INCOMPRESSIBLE FLUID FLOW IN COLLAPSIBLE TUBES

By

DAVID LEE SMITH

Bachelor of Science
Oklahoma State University
May, 1971

Master of Science
Oklahoma State University
July, 1972

Submitted to the Faculty of the
Graduate College of the
Oklahoma State University
in partial fulfillment of
the requirements for
the Degree of
DOCTOR OF PHILOSOPHY
December, 1979

INCOMPRESSIBLE FLUID FLOW IN COLLAPSIBLE

TUBES

Thesis Approved:

Karl N. Reid

Thesis Adviser

Thomas E. Blejwas

J W Harvey

David G. Lilley

Norman N. Durham

Dean of Graduate College

PREFACE

This study was concerned with the analysis of a hybrid fluid mechanical problem. That is, the steady state achieved by the fluid flow was strongly dependent upon an interaction with the confining structure. The tube walls moved in response to the fluid flow forces. Although the apparent emphasis in this manuscript is upon a fluid mechanical result, the bulk of the work actually concentrated on a finite element structural description of the tube where two major stumbling blocks were encountered. The first, which was a singularity of the unconstrained stiffness matrix, has been observed by a colleague working on a similar problem. This difficulty suggests that the collapsing cylindrical shape needs to be guided or constrained in the proper direction. The second difficulty arose when the wall deflections became very large and was due to inter-element discontinuity. The cure for this ailment was found in a redefinition of the element displacements.

Regarding the organization of this document, the view was adopted that most readers are generally familiar with these methods. The bulk of the derivations and matrix manipulations are given in the appendices. Annotated deck listings are furnished in order to encourage the further use and development of these computational methods. Furthermore, it was felt that the readability of the manuscript would be enhanced if the literature review was integrated with the appropriate chapters. That is, the review of previous experimental work is presented in Chapter II, while the review of previous analytical work is presented in Chapter III.

Financial support for the author was derived in part from a Gulf Foundation Fellowship and a National Institutes of Health Biomedical Sciences Research Support Grant. This support is gratefully acknowledged as well as that which was derived from Oklahoma State University departmental sources.

The author wishes to offer an expression of appreciation to the advisory committee members: Those who guided the early work; E. W. Jones, DVM; Dr. R. Mulholland; and Dr. W. Tiedermann; and those who have encouraged and guided the majority of the work which is represented by this manuscript; Dr. T. Blejwas, Dr. J. Harvey, and Dr. D. Lilley. Special gratitude is extended to Dr. Karl N. Reid whose recruiting ability brought me back to Oklahoma State University for this third time and whose advice and constant support in the role of major adviser has made every step of this educational exercise very logical and very enjoyable.

A note of thanks is extended to Mr. George Cooper whose talent with hardware and willingness to work on short notice made him irreplaceable in constructing the experimental apparatus.

My deepest appreciation is extended to my partner, Jeanne, whose many sacrifices made it possible for me to attempt and complete this contribution.

TABLE OF CONTENTS

LIST OF TABLES

LIST OF FIGURES

NOMENCLATURE

List of Symbols

The list of symbols has been extended to include computational variables from the COMMON block of the subroutines in the appendices.

a	coefficient of the displacement polynomial, also called the generalized coordinate
A	Area (cm^2)
[B]	proportionality of $d\varepsilon$ to dq
[B*]	proportionality of $d\varepsilon$ to da
[C]	proportionality of q to a or dq to da
[CC]	matrix of constraint coefficients
CI	same as $[C]^{-1}$
d	tube diameter (cm)
[D]	Hookean elasticity proportionality matrix
DIA	tube undeformed diameter (cm)
DMAX	the computed maximum node position change
DP, DU, DPSI	convergence parameters
DPDX	fluid pressure gradient
DRO	initial cross-section ellipticity parameter, 1/2(major axis length - minor axis length)
DXIN, DXOUT	lengths of the tube mounting fixtures

E	Young's modulus of elasticity (dynes/cm^2)
ε	linear strain (dimensionless)
eps	general numerical convergence criteria
f	surface traction force (dynes/cm^2)
F	force (dynes)
FMU	Poisson's ratio
γ	shear strain (dimensionless)
[G]	proportionality of dq to q
h	thickness (cm)
[H]	proportionality of dq to a
hd	hydraulic diameter (cm)
HX, HY	grid spacing distances (cm)
IELEM	stores three nodes which comprise an element
IFORCE	a flag to bypass the fluid model
IIN, IOUT	logical input/output unit assignments
INFLAG	a flag signalling the completion of initialization
κ	change in reciprocal radius of curvature from an initial value (cm^{-1})
$[K_N]$	stiffness matrix containing linear and geometrically nonlinear parts
$[K_T]$	tangential stiffness matrix
$[K_\sigma]$	initial stress or geometric matrix
l	length (cm)
LASTEL	the number of the last element in the structure, including the rigid mount approximations
LASTJ	the index of the next-to-last X location

LASTND	the number of the last node in the structure, including the rigid mount approximations
lp	wetted perimeter (cm)
λ	Lagrange multipliers
M	bending moment per unit area (dyne-cm/cm^2)
[M]	matrix of stress values
m	slope of the linear fluid pressure approximation
μ	fluid dynamic viscosity (poise)
$\hat{n}$	outward directed unit normal
ν	fluid kinematic viscosity (stokes)
NDOF	stores the numbers of the constrained degrees of freedom
NELEM	the number of finite elements in the tube
NIN	the number of grid increments which lie under the inlet mount approximation
NNODES	the number of nodes in the tube
NTUBE	the index of the last X-location which lies under the flexible tube
NTUBEX, NTUBEY	finite element subdivision of the tube
NUMBC	the total number of constrained degrees of freedom
NX, NNY	number of X-Y grid increments
NY	number of grid points in the Y direction
P	static fluid pressure (in. H_2O, mm Hg, dynes/cm^2)
P1	the inlet pressure (dynes/cm^2)
P2	the outlet pressure (dynes/cm^2)
PE	the collapsing pressure (dynes/cm^2)
PSI	same as Ψ, the equilibrium index

Ψ	equilibrium index (dynes)
PTEST	an internal variable used to store the maximum change in pressure at a location computed on a step
PXB	fluid static pressure gradient in the axial direction (dynes/cm^2)
q	displacement evaluated at a finite element node
Q	flowrate (cm^3/sec = ml/sec)
R	adjustable orifice fluid resistance
r	Poisson's ratio
RC	radius of curvature (cm)
Re	Reynolds number (dimensionless)
REY	Reynolds number (dimensionless)
RHO	fluid density (gm/cm^3)
ρ	fluid density
RL	tube length (cm)
RLP	same as lp, the wetted perimeter (cm)
RLS	circumference of the tube cross section (cm)
RMU	fluid dynamic viscosity (poise)
RNU	fluid kinematic viscosity (stokes)
S	scale factor
SCALE	sets the maximum allowable computational step
SIGMA	stores the initial global stress in the elements
SIGXO	initial global prestress in the axial direction
STIFF	augmented tangential stiffness matrix

STRAIN	same as ε, the element strains
σ	stress (dynes/cm^2)
t	time (sec)
[T]	transformation matrix of global to local coordinates
τ	shear stress (dynes/cm^2)
$d\tau$	volume increment
θ	structural orientation (radians)
$\Delta\theta$	rotational deflection (radians)
THK	the thickness of the elements (cm)
TR	same as [T], the axes transformation
TWX, TWY, TWZ	fluid wall shear forces (dynes/cm^2)
TX	slope of the structural surface (radians)
TXO	initial slope of the structural surface (radians)
U^i	internal work (dyne-cm)
u, v, w	deflections in local coordinates (cm)
U, V, W	deflections in global coordinates (cm)
UTEST	an internal variable to store the maximum change in average velocity at a location computed on a step
$\bar{V}$	average fluid axial velocity (cm/sec)
$\underset{\sim}{V}$	fluid velocity vector (cm/sec)
VOL	element volume (cm^3)
VU	same as $\bar{V}$
W	external work (dyne-cm)
x, y, z	local coordinates (cm)
X, Y, Z	global coordinates (cm)
XC, YC	local coordinates of the element centroid (cm)

XNODE, YNODE, ZNODE	global position of the finite element nodes (cm)
XO, YO, ZO	initial global position of the finite element nodes (cm)
YMAX	maximum Y dimension of the tube cross-section at a given X location (cm)
ZMAX	maximum Z dimension of the tube at a given X-Y location (cm)

Subscripts

1	inlet
2	outlet
a	atmospheric
d	downstream
e	exterior
G	global
h	hoopwise (circumferential)
i	internal
j, k, l	nodes of a finite element
L	local
m	generalized node number
n	generalized element number
o	initial
p	predicted
r	measured or reading
u	upstream
w	interior tube wall
x, y, z	in direction of local x, y, or z axes

X, Y, Z	in direction of global X, Y, or Z axes

Notation

$\overline{A}$	overbar indicates average value
$\utilde{A}$	underwave indicates a vector
[A]	brackets indicate a matrix
dA	indicates first variation
ΔA	indicates difference; i.e., $A_1 - A_2$
$[A]^{-1}$	indicates the inverse of matrix [A]
A^n	is A at computation step n
$[A]^T$	indicates the transpose of [A]

CHAPTER I

INTRODUCTION

Overview

The problem of predicting fluid flow variables in a collapsible tube appears to be most often encountered in a physiological setting. A variety of spontaneous as well as forced physiologic fluid flow situations exhibit complications which suggest that tube collapse exerts a significant modulating effect on the fluid flow. It has also been suggested that a thorough understanding of the mechanics of this problem may lead to exploitation in fluid power control circuitry and other engineering applications. This later observation is underscored by the choice of experimental apparatus which is typically used in investigation of the problem. In this study, as in previous investigations, a non-physiologic experimental idealization was used to define the tube/fluid mechanical response to collapsing pressure and to provide a basis of comparison for a new analytical model of the mechanics. Nevertheless, the importance of the problem at this time stems primarily from physiologic reasons and particularly from venous blood flow prediction difficulties.

The important role of the veins as a return for blood flow to the heart has received scant attention in theoretical circulatory analysis. It would appear that the more regular geometry of the arteries has prompted numerous analytical studies of arterial blood flowrate, pressure, phase velocity, etc., thus diverting attention from equally important venous blood flow problems. By way of complication, the thin-walled, low pressure, highly flexible venous tubes are especially susceptible to states of collapse at any time due to excessive external pressure. In addition, the collapse condition entails complex geometries and, hence, difficult analyses. More importantly, venous blood flow must be addressed in any study of the complete circulation. In fact, an overall circulatory regulation may occur due to the fluid flowrate modulation caused by the collapsing veins (1).

Historical Perspective

Physiologists have long recognized the occurrence and importance of collapsed tube flows. Perhaps one of the earliest descriptions of the natural occurrence of the phenomenon was offered by Bayliss (2) in 1895 in a discussion of the cerebral circulation. In 1912, Starling (3) presented a controllable hydraulic resistor based on this principle which was designed to vary the load on an isolated mammalian heart. In recognition of his achievements, physiologists now widely describe collapsed tube flows as "Starling resistors." Important spontaneous occurrences of the phenomenon have been recognized in the following physiologic tube systems: veins, arteries, pulmonary circulation, pulmonary airways, urethra, eustachian tubes, and vocal cords (4). Tube collapsibility is also important in the following clinical practices: positive pressure lung ventilation, listening for Korotkoff sounds, vascular diagnosis with pressurized cuffs, intra-Aortic balloon counterpulsation, artificial heart pumping, heart assist by external leg counterpulsation, and blood withdrawal with vein cannulation. An important difference between these two groups is that the flows in the second group are controlled by external forcing. Thus, the clinician creates a forced response. Clearly, a deeper understanding of the mechanics of cause and effect could improve the effectiveness of these procedures and perhaps indicate new ones as yet undiscovered.

The principal interest of this study was the relationship of Starling resistor effects to the design and control of positive pressure lung ventilation equipment. It has been suggested that venous portions of the circulation act like Starling resistors during this type of lung ventilation (5). This description is in excellent agreement with contemporary concepts of hemodynamics (6-10). Thus, positive pressure lung ventilation creates elevated pulmonary pressures which apparently operate to modulate the net cardiac output. Consequently, this type of ventilation creates an undesirable mechanical effect (reduction of blood flowrate) as well as a desirable chemical effect (increased blood oxygenation), and leads to an important tradeoff in order to optimize controlled gaseous exchange.

Motivation for this study of the collapsible tube is not limited to physiologic situations, however. Exploitation of collapsible tube flows has been described in the design of the following engineering devices: oscillators, amplifiers, switches, logic devices, and resistors (4).

Scope

Any fluid mechanical study of the venous collapse problem is initially complicated by inherent measurement difficulties. The simultaneous measurement of pressure and flowrate in veins *in situ* has been termed a "difficult and unreliable art" (11, p. 333). Thus, for the most part, analytical and experimental findings to date have been derived from a laboratory apparatus which is used as a physical idealization of venous mechanics. The classical experimental apparatus is shown in Figure 1a. This device is composed of a thin-walled latex tube, often Penrose surgical drain tubing, freely suspended in air between rigid circular mounts. Liquid flow through the device can be modulated by the adjustable orifices (R_1 and R_2), or the collapsing pressure, P_e.

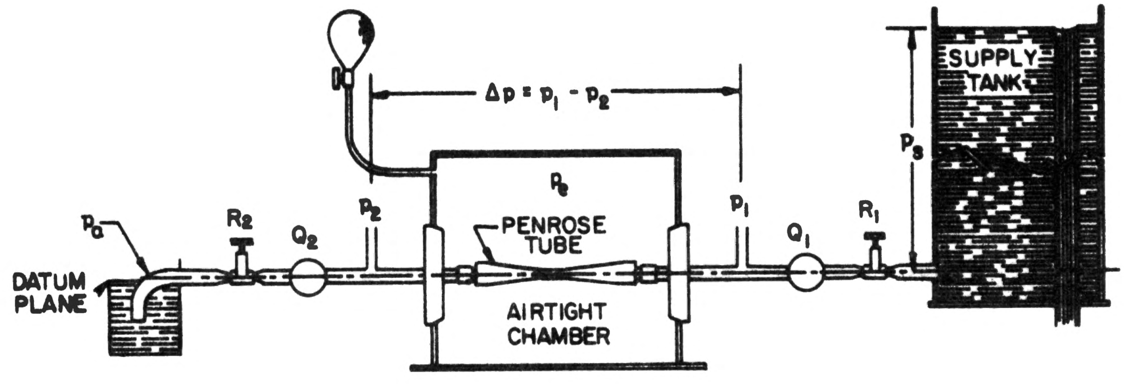

(a)

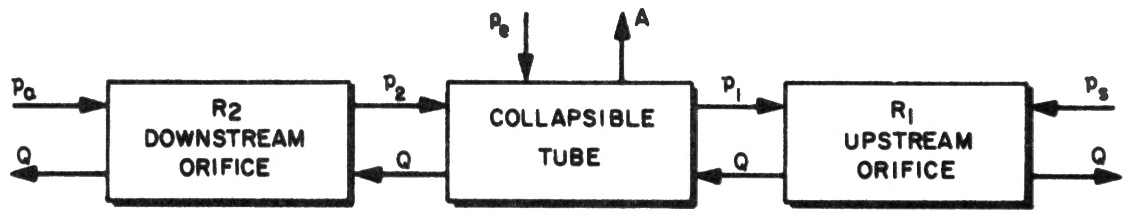

(b)

Figure 1. Classical Apparatus for the Study of Flow in Collapsible Tubes (a) Apparatus, from Katz (12, p. 1263), (b) Block Diagram

A block diagram of the classical hydraulic system is shown in Figure 1b. This block diagram portrays the interdependence of the collapsible tube and the remaining circuit elements. Thus, the steady-state operation of the system is represented by the constant flowrate, Q, between all blocks, each block representing a circuit element. Each element, in turn, responds to its input variables in order to produce one or more outputs. For example, the downstream orifice responds to inputs of flowrate, Q, and outlet pressure, P_a, (Q and P_a labelled inward pointing arrows) and gives P_2 as its output. At the inlet side of the system, the flowrate through the upstream orifice responds to pressure inputs, P_s and P_1. The inputs to the collapsible tube are the collapsing pressure, P_e, the downstream pressure, P_2, and the system flowrate, Q. The collapsible tube outputs are the upstream pressure, P_1, and the cross-sectional area, A, which varies along the tube axis.

Measurements made with the classical apparatus of Figure 1 have introduced some confusion regarding the fluid mechanical behavior of the collapsible section. This confusion stems from a failure to distinguish between a <u>characteristic</u> response and the <u>in-circuit</u> performance (11). A characteristic response is observed when a circuit element is isolated from interacting elements while input versus output relationships are determined. On the other hand, circuit performance is composed of the responses of the interacting elements. The element characteristic responses can be used to predict circuit performance, but the characteristic response may not be recoverable from the circuit performance data.

Isolation of the collapsible tube in order to measure its characteristic can be achieved in several ways. One way is to eliminate both the orifices of Figure 1 and use a pressure drop to force the fluid through the tube (e.g., Figure 2a). This approach requires that P_s (P_1), P_2, and P_e

all be independently controlled variables (i.e., inputs). Shapiro (13), Griffiths (14), and Lambert and Wilson (15) all used pressure forcing of the collapsible tube. However, the characteristic that coincides with the classical experiment results from flowrate forcing. That is, the flowrate, Q, is an input to the collapsible tube. In both cases, as shown in Figure 2, P_e and P_2 are independent variables.

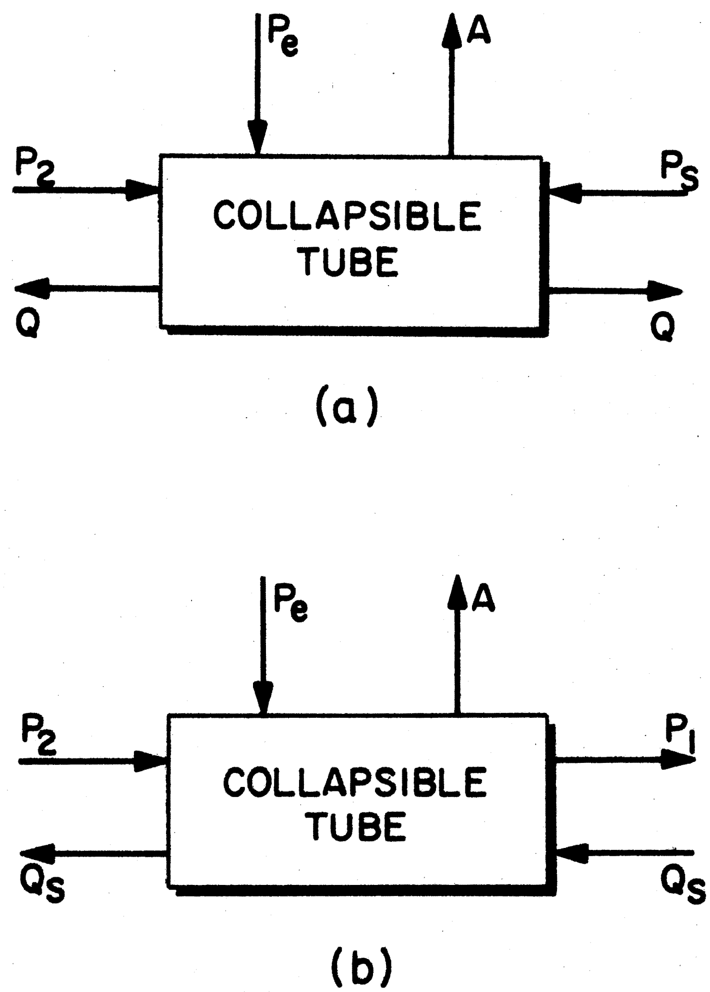

Figure 2. Input-Output Variables in a Collapsible Tube (a) Pressure Forcing, (b) Flowrate Forcing

It was assumed that the input-output causality of Figures 1 and 2b corresponds to the venous case. The experimental apparatus was designed to isolate the characteristic with this causality, but the apparatus was not intended as a rigorous physical venous model.

The analytical goal was to predict the pressure drop versus flowrate characteristic given knowledge of fundamental tube and fluid properties. In this approach, it was assumed that flowrate, collapsing pressure, and outlet pressure are known while inlet pressure is to be calculated. The analysis was restricted to the steady-flow case.

The object of this study was thus twofold: to experimentally clarify the pressure drop-flowrate steady-flow fluid response to a collapsible tube as a function of external collapsing pressure, and to develop an analytical model capable of describing the observed fluid flow behavior through the collapsed tube.

The organization of this study is into five chapters: the first is introductory; the second discusses past and present experimental approaches; the third presents previous analytical attempts which lead to a new, more fundamental model; the fourth shows experimental results and compares analysis to experiment; the last summarizes and gives some conclusions and recommendations. The body of this thesis is intended to highlight the approach and, consequently, much theoretical and analytical detail is relegated to the appendices.

CHAPTER II

EXPERIMENT

The early experimental investigators made measurements with the apparatus shown in Figure 1 (12,16). They suggested that the performance curves obtained were "characteristic" curves, yet they also observed that the value of the downstream resistance had a strong effect on the results. Therefore, in the light of the introductory remarks, these results were really a representation of in-circuit performance rather than the true characteristic fluid flow response to the collapsible tube. More recently, investigators have realized the necessity to isolate the collapsible tube in order to determine its characteristic (17). Consequently, the following literature survey is divided into two sections, a section on in-circuit performance and a section on the characteristic response.

Literature Survey

In-Circuit Performance

A summary of experimental results from the early investigations is shown in Figure 3. At a fixed value of collapsing pressure, P_e, a single highly nonlinear pressure-flow relationship exists, as shown in Figure 3a.

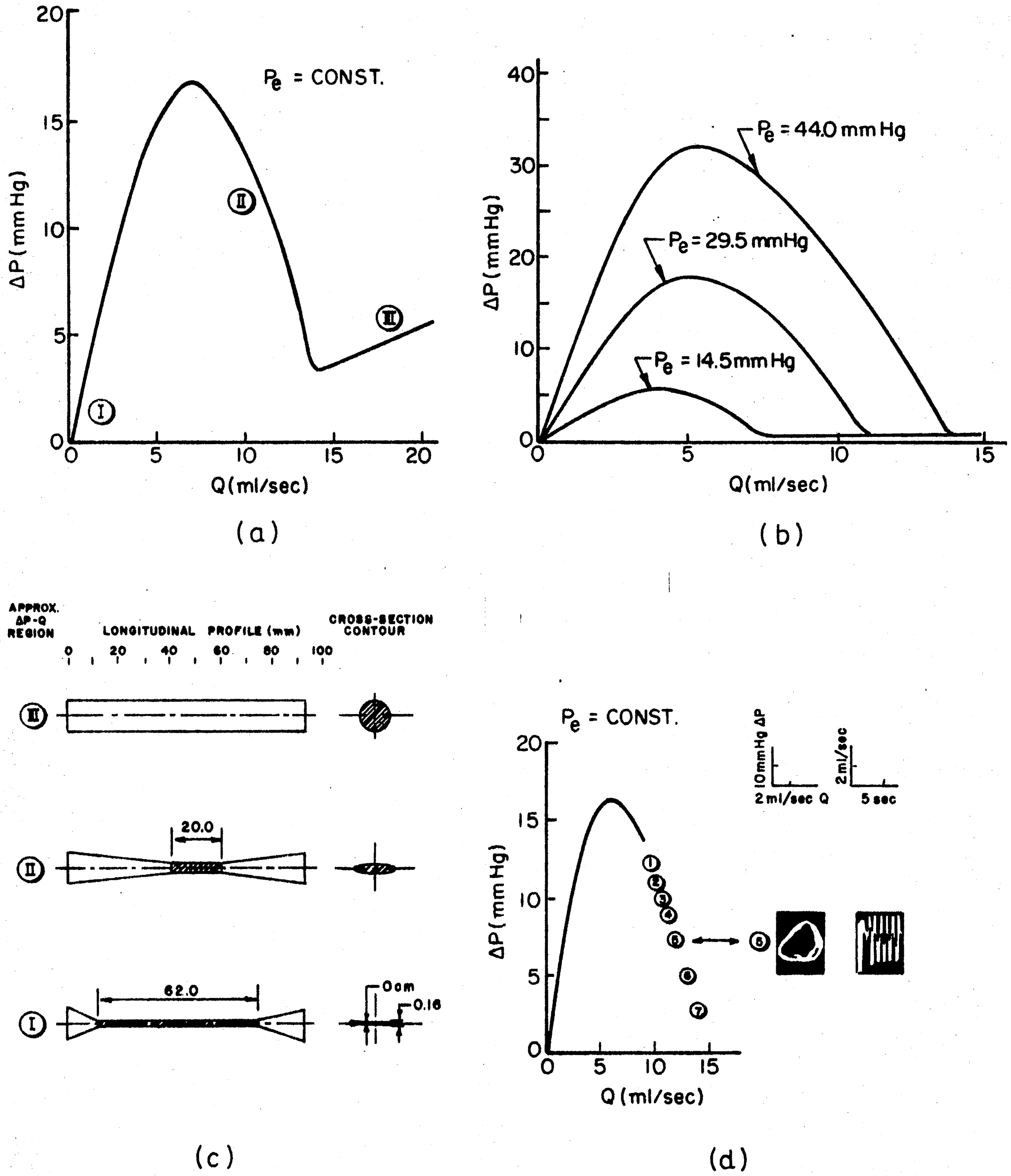

Figure 3. Experimental Data for a Collapsible Tube in a Hydraulic Circuit (a) from Conrad (16, p. 288), (b) from Katz (12, p. 1267), (c) from Katz (12, p. 1272), (d) from Conrad (16, p. 291)

Furthermore, a family of nonlinear pressure-flow curves can be generated, each curve corresponding to a different value of collapsing pressure as shown in Figure 3b. Figures 3a and 3b were generated with the same circuitry (e.g., Figure 1) with different settings of R_2 for each figure. Mechanical coupling between tube and fluid dictates that the tube assume certain shapes, which are shown in Figure 3c and are correlated to the pressure-flow relationship of Figure 3a. The geometries of Figure 3c occurred with a flow direction of left-to-right. Photographs taken by Conrad (16) show the constriction (shape II) formed closer to the downstream end than that shown in Figure 3c. However, comparison of these data was not possible owing to non-standardization of experimental parameters (e.g., tube pretension and length, R_1 and R_2 settings, supply pressure setting, etc.). Oscillatory tube behavior has been observed and several recordings of this are shown in Figure 3d. Katz et al. (12) suggested that the value of R_2 was important to oscillation onset.

Qualitatively, the mechanics passed through four distinct regimes. These regimes can be separated by the relative magnitudes of the three controlling pressures: the inlet pressure, P_1, the outlet pressure, P_2, and the collapsing pressure, P_e.

1. $P_1 > P_2 > P_e$ The tube is inflated and the flowrate Q is determined by P_1 and P_2 with only a weak P_e dependence. This is similar to the arterial flow case (3).

2. $P_1 > P_e > P_2$ Here, part of the tube is inflated while part is collapsed. This condition has received no apparent discussion in the literature.

3. $P_e > P_1 > P_2$ Now the tube is collapsed to varying degrees along its entire length. An oscillation has been observed with this pressure arrangement and frequencies have been measured (16,18). Conrad (16) has described this behavior as a relaxation oscillation which builds up to a limit cycle, while Rodbard (18) has described it as an interrupted series of jets with production of audible sound.
   Prediction of the steady flow observed in this regime was of primary interest to this study.

4. $P_e >> P_1$ Ultimately in the physiologic case, P_e will reach a value, commonly known as the Critical Closing Pressure, which prohibits fluid flow through the tube (19). Observation of critical closing has not been documented in previous collapsible tube experiments.

The Charactertistic Response

The need to isolate the collapsible tube in order to measure the fluid pressure-flow characteristic was perhaps first recognized by Brower (17). His analytical work showed that the tube characteristic could be extracted from previously reported circuit performance data. He conducted confirming experiments of this concept and the results are shown in Figure 4.

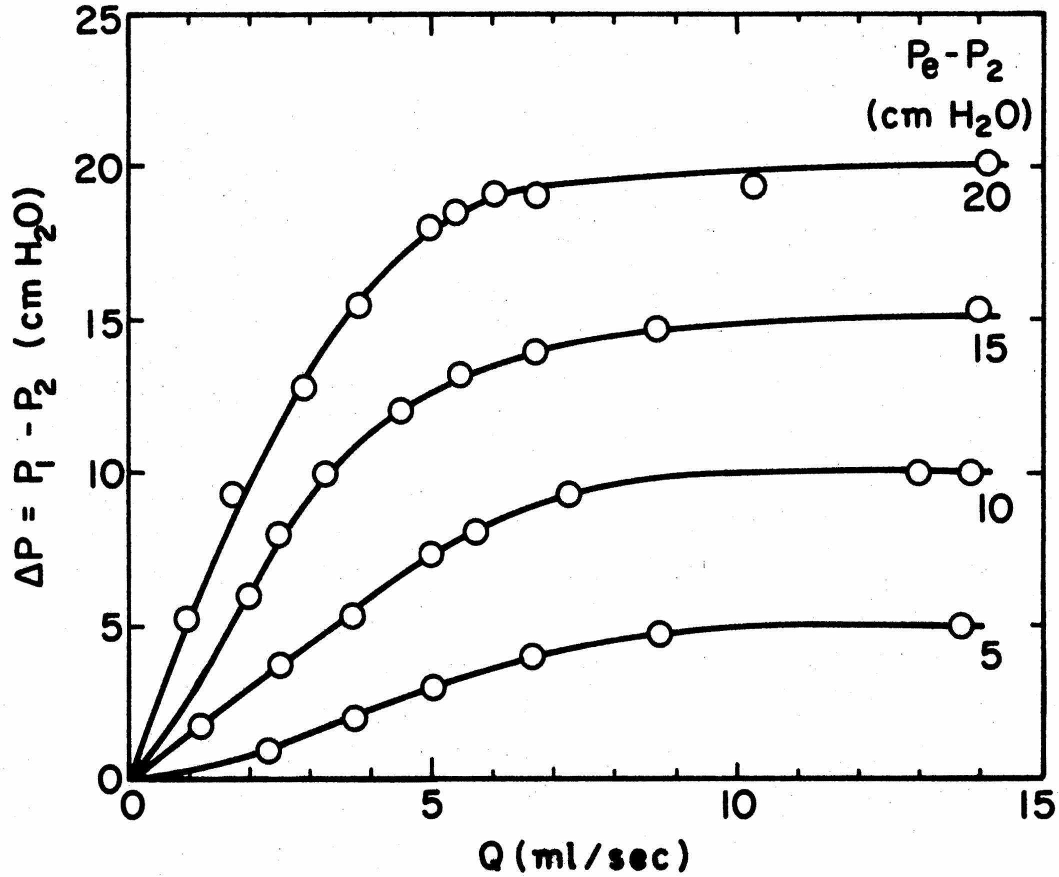

Figure 4. The Pressure Drop-Flowrate Characteristic of a Collapsible Tube, from Brower and Noordergraaf (11, p. 338)

Experimental Approach

The goal of the present experimentation was to clarify the fluid pressure-flowrate characteristic response to a collapsible tube. Two types of experimental studies were conducted in these experiments: The effect of tube axial prestrain on the characteristic was studied, and the axial distribution of tube internal fluid pressure was measured.

The effect of prestrain on the characteristic appears to have been ignored by previous investigators. For example, Brower and Noordergraaf (11) used a prestrain in excess of 15%, Conrad (16) attempted a strain-free experiment, while Katz et al. (12), and Lambert and Wilson (15) did not report the prestrain value.

In order to determine the role of prestrain, two sets of inlet pressure versus flowrate measurements were made: a set at an initial tube axial strain near 10% and a set at an initial tube axial strain near 1%. The two cases were somewhat arbitrarily denoted as high and low prestrain cases, respectively. The axial strain was estimated by placing marks on the tube and measuring their separation before and after mounting. That is,

$$\varepsilon_X = (l - l_o)/l_o \tag{1}$$

where ε_X is the axial strain, l is the stretched length, and l_o is the unstressed length.

Figure 5a shows a schematic of the experimental apparatus. Here, the supply pressure was set at a value large enough (10 ft H_2O) to ensure that the upstream orifice, R_1, functioned as a flowrate source which was nearly independent of its downstream pressure, P_1. In addition, the downstream resistance, R_2, was eliminated so

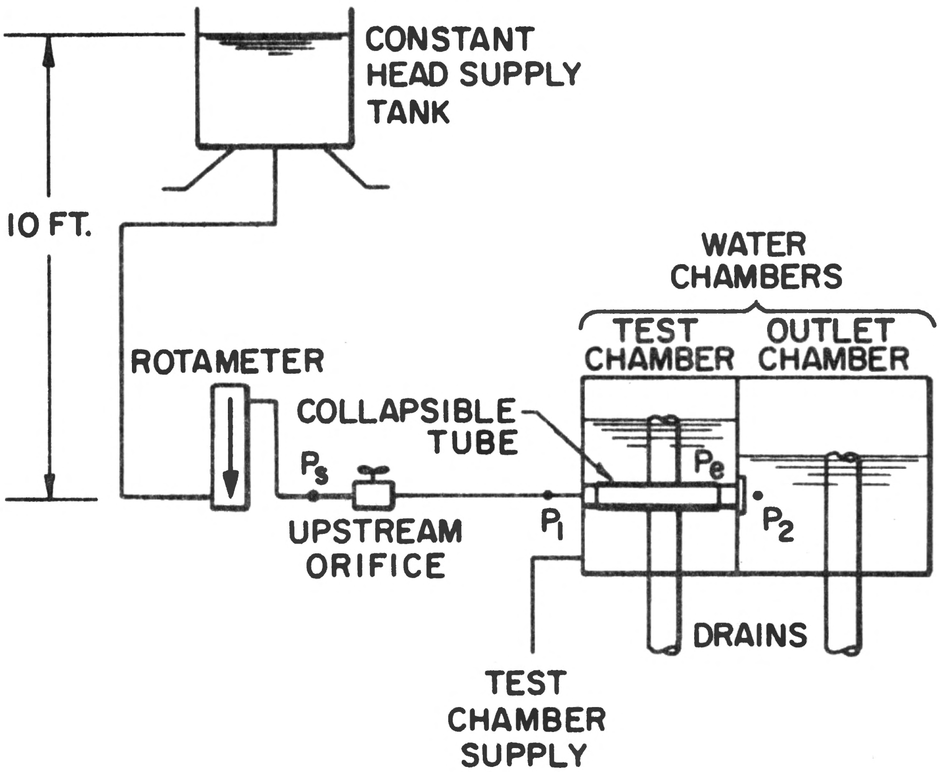

(a)

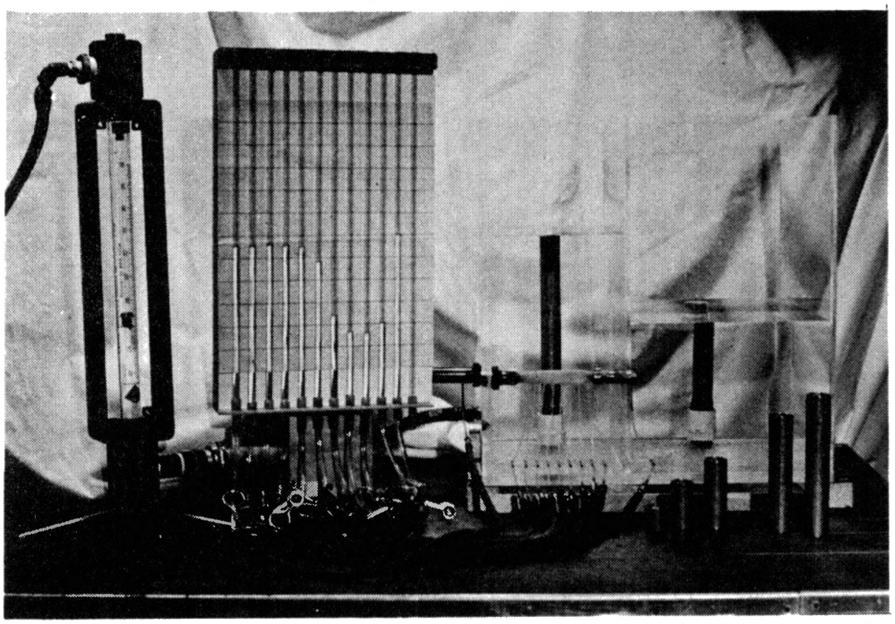

(b)

Figure 5. Experimental Apparatus (a) Schematic, (b) Photograph of Rotometer, Manometers, and Water Chambers

that the pressure, P_2, downstream of the tube was very nearly equal to the back pressure created in the outlet chamber. Thus, the tube was isolated in order to generate the characteristic pressure-flowrate fluid response. Contrary to previous experiments, the tube was immersed in water in order to minimize bouyancy effects.

Water flowrate through the flexible tube was measured with a Fisher-Porter flowmeter (No. 1/2-21-G-10/20).

In Figure 5b, the collapsible tube is shown connected to the manometers. This configuration was used to measure the distribution of interior fluid pressure, which is indicated on the manometers in the figure. The water level in the test chamber was adjustable through the interchangeable sections of pipe shown in the right foreground of the figure. The outlet pressure, P_2, was maintained at a constant value of 3.10 in H_2O above the centerline of the collapsible tube. The free length between the collapsible tube supports was adjustable between 9 and 11 cm.

Samples of 1/2 inch Penrose surgical drain tubing (latex rubber) were used as the flexible tube ($E = 1.9 \times 10^7$ dynes/cm^2, thickness = 0.028 cm, Poisson's ratio = 0.5). The measurement of axial pressure drop was done with a piece of this tubing suspended between the circular mounts. However, it was necessary to affix manometer connecting tubes to the main Penrose tube in order to measure the distribution of interior pressure. This modification is shown in Figure 6. Conrad (16) has observed that the initial elliptic cross-section of the tube predetermines its circumferential collapsed shape. That is, the long axis of the initial cross-section remains the long axis of the collapsed cross-section. This fact made it possible to locate the manometer connecting tubes a priori so that they continue to measure the fluid pressure in the side channel formed during extreme collapse (condition I in Figure 3c). Thus, small holes (0.5 mm) were made in the Penrose tube wall along a lengthwise extension of the major axis of initial cross-section. The manometer connecting tubes were glued to the penrose tube over the holes. The wall tap spacing (1 cm) was somewhat arbitrarily selected based on a tradeoff between minimizing the interference with the solid mechanics of collapse and maximizing the number of fluid pressure sampling points.

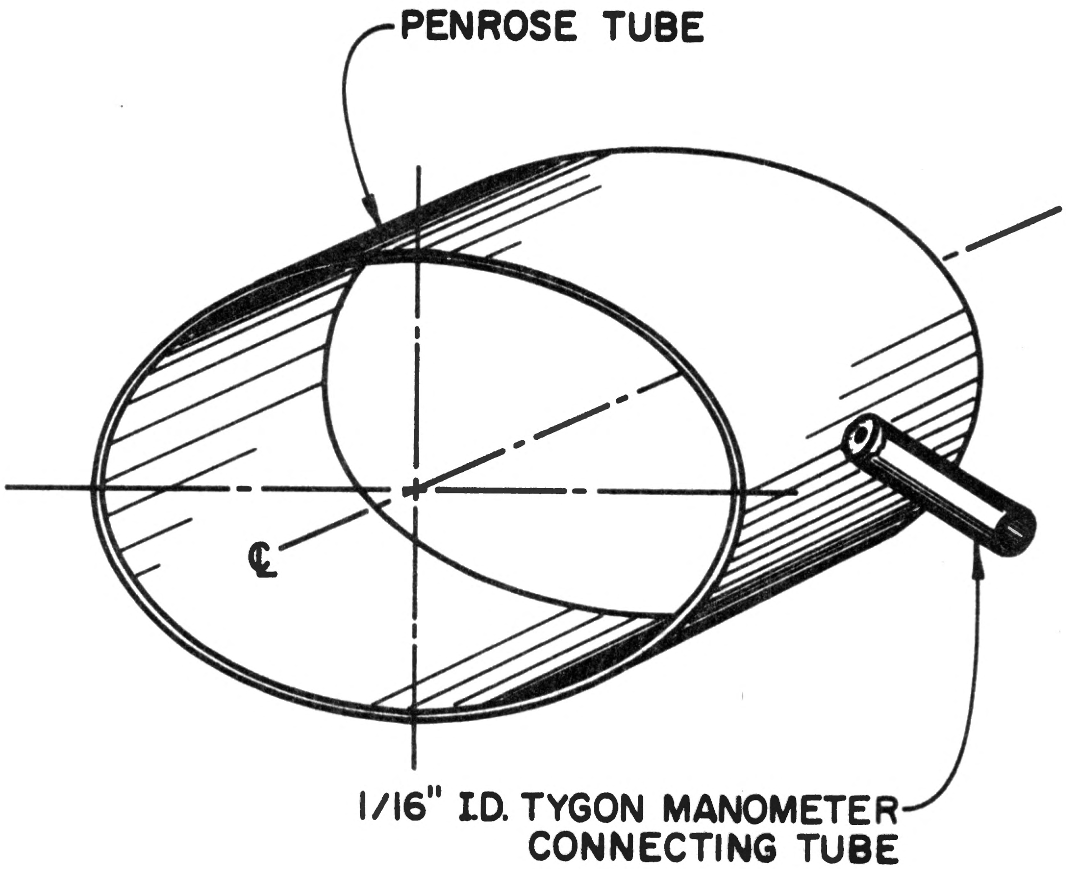

Figure 6. Modification of a Section of the Flexible Tube for Interior Wall Pressure Measurement

CHAPTER III

ANALYSIS

The major analytic difficulty experienced by previous investigators has been the treatment of tube structural mechanics. The fluid mechanics has been uniformly treated as one-dimensional. In order to assess the accuracy of predicted variables, a relative error was used

$$\text{error} = (x_p - x_r)/x_r \tag{2}$$

In Equation 2, and throughout this study, the standard of comparison is the measured (reading) value which is represented by x_r; x_p represents the predicted value.

Literature Survey

Rodbard (18,20,21) and Holt (22,23) were among the first to discuss flowrate prediction in collapsible tubes. As physiologists, they attempted to use the simplest fluid flow model available, a linear Hagen-Poiseulle relationship. This linear pressure drop-flowrate model has repeatedly appeared in analyses of collapsible tube flows; however, the nonlinear nature of the characteristic previously discussed (e.g., Figure 4) would seem to preclude accurate prediction by so simple a fluid model.

Conrad (16) was among the first to study both the steady and oscillatory behavior of the flow through the tube. His fluid models were used to explain the experimental data and a prediction of the data was not attempted. His experimental apparatus was the clasical apparatus shown in Figure 1, so that isolation of the tube in order to determine its characteristic was not accomplished.

Almost simultaneously with Conrad, Katz et al. (12) attempted a study of the collapsible tube. They measured experimental collapsed tube shapes and correlated them to a fluid energy loss coefficient for the tube. This model of the flow through a collapsible tube was utilized in a fluid mechanical analysis of the classical apparatus (Figure 1). Thus, Katz et al. attempted to predict the in-circuit performance of the tube. Their results are presented in Figure 7. The large error (56%) in predicted pressure drop at a given flowrate was attributed to slight errors in the measurement of cross-sectional area and the accompanying underestimation of the viscous losses.

In a milestone study, Brower and Noordergraaf (11) presented the first characteristic data for a collapsible tube. The analysis that they conducted was based on a best fit to the experimental data. An important study conclusion was that the analysis should be developed from basic physical principles.

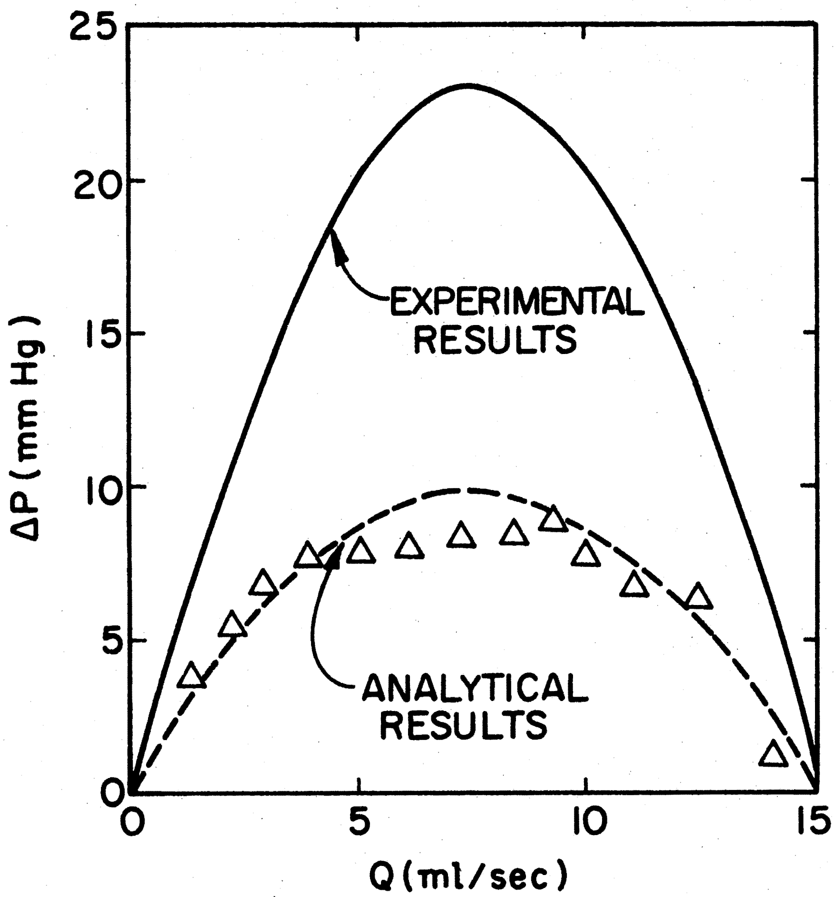

Figure 7. Comparison of Data for a Semi-Empirical Model, from Katz (12, p. 1273)

In 1972, Lambert and Wilson (15) proposed an inviscid, irrotational model of the fluid flow coupled to a theoretically derived model of the tube mechanics. In this model, the tube was assumed to possess hoopwise bending rigidity only. Two aspects of this model are important. First, the model was fully predictive. That is, given the basic properties of the fluid and tube, a flowrate was predicted, albeit inaccurately. Secondly, the large errors manifest in the results were attributed by the authors to the neglected fluid viscous effects.

In a later study, Wild et al. (24) presented a model specifically addressed to steady flow at low Reynolds numbers. The model was derived from a lubrication theory solution. The lubrication theory is useful when the Reynolds number is small (e.g., order 1) and the tube radius is very small compared to the length. Wild modified the basic lubrication theory to account for an elliptic tube cross-section, with ellipse parameters which vary in the axial direction. This model is important in that it was one of the first to utilize a distributed geometric shape as a tube description. However, noteworthy shortcomings of the model include its requirement for an elliptic tube cross-section, and the constraint to low Reynolds number flow.

In 1977, Shapiro (13) published his approach to the problem. He offered a one-dimensional fluid model and emphasized the importance of coupling the mechanics of the flow to the mechanics of the tube. His model of the tube was an empirical one and fluid frictional effects were lumped into a coefficient of friction. Shapiro emphasized the importance of the tube-support interaction at the downstream, exiting end of the tube on the fluid mechanics. He also suggested that these end effects may limit the usefulness of the apparatus as a rigorous venous model.

Shapiro presented a general theory of flow in collapsible tubes, but perhaps the greatest limitation of his theory rests in his assumption that the fluid pressure distribution and viscous wall shear distribution are known quantities. In the light of inherent measurement difficulties discussed previously (11), this would seem to be an unjustifiable assumption at the present time.

Analytical Approach

The goal of the present analysis was to predict the fluid flow characteristic pressure drop-flowrate response to the collapsible tube. In this approach it was assumed that flowrate, outlet pressure, and collapsing pressure are known while inlet pressure is to be calculated. A finite-element model of the flexible tube was assembled and coupled to a one-dimensional fluid mechanical model. The nonlinear combined model was programmed for iterative solution on a digital computer. The solution algorithm was composed of a set of task-oriented subroutines which are highlighted in the following sections and discussed in detail in Appendices A through F.

Analysis inputs were separated into four types: geometric, material, initial value, and numerical parameters. The inputs are summarized in Table I. These fifteen inputs are all that was required for the analysis and thus fulfill the scope requirement for an input list of fundamental parameters.

TABLE I

ANALYSIS INPUTS

Type	Tube	Fluid
GEOMETRIC		
	Thickness Circumference Length Ellipticity	
MATERIAL		
	Poisson's Ratio Young's Modulus	Kinematic Viscosity Density
INITIAL VALUE		
	Stress Levels	Flowrate Downstream Pressure Collapsing Pressure
NUMERICAL		
	Global Axes Subdivision Finite Element Distribution Convergence Parameters	

The Tube Model

The tube was viewed as a shell structure which shows membrane stiffness in the axial direction and bending rigidity in the hoop direction. Katz et al. (12) showed the importance of accurate tube shape prediction to the coupled fluid mechanical prediction. Lambert and Wilson (15) have shown the importance of hoopwise bending in the tube, but they ignored effects in the axial direction. Shapiro (13) suggested that the short length of the tube would also make axial membrane stresses important to tube shape prediction, but he observed that such a distributed tube model could be forbiddingly complex. Nevetheless, such a model was the next logical step and it was employed for this study.

The observed collapse shapes (Figure 3) show that the analysis must account for wall deflections which are very large with respect to wall thickness (e.g., 20 times). These large deflections give rise to a form of "geometric" nonlinearity which may be best treated with a finite element approach (25). Furthermore, the deflections occurred in such a way that the thin plate assumptions which are usually used in a shell analysis became invalid.

Finite elements which possess inter-element discontinuities in position or slope have often been used in the analysis of shell problems, such elements are usually termed non-conforming (25). In the present study, a variety of non-conforming triangular elements were examined, none of which achieved consistent numerical convergence. That is, at sufficiently large displacement, all the non-conforming elements that were examined produced a singular stiffness matrix. The cure for this ailment was found in a redefinition of the displacement functions. In contrast to a classical finite element analysis, the linear deflections (u, v, w) were associated with a pure membrane finite element, while the element rotational orientation ($\bar{\theta}$) was interpreted as a mean value for the slope of the curving structure. Thus, nodal rotational deflections ($\Delta\theta$) were defined independently of the linear deflections, and the two types of deflections were related through an intuitive geometric relationship which was enforced by the use of Lagrange multipliers. This scheme permitted position continuity in order to predict membrane effects as well as slope continuity in order to predict bending effects.

Following the finite element method, the structure was subdivided into an interconnected set of small but finite structural elements. Planar triangular elements were defined such that they stretch in-plane in order to show membrane action. Hoop bending forces were calculated from the nodal rotational deflections. The element linear U, V, W deflections are associated with the global coordinate directions X, Y, and Z, as shown in Figure 8; $\Delta\theta_x$ is the rotational deflection of a line tangent to the structure about the global X-axis defined in a right-handed manner. For example, at node ℓ in Figure 8, the structural orientation, θ_x, arises due to a deflection, $\Delta\theta_x$, from the initial orientation, θ_{xo} .

Two coordinate systems were needed for the analysis. The local coordinate system was used to take advantage of the structure modelling assumptions (e.g., the "shallow shell" assumptions which are discussed in following paragraphs), while the global coordinates were used as a reference for the assembled structure and the fluid mechanics. In order to facilitate the analysis, x and X must be chosen to be colinear. If this is not done, a more complete set of rotations would be required.

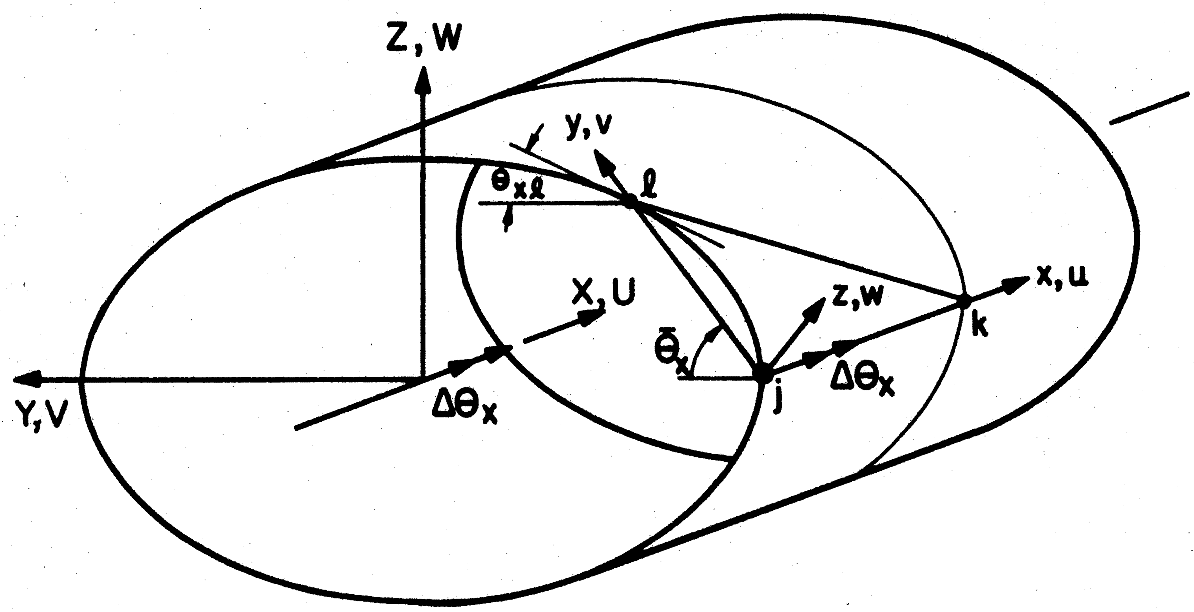

Figure 8. The Tube and a Finite Element in the Initial Configuration with Corresponding Deflection Directions

A "tangential stiffness" approach was used to analyze the anticipated non-linear load-deflection curve. The analysis used an incremental tangential stiffness to represent the stiffness of an element's degrees of freedom to the applied nodal loads. The degrees of freedom occur at the element corners (nodes) and are specified in Figure 9. The elemental matrices were assembled into a single "global" stiffness matrix which represents the incremental stiffness behavior of the entire structure as a set of coupled linear algebraic equations.

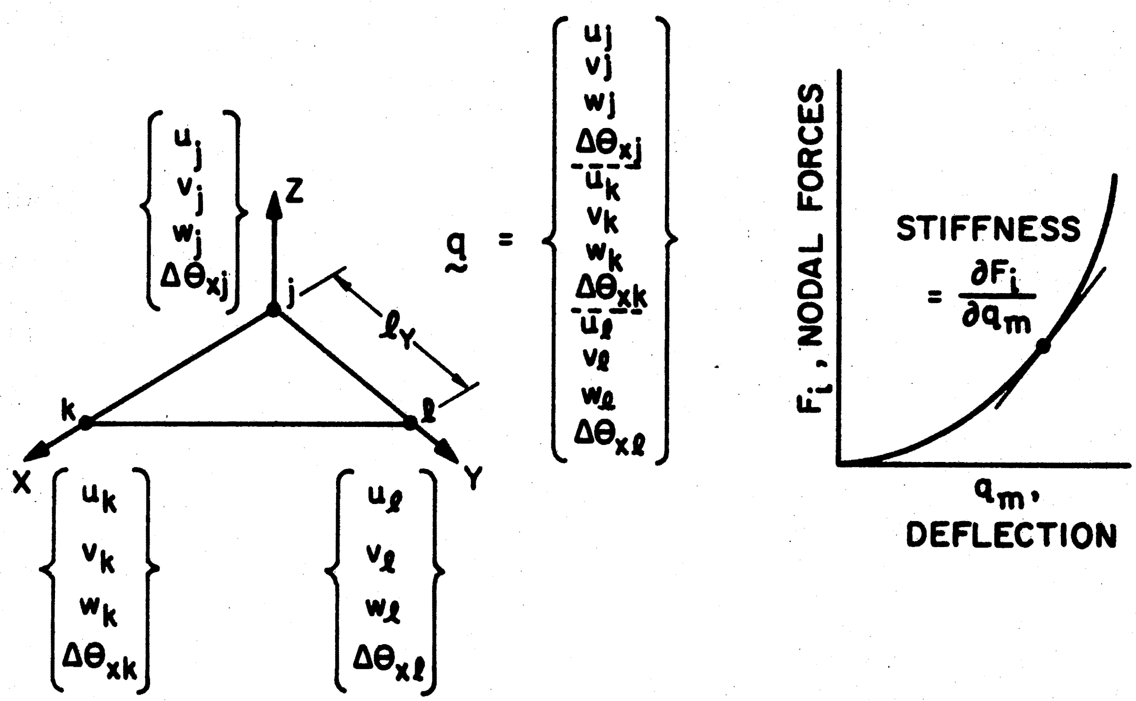

Figure 9. A Finite Element, the Deflection Vector, and the Load-Deflection Curve

The analysis was based on a set of shallow shell assumptions:

1. Due to the thinness of the shell, the displacements, expressed in local coordinates (u, v, w, $\Delta\theta_x$), were assumed independent of the coordinate normal to the initial local surface (z-direction). Thus, a complete first-order two-dimensional polynomial was used to represent the displacements.

$$u = a_1 + a_2x + a_3y \tag{3}$$

$$v = a_4 + a_5x + a_6y \tag{4}$$

$$w = a_7 + a_8x + a_9y \tag{5}$$

$$\Delta\theta_x = a_{10} + a_{11}x + a_{12}y \tag{6}$$

The incompatibility of the linear and rotational deflections was compensated by an intuitive geometric relationship. That is, in terms of the coordinates of the nodes

$$\bar{\theta} = (\theta_{XJo} + \Delta\theta_{XJ}) + (\theta_{XLo} + \Delta\theta_{XL}) \tag{7}$$

$$\sin\bar{\theta} = (Z_{Lo} + W_L) - (Z_{Jo} + W_J)\,/\ell_Y \tag{8}$$

Here, the finite element orientation, $\bar{\theta}$, shown in Figure 8, was treated as an average of the two hoopwise structural rotations at nodes j and ℓ. This geometric relationship was implemented through Lagrangian constraint of the displacements (see Appendix A). In other words, a Lagrangian constraint of the stiffness matrix was applied to enforce Equation 8 during all computed position increments.

2. The effects of initial curvature were slight and were disregarded. This "shallowness" assumption permitted the use of the large

deflection strain expressions sometimes called Green's Strain Tensor (25):

$$\varepsilon_x = \frac{\partial u}{\partial x} + \frac{1}{2}\left\{ \left(\frac{\partial u}{\partial x}\right)^2 + \left(\frac{\partial v}{\partial x}\right)^2 + \left(\frac{\partial w}{\partial x}\right)^2 \right\} \quad (9)$$

$$\varepsilon_y = \frac{\partial u}{\partial y} + \frac{1}{2}\left\{ \left(\frac{\partial u}{\partial y}\right)^2 + \left(\frac{\partial v}{\partial y}\right)^2 + \left(\frac{\partial w}{\partial y}\right)^2 \right\} \quad (10)$$

$$\gamma_{xy} = \frac{\partial u}{\partial y} + \frac{\partial v}{\partial x} + \frac{\partial u}{\partial x}\frac{\partial u}{\partial y} + \frac{\partial v}{\partial x}\frac{\partial v}{\partial y} + \frac{\partial w}{\partial x}\frac{\partial w}{\partial y} \quad (11)$$

3. Furthermore, the strain in the hoop direction, ε_H , was constrained in order to prevent the elements from carrying the load through hoopwise membrane compression. If membrane compression were to occur, then this would be characterized numerically by a singular stiffness matrix. However, this behavior is not observed physically and should not be allowed to occur numerically. Proper choice of local axes gave $\varepsilon_H = \varepsilon_Y$ so that a second constraint equation was introduced:

$$\varepsilon_y = 0 \quad (12)$$

4. A straight line normal to the initial surface remained straight and normal to the deflected surface. This assumption is very much like the Love-Kirchoff approximation where it is assumed that transverse shear strains (γ_{XZ}, γ_{YZ}) are negligible (26). Yet, in contrast, here the thickness was allowed to change.

5. A state of plane stress was assumed. A change in internal energy associated with the transverse normal strain, ε_Z , was zero since the transverse normal stress, σ_Z , was zero. This means that effects due to a change in thickness can be ignored in a state of plane stress. Furthermore, the assumption of a state of plane stress automatically gave a zero volume strain for Poisson's ratio of 0.5.

6. Out-of-plane distortion of the initial cross-section has negligible effect on the hoopwise

radius of curvature (RC). Thus, the change in hoopwise reciprocal curvature becomes

$$\kappa = \frac{\partial \Delta\theta_x}{\partial y} \tag{13}$$

In addition to these shell assumptions, the following boundary behavior assumption was adopted:

7. The effect of stretching the tube over the circular mountings on the initial stress-strain state of the tube was neglected. The mountings were assumed to be in the same shape as the undeformed cross-section of the tube.

The relationships above were interpreted on a Lagrangian frame of reference. That is, once the local axes were specified, they remained fixed and all displacements and strains were referred to the original axes positions.

Given these assumptions, a tangential global stiffness matrix $[K_T]$ was formulated, a task which is discussed in Appendix A. The applied loads were thus used to compute a step in incremental displacement. This, in turn, led to a new wall position and a corresponding new stiffness matrix. Essential to this stepping process was an evaluation of the applied loads. These applied loads were due to an imbalance of the force of hydrostatic collapsing pressure and the forces exerted by the flowing liquid.

The Fluid Mechanical Model

In the fluid mechanics analysis, the fluid volume was divided into a series of finite incremental regions separated by successive X = c planes. A schematic of the volume division is shown in Figure 10. Starting at the downstream end, the fluid pressure and velocity were calculated to satisfy a momentum and continuity balance for each successive region. When the inlet was reached, an estimate of the internal distribution of fluid variables was obtained.

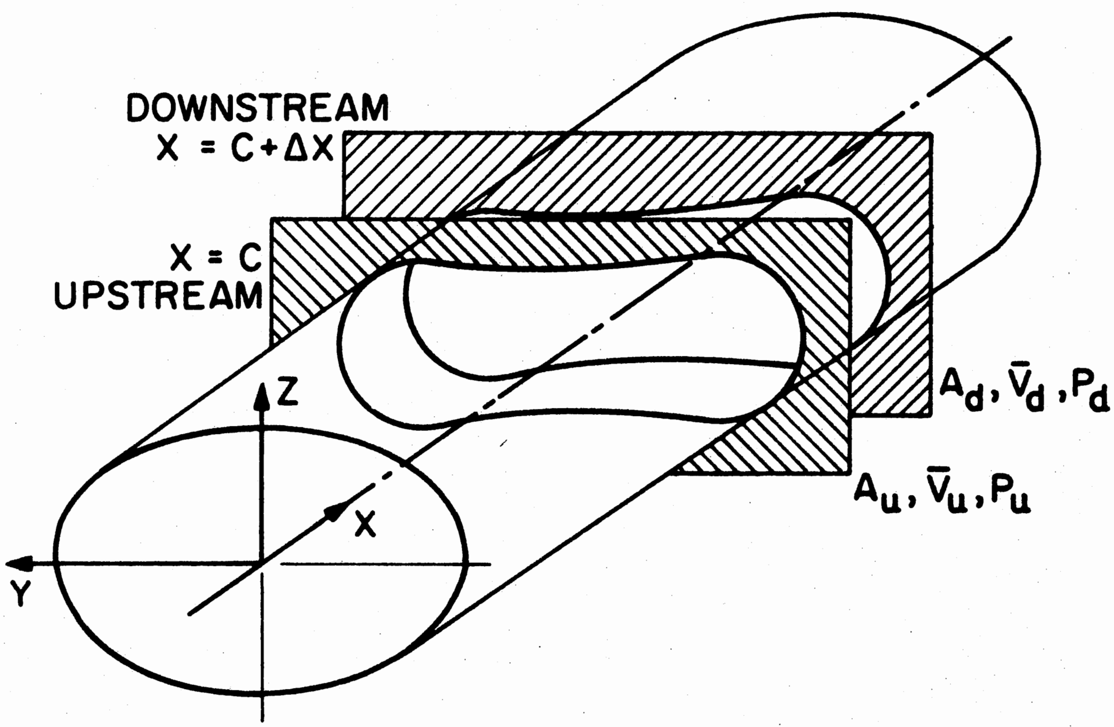

Figure 10. Division of the Fluid Volume into Finite Regions

The governing equations included mass continuity:

$$Q = A\bar{V} \tag{14}$$

where $\overline{V}$ is the continuity averaged axial fluid velocity, A is the tube cross-sectional area, and Q is the fluid volume flowrate. Equation 14 shows that, given the tube shape, the continuity averaged fluid velocity can be calculated at each location along the tube.

In addition, the integral form of momentum balance was satisfied over each region:

$$\frac{\partial}{\partial t} \int \rho \underset{\sim}{V} d\tau = -\int \underset{\sim}{V}(\rho \underset{\sim}{V} \cdot \hat{n}) dA + \int \underset{\sim}{f} dA - \int P\hat{n} dA \qquad (15)$$

In this approach, the fluid mechanics was assumed to be dominated by changes in the axial, X-direction. This allows simplification of the general momentum equation to

$$0 = \rho \overline{V}_u^{\,2} - \rho \overline{V}_d^{\,2} + P_u A_u - P_d A_d + \int_w f_X dA - \int_w P dA_X \qquad (16)$$

For this steady flow analysis, the time-derivative term has been discarded. The f_X integral term represents the contribution of the wall shear force. This term was estimated via a hydraulic diameter modification of the classic pipe Hagen-Poiseuille shear force calculation (27). That is,

$$\int_w f_X dA = 8\mu \overline{V}_d A_w / hd \qquad (17)$$

with the hydraulic diameter given by

$$hd = 4A_d / lp \qquad (18)$$

Here, $\overline{V}_d$ and A_d are downstream velocity and cross-sectional area which are used to include some account of taper, and lp is the wetted perimeter of the fluid region. Notice that since the hoop strains were constrained to be zero, lp is constant.

The procedural difficulty in evaluating Equation 16 entered in the integration of the pressure over the wall surface; that is, the difficulty entered in coupling the one-dimensional fluid model to the three-dimensional tube model. Here, the fluid pressure, P, was assumed to be a linear function of X within a given region. This linear relationship, in conjunction with Equation 16, forms two equations in the three unknowns, P_u, P_d, and axial rate of pressure change, m. Thus, the downstream pressure was assumed known, the last term in Equation 16 was numerically integrated, and the upstream pressure was calculated from a closed form of Equation 16. This technique was stepwise applied beginning at the outlet end of the tube and proceeding upstream until the inlet was reached in order to obtain an estimate for the axial fluid pressure distribution. These calculations were made by subroutine FLOW1D which is discussed in Appendix B.

Subsequent to the calculation of the fluid pressure exerted on the interior wall surface was the estimation of the loads on the tube. Here, it was assumed that the fluid pressure forces were dominant, so that fluid viscous forces on the tube could be neglected. The subroutine which calculates the external forces on the tube and reduces them to an equivalent set of nodal forces is called subroutine FORCES and is discussed in Appendix C.

Solution Algorithm

The solution began with the definition of an equilibrium index, Ψ,

$$\underset{\sim}{\Psi} = \underset{\sim}{F}_i - \underset{\sim}{F}_e \tag{19}$$

The internal forces, F_i, were related to the amount of strain the tube experienced and the elasticity of the tube material. The external forces, F_e, were calculated from the fluid hydrostatic and flow pressure loads.

Computing the first variation of Equation 19, with the external forces held constant, yields

$$d\underset{\sim}{\Psi} = [K_T]\, d\underset{\sim}{q} \tag{20}$$

The global tangential stiffness matrix $[K_T]$ represents the stiffness of the structure to an incremental change in position, dq. Conversely,

$$d\underset{\sim}{q} = [K_T]^{-1}\, d\underset{\sim}{\Psi} \tag{21}$$

was used to calculate an incremental change in position due to a small change in load, $d\Psi$. Thus, at computational step n, $d\Psi = \Psi^{N+1} - \Psi^{N}$. In addition, $\Psi^{N+1} = 0$ was used to guide the solution toward equilibrium. Then,

$$d\underset{\sim}{q}^{n} = -[K_T]^{-1}\,\underset{\sim}{\Psi}^{n} \qquad (22)$$

was used to compute an incremental correction to the position. Here, the stiffness matrix $[K_T]$ was augmented to account for the two constraint equations previously introduced (see Appendix A):

$$\begin{Bmatrix} d\underset{\sim}{q}^{n} \\ \underset{\sim}{\lambda}^{n} \end{Bmatrix} = - \begin{bmatrix} [K_T]^{n} & [CC]^{T\,n} \\ [CC]^{n} & [0] \end{bmatrix}^{-1} \begin{Bmatrix} \underset{\sim}{\Psi}^{n} \\ \underset{\sim}{0} \end{Bmatrix} \qquad (23)$$

where $[CC]$ is a matrix of the constraint coefficients and $\underset{\sim}{\lambda}$ is the Lagrange multipliers. Subroutine STEP applied the boundary conditions, computed the inversion of the augmented stiffness matrix, and tested for convergence based, in part, on the smallness of the correctional step, dq . The details of subroutine STEP are discussed in Appendix D.

It is now possible to establish the algorithm flowchart as in Figure 11. Two subroutines are shown which have not been previously discussed, INIT and MESH. Subroutine INIT was the solution initializer which defined the finite elements as well as various constants (Appendix E). MESH defined the global cartesian mesh contained in the interior volume of the tube plus rigid supports (Appendix F).

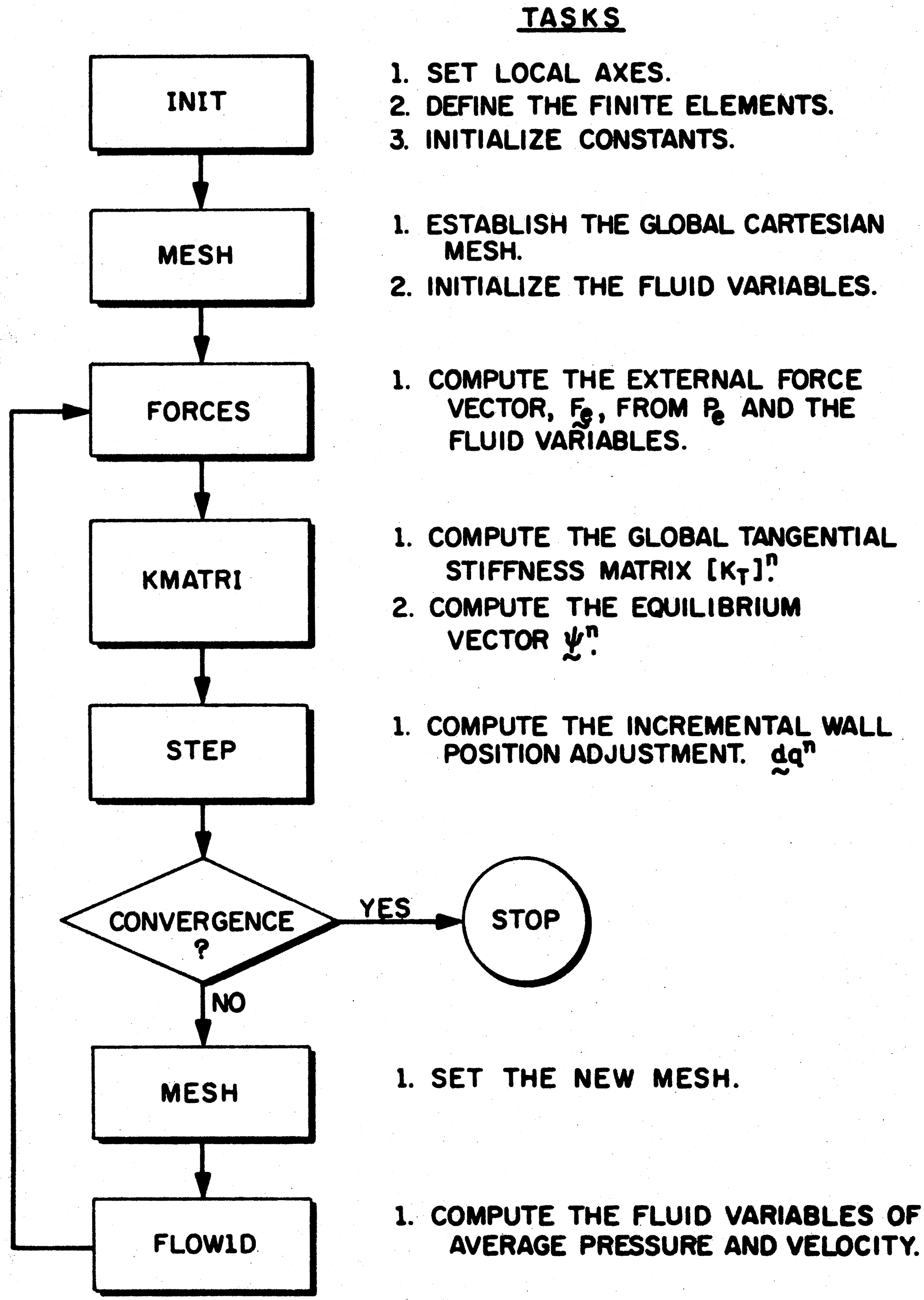

Figure 11. The Algorithm Flowchart

The solution algorithm used a modified Newton-Raphson technique which followed the path shown in Figure 12. Although the figure only shows the path for a single degree of freedom, it is indicative of the overall process. The first step 1-2 is a simple inversion of the stiffness matrix with scaling of the step to ensure its smallness. The step must not be allowed to become excessive, otherwise the assumption of constant external force during a step may lead to a non-physical solution. Nevertheless, due to non-linearity, the internal stresses may not produce the expected value of Ψ at step 2. Thus the true Ψ occurs at point 3. Subsequently, the tangential stiffness is recomputed and another step is taken from 3-4. This process is continued until convergence at step 6 is achieved.

The apparent $\Psi=0$ point changed on each step as shown in Figure 12. This occurred since the pressure loads created a changing nodal force vector for the elements as they changed orientation. This presented no problem as long as the step size was kept small.

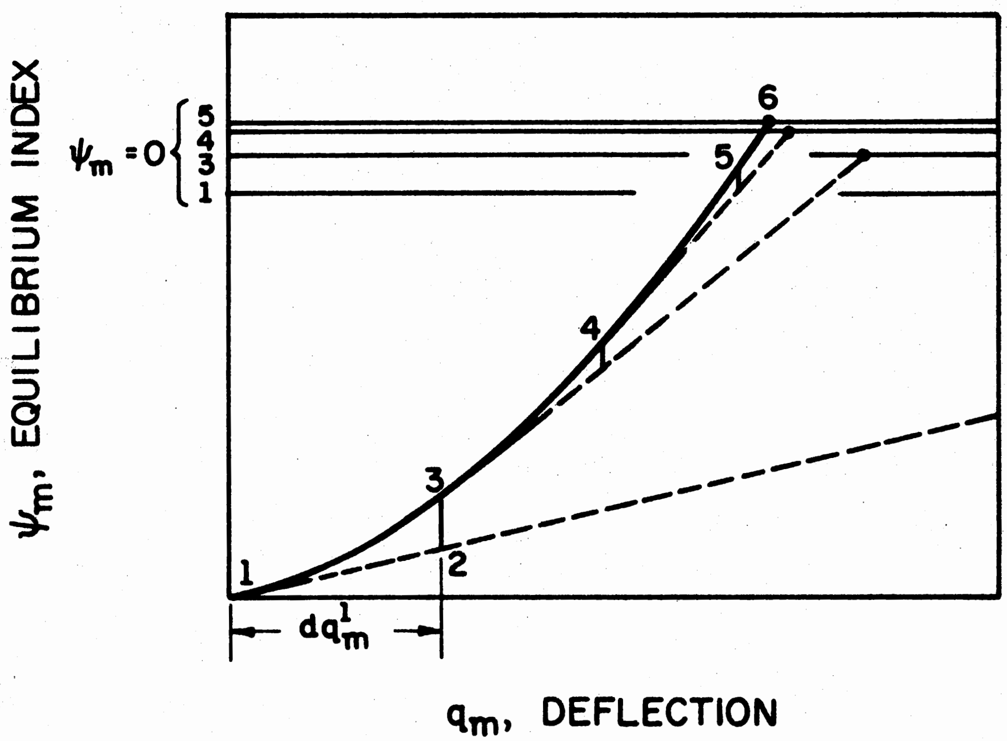

Figure 12. The Solution Path on a Load-Deflection Plot

CHAPTER IV

RESULTS AND DISCUSSION

In this chapter, the experimental and analytical fluid pressure-flowrate characteristic of a collapsible tube is presented. The role of pretension was investigated as well as the demarcation of the oscillatory regime and the definition of the axial pressure distribution. The reference height for the measurement of all pressures was the axis of the collapsible tube.

Experimental Results

The Pressure Drop-Flowrate Characteristic

Figure 13 shows the experimental characteristic fluid pressure response to tube collapse due to flowrate and collapsing pressure variation. The downstream pressure, P_2, was held at 3.10 in H_2O. Each curve represents a different value of collapsing pressure, P_e. The prestrain was set at about 1%. Imprecision of the prestrain occurred due to the difficulty of achieving a uniform mounting of the tube on the experimental apparatus.

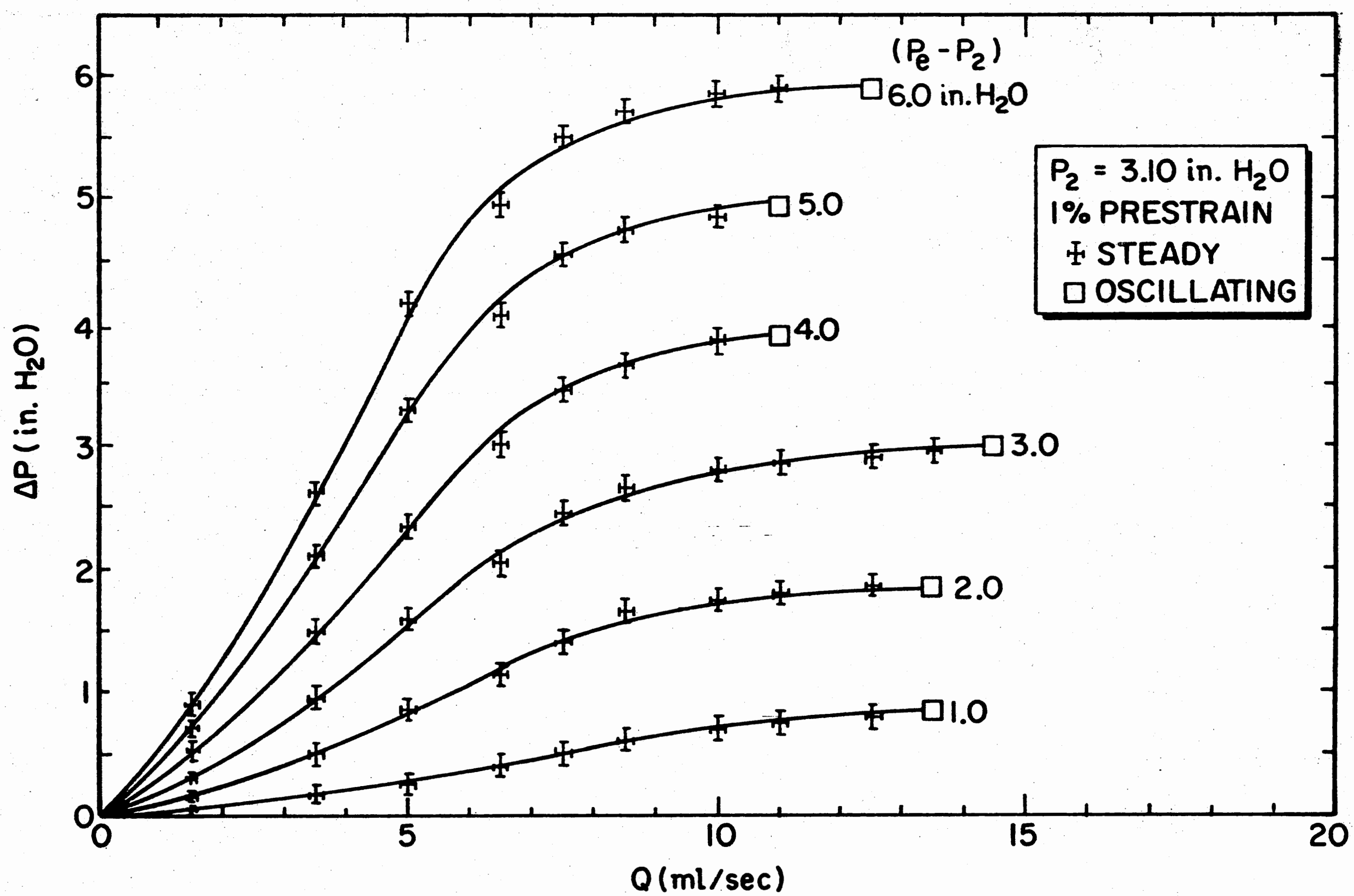

Figure 13. The Experimental Steady Flow Pressure Drop-Flowrate Characteristic of a Collapsible Tube

Qualitatively, the tube characteristic response was similar to that presented by Brower and Noordergraaf (Figure 4), but differences in tube length and pretension exclude a rigorous comparison to their experimental data. The fluid mechanics underlying Figure 13 are perhaps best described by observing the dependent inlet section pressure response, P_1, as flowrate was increased with constant P_e:

1. At extremely low flowrate (less than 3 ml/sec) two side channels were created and the tube was in a state of extreme collapse (I in Figure 3). Due to the low flowrate, however, the fluid forces were small and, consequently, the upstream pressure was small at all values of collapsing pressure.

2. At moderate flowrates (3-9 ml/sec), the tube began to open due to increasing upstream pressure. This increase in upstream pressure was due to the increase in fluid viscous forces which accompanied the increased flowrate. Now the tube appeared to be mostly open at the upstream end and closed, or collapsed, at middle and downstream locations.

3. As the flowrate was increased still further (greater than 9 ml/sec), the upstream pressure approached the collapsing pressure in magnitude. At these flowrates, the tube shape took on the character described by previous investigators as "pinched" (12,16). That is, a small but complete collapse dimple was formed at the downstream end.

4. At some critical value of flowrate, the tube and flow began to oscillate. These data points have been given an identifying symbol in Figure 13. The tube wall oscillation might be best characterized as a large amplitude (of the magnitude of the tube radius) and low frequency (1-2 Hz) oscillation.

Effect of Pretension

Figure 14 shows the effect of pretension on the flow characteristic at three levels of collapsing pressure.

The high level of collapsing pressure (P_e - P_2 = 6.0 in H_2O) shows only a slight response to pretension. Here, flowrates less than 7 ml/sec provided a slightly increased upstream pressure, otherwise the characteristic was affected very little.

The moderate level of collapsing pressure (P_e - P_2 = 4.0 in H_2O) shows a uniformly lower upstream pressure. This response was attributed to the increased tension associated with high prestrain holding the tube more open. Thus, the fluid channel was widened so that the fluid forces were reduced, as was the upstream pressure.

At the low collapsing pressure (P_e - P_2 = 2.0 in H_2O), the effect of pretension was most pronounced: All flowrates produced a smaller upstream pressure.

Table II shows the effect of pretension on the oscillation onset. The flowrate values which are shown were the first at which oscillation was observed, all other conditions held constant. No overall pattern emerged from this data. Nevertheless, two points are of interest:

1. At a very low collapsing pressure (P_e - P_2 = 1.0 in H_2O) and a high prestrain, contact of opposite walls did not occur. Neither did oscillation. The occurrence of this case suggests that oscillation and collapse with contact of opposite walls are closely related.

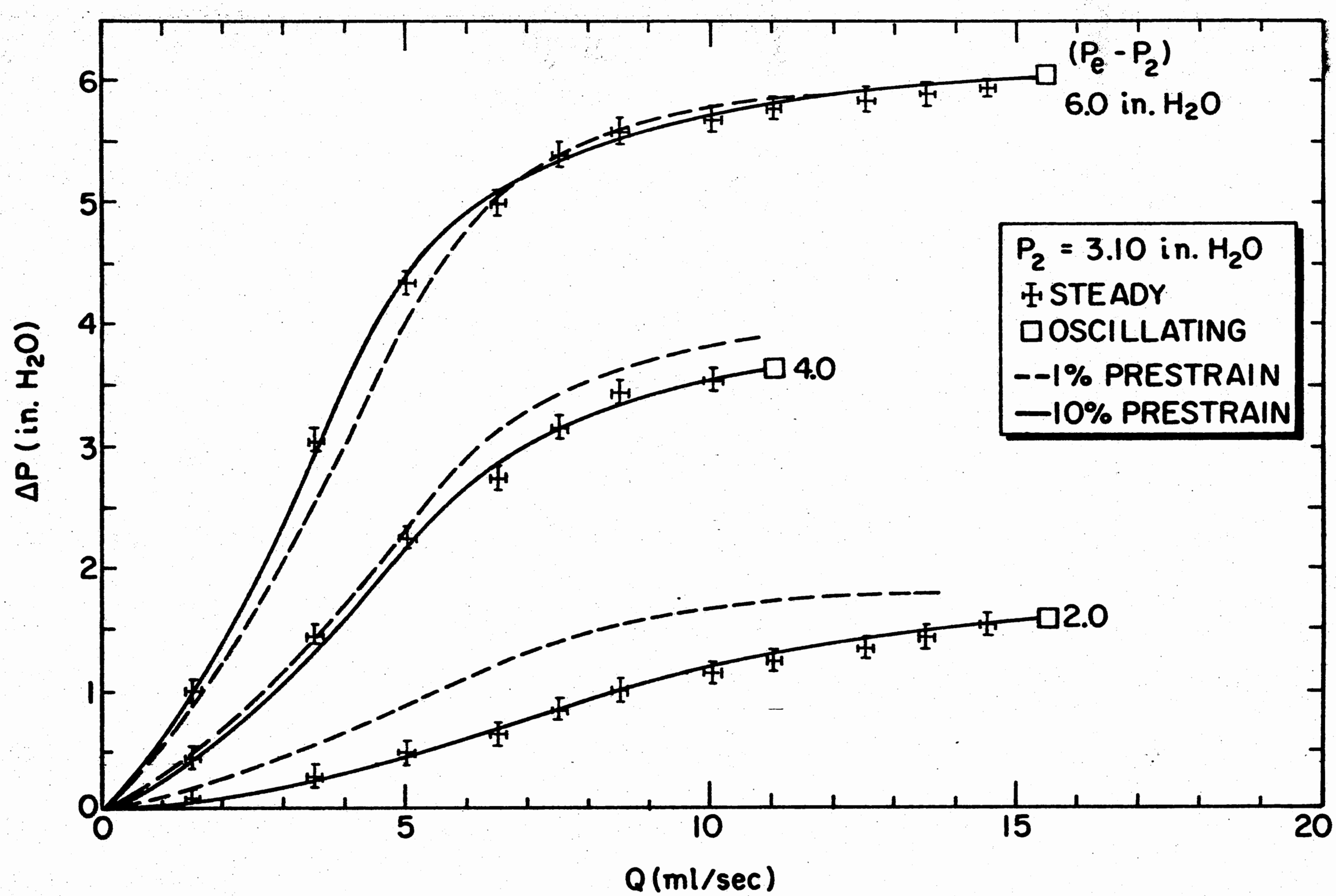

Figure 14. The Effect of Pretension on the Experimental Characteristic of a Collapsible Tube

2. With a high prestrain and a high collapsing pressure ($P_e - P_2 = 6.0$ in H_2O), a very high frequency, low amplitude (radius/10) oscillation began at about 15.5 ml/sec. This high frequency oscillation persisted until the flowrate reached 23.5 ml/sec when the large amplitude oscillation began as in other cases.

TABLE II

FLOWRATE (ML/SEC) AT ONSET OF OSCILLATION

$(P_e - P_2)$ (in. Water)	1% Prestrain	10% Prestrain
6.0	11.5	15.5/23.5
5.0	11.0	12.5
4.0	11.0	11.0
3.0	14.5	10.0
2.0	13.5	15.5
1.0	13.5	none

(Downstream pressure = 3.10 in H_2O)

Axial Pressure Distribution

The four figures which follow show the axial distribution of fluid pressure as measured by the tube wall taps, and the corresponding shape assumed by the collapsed tube. In all cases, the flow direction was left-to-right.

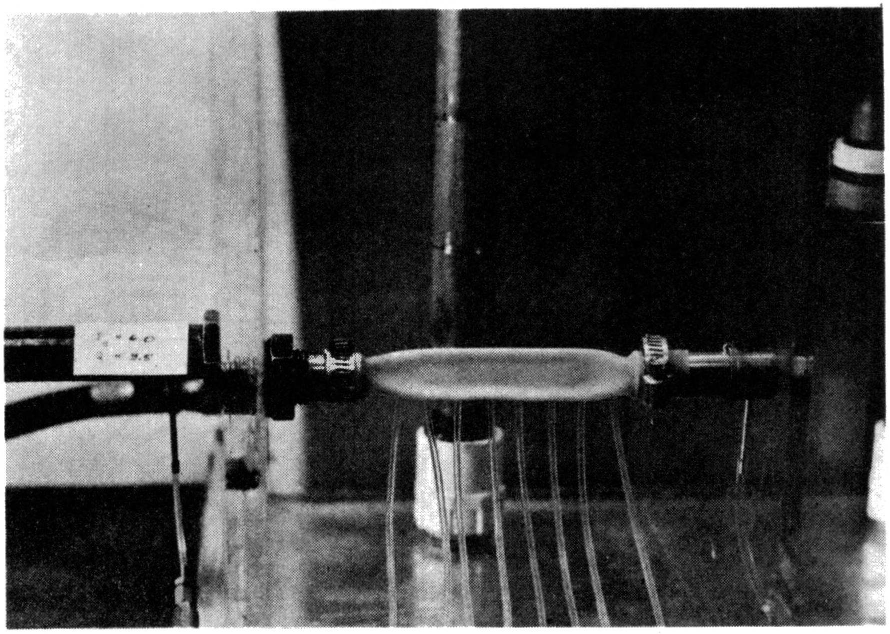

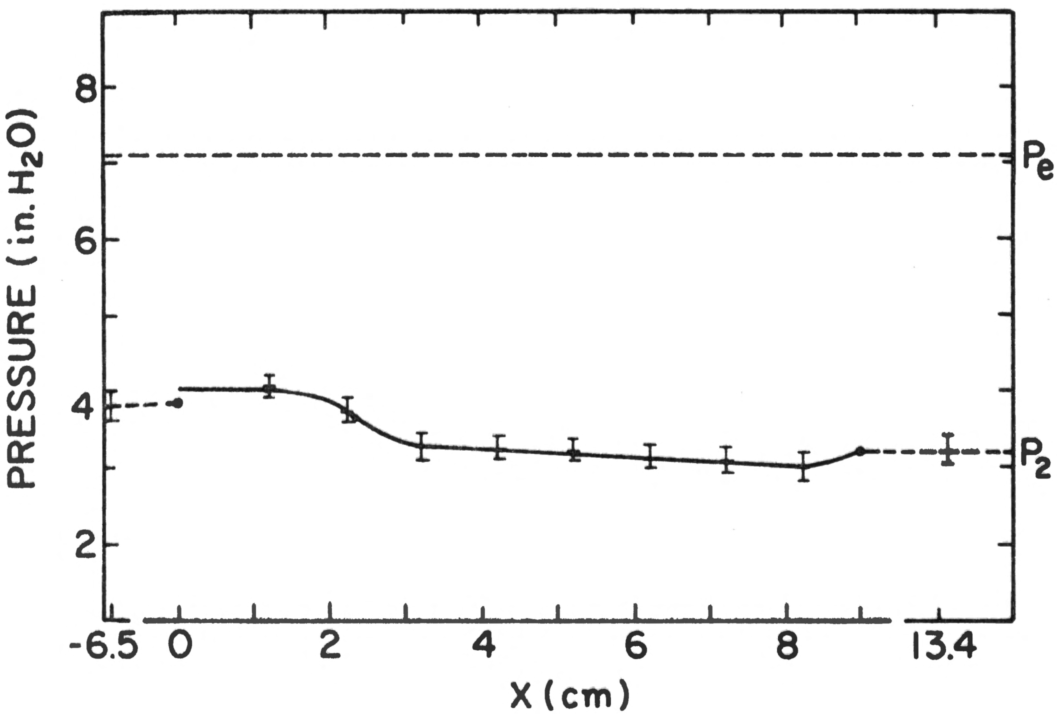

Figure 15. Photograph of Tube Shape and the Corresponding Fluid Wall Pressure Distribution at 3.5 ml/sec

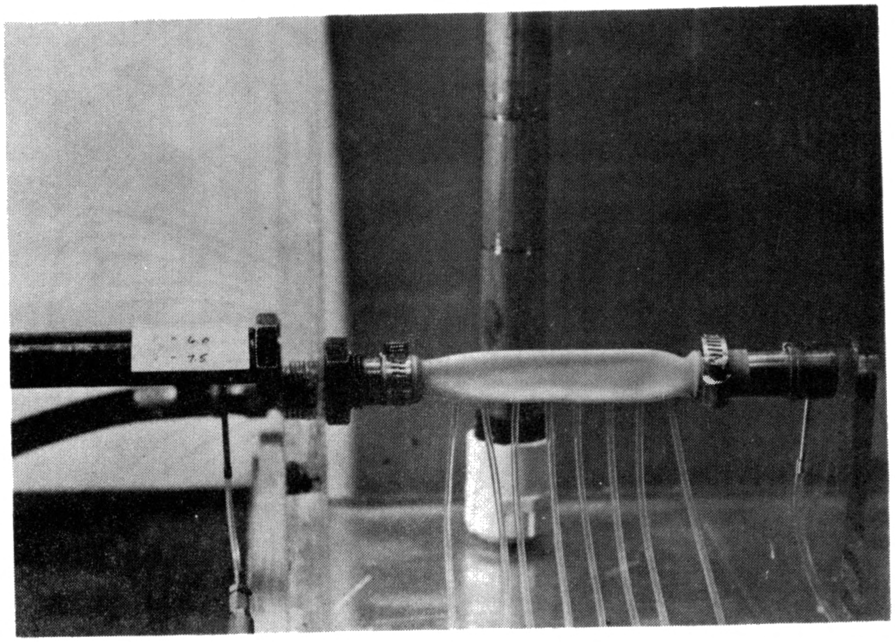

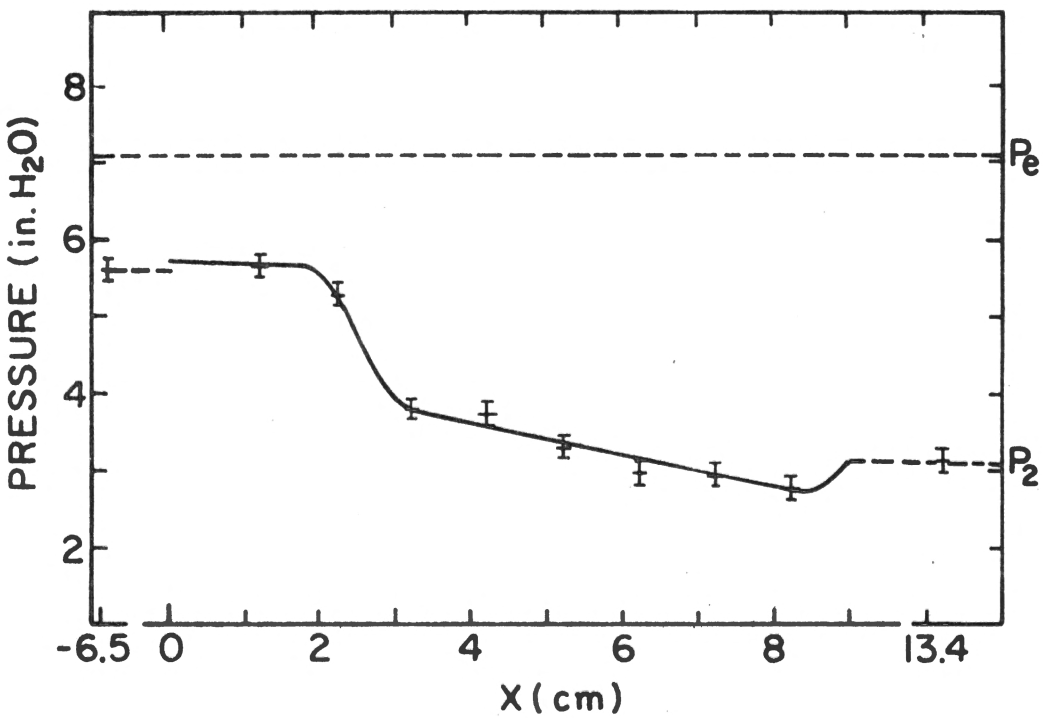

Figure 16. Photograph of Tube Shape and the Corresponding Fluid Wall Pressure Distribution at 7.5 ml/sec

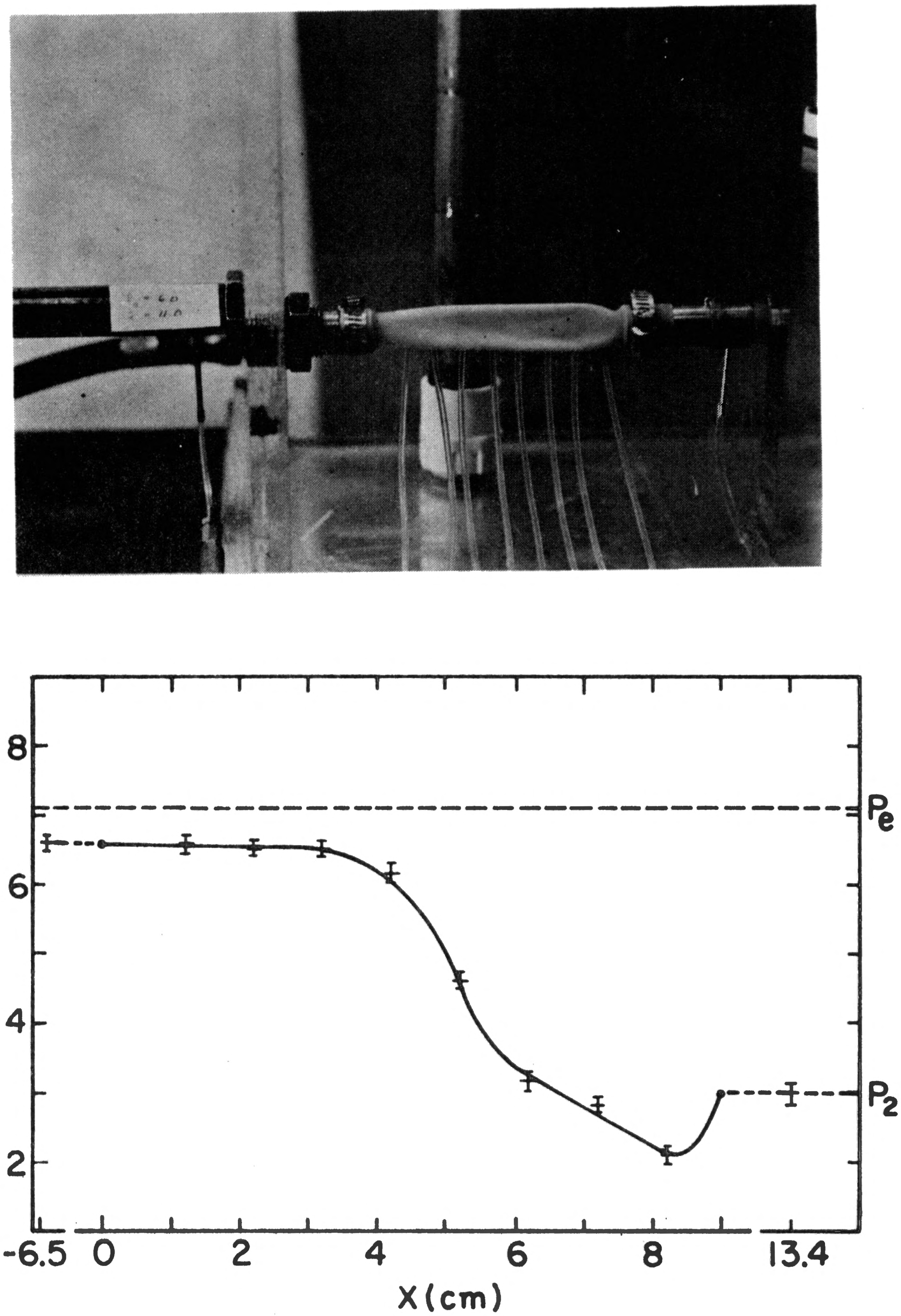

Figure 17. Photograph of Tube Shape and the Corresponding Fluid Wall Pressure Distribution at 11.0 ml/sec

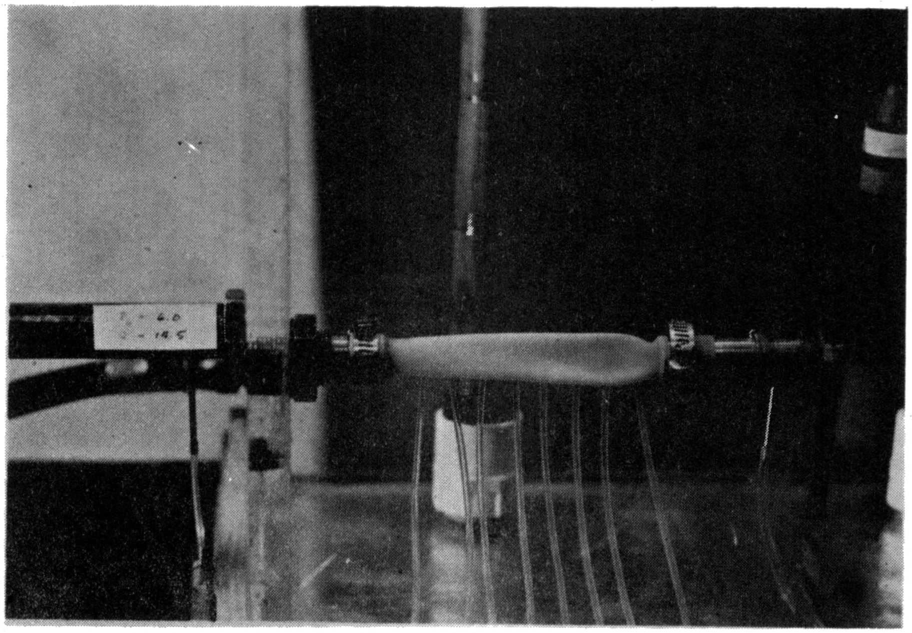

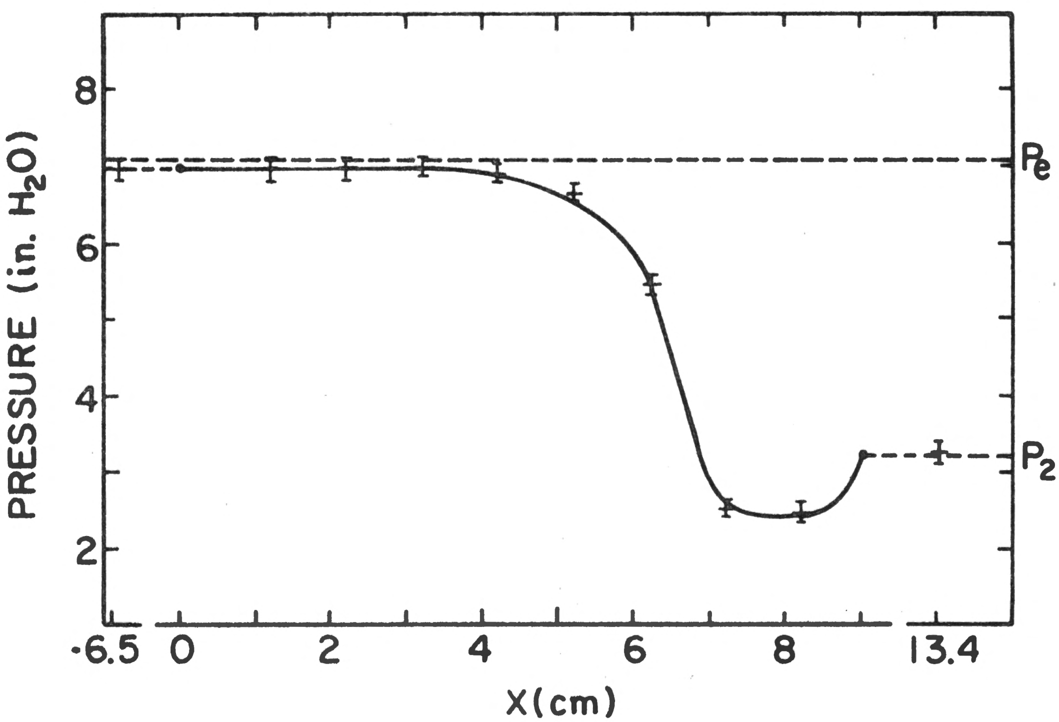

Figure 18. Photograph of Tube Shape and the Corresponding Fluid Wall Pressure Distribution at 14.5 ml/sec

The prestrain was set at the low value. The intent was to demonstrate the development of the axial pressure distribution as the flowrate was increased. Consequently, the collapsing pressure was held constant, ($P_e - P_2 = 4.0$ in H_2O), as was the downstream pressure (3.10 in H_2O), while the flowrate was increased and the fluid wall pressure measured for each successive case. In all cases, contact of opposite walls was indicated by the flat area down the center of the tube. The pressure distribution demonstrates the interplay of the two major opposing fluid reactions: An upstream pressure rise due to viscous effects, and a downstream static pressure drop due to a venturi effect.

In the final figure of the series, Figure 18, the tube has assumed the "pinched off" shape described by previous investigators (12,16). Complete collapse was confined to a small region in the downstream end of the tube. The interior fluid pressure was very nearly equal to the collapsing pressure over the entire upstream half of the tube. At this high flowrate, oscillation was imminent.

It was observed that a slight increase in flowrate above that in Figure 18 caused the tube to open completely due to the further increase in upstream pressure. This opening motion caused an increase in the cross-sectional area at the constriction with large reduction in viscous effects. Subsequently, the loss of viscous effects made the interior distending pressure less than the exterior collapsing pressure, which encouraged recollapse of the tube. The cycle was completed when recollapse caused a rise in upstream pressure. In this scheme, the limits of the cycle were determined by the tube machanics. That is, the opening motion was limited by the increase in stiffness associated with the fully inflated tube cross-section, while the closing motion was limited by contact of opposite tube walls.

Analytical Results

In the remaining portion of this chapter the computational results are examined. These results are separated into two groups: a high pressure group with collapsing pressure greater than 6.5 in H_2O, and a low pressure group with collapsing pressure less than 6.5 in H_2O. This approach was adopted for three reasons: First, for clarity of presentation; second, since the low collapsing pressures are more likely to occur in the physiology, more attention was focused on them; and lastly, less computational data was generated for the high pressure group since it was extremely expensive to do so. This last consideration was a concession to the finite size of both the computing storage capacity and the project budget.

Configurations and Cost

Nonlinear finite element methods have been traditionally recognized as being computationally time consuming (25,29,30). This occurs partly because the stiffness matrix is dependent on position and, therefore, must be reformulated on each computational step, and partly because of the inversion cost of the large stiffness matrix. In the present study, the introduction of constraint equations created an augmented stiffness matrix which no longer possessed the banded matrix structure of the stiffness matrix alone. This presented an even greater computational burden on the stiffness matrix storage and inversion techniques. In addition, the routines in this study were written for understanding and debugging versatility, rather than program efficiency. However, as a concession to optimization, an optimizing compiler (FORTRAN, level G compiler) was used. Nevertheless, accurate solutions were obtained at high cost.

At the outset of the computation, it was assumed that seven equidistant circumferential nodes would be adequate to predict hoopwise bending effects. It was felt that fewer nodes would be inadequate to accurately predict the extreme collapsed condition and more nodes would be wasteful. In accordance with this assumption, only the fineness of the tube lengthwise subdivision was varied in order to study convergence. Two axes of symmetry were used to minimize computations.

Figure 19 shows a coarse finite element arrangement. Here, 48 elements were used to predict wall position; the arrangement was denoted M48. Similarly, M72 was a configuration with 72 elements. Both configurations had six equal hoopwise increments.

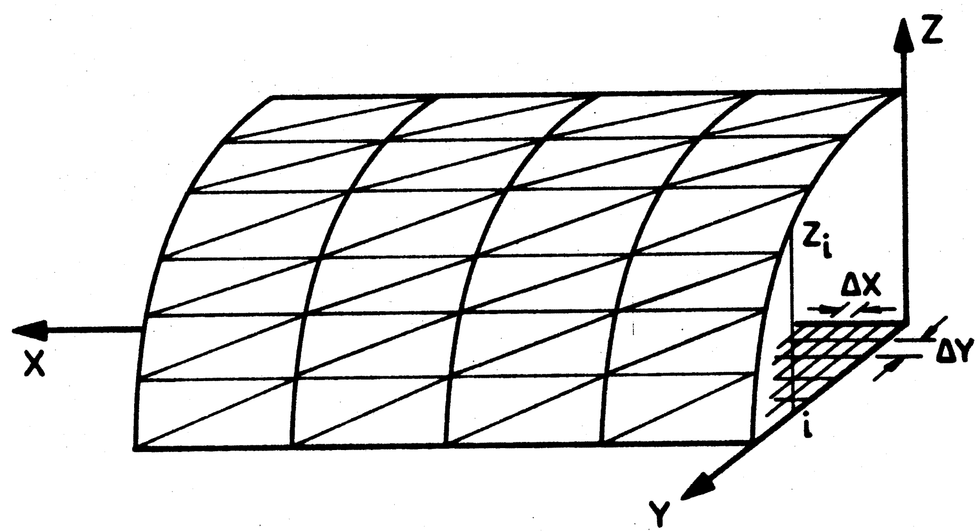

Figure 19. The M48 Finite-Element Configuration with Underlying Grid

Table III shows a comparison of the computational requirements of the two element densities for an IBM 370/158 digital computer. The larger stiffness matrix was acompanied by a twofold increase in storage and a nearly threefold increase in the execution time. Fortunately, these increased costs were offset somewhat by an increase in accuracy.

TABLE III

ELEMENT DENSITY VERSUS COMPUTATIONAL PARAMETERS

	Single Step Execution Time	Augmented Stiffness Matrix Storage Requirement Upper 1/2 Only--Double Precision Words
M48	26.7 sec	13k
M72	1 min 8.4 sec	27k

Prediction and Measurement Comparison

Figure 20 shows the experimental and predicted inlet pressure for low axial tube prestrain. The experimental and analytical cases had the outlet pressure, P_2, constant at 3.10 in H_2O. The 48-element distribution was used to predict P_1 at all the experimental values of collapsing pressure shown. The maximum error for the M48 pressure predictions was about 13% of the measured value at the same flowrate (e.g., Equation 2), and it occurred at the mid-range of collapsing pressure and flowrate of the points examined. The maximum M72 error in predicted pressures was about 9% compared to measured pressures at the same flowrate. Predicted pressures tended to be high at the low flowrates and low at the high flowrates. The improvement in accuracy shown by the M72 predicted pressure at high

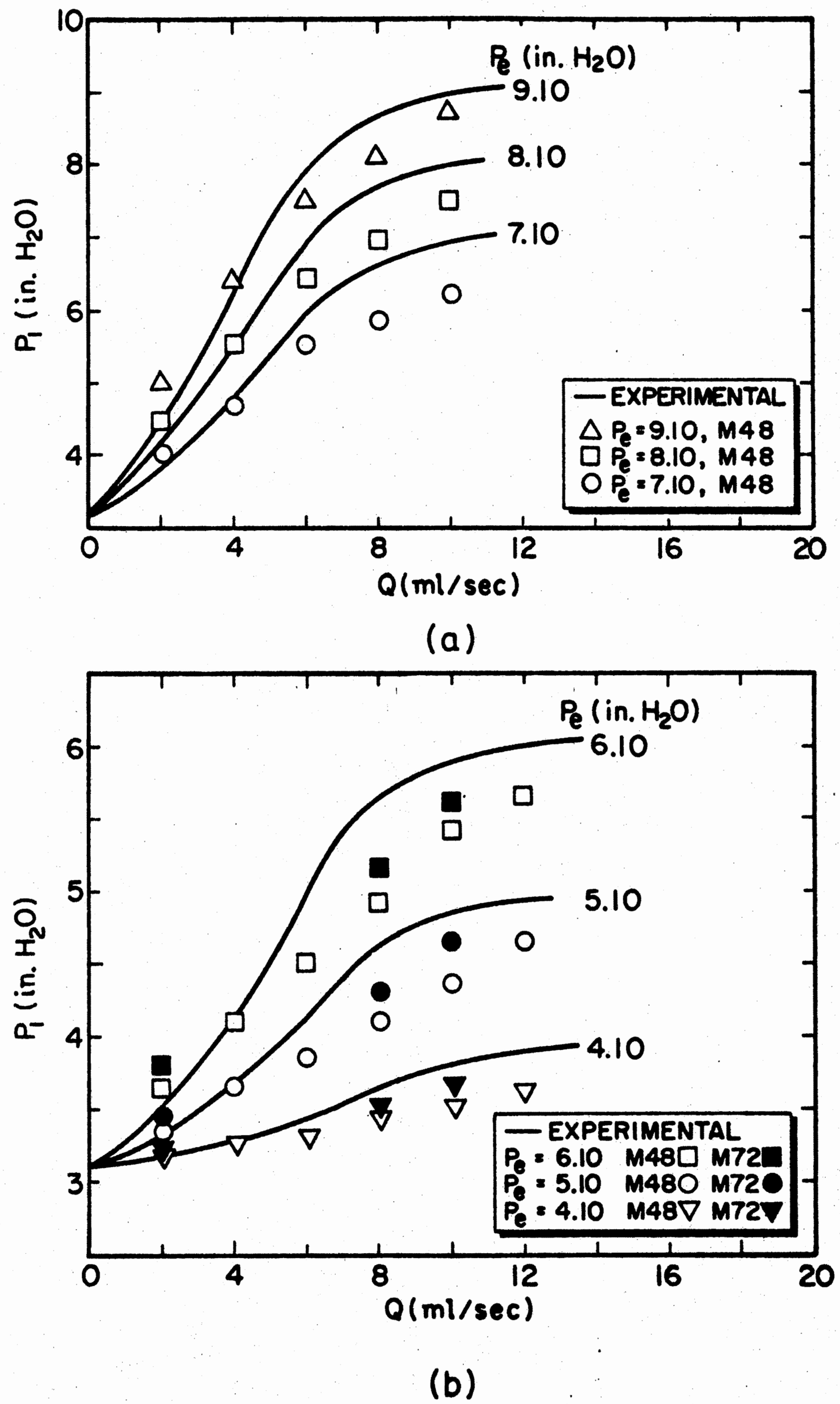

Figure 20. Prediction of the Characteristic at Low Tube Axial Prestrain with P_2 = 3.10 in H_2O (a) High Collapsing Pressures, (b) Low Collapsing Pressures

flowrates occurred due to an increase in structural flexibility associated with the greater element density. That is, the increase in element density gave rise to a decrease in predicted structural stiffness. This decrease in stiffness resulted in a decrease of cross-sectional area and a corresponding rise in upstream pressure through increased viscous forces. This effect was demonstrated at all flowrates examined.

Figure 21 shows the correlation between predicted and measured inlet pressure for the high prestrain case. Here, the M48 values demonstrated much larger errors in predicted pressures than the M72 results (24% maximum error versus 8% maximum error). This further suggests that the improvement in accuracy of the M72 configuration was due, in part, to the ability of the 72-element model to accurately predict the membrane forces since these had more effect on displacement in the high prestrain case.

Two important shortcomings of the model are evidenced in Figure 22. First, an excessive fluid pressure minimum was predicted. This suggests that the fluid viscous forces were somewhat under-estimated, while the wall structural model appeared to be overly flexible. Compared to the physical case, this combination would lead to a smaller cross-sectional area at collapse and a corresponding higher fluid velocity at the minimum cross-section. Thus, the fluid inertial effects would assume too important a role and cause the excessive pressure depression which was predicted. Secondly, the predicted pressure minimum was located upstream of the minimum in the experimental data. Comparison between predicted and observed tube shapes showed that the predicted wall shape had a tendency to form a minimum in area which was too close to the mid-line (x = 4.5 cm) of the tube. This would cause the predicted pressure minimum to occur further upstream than was observed experimentally. Nevertheless, care must be exercised in these comparisons. The fluid flow in the inlet and outlet regions to the collapsed portion of the tube was three-dimensional. Thus, comparison of measured wall pressure data to predictions from a one-dimensional fluid model may be suspect.

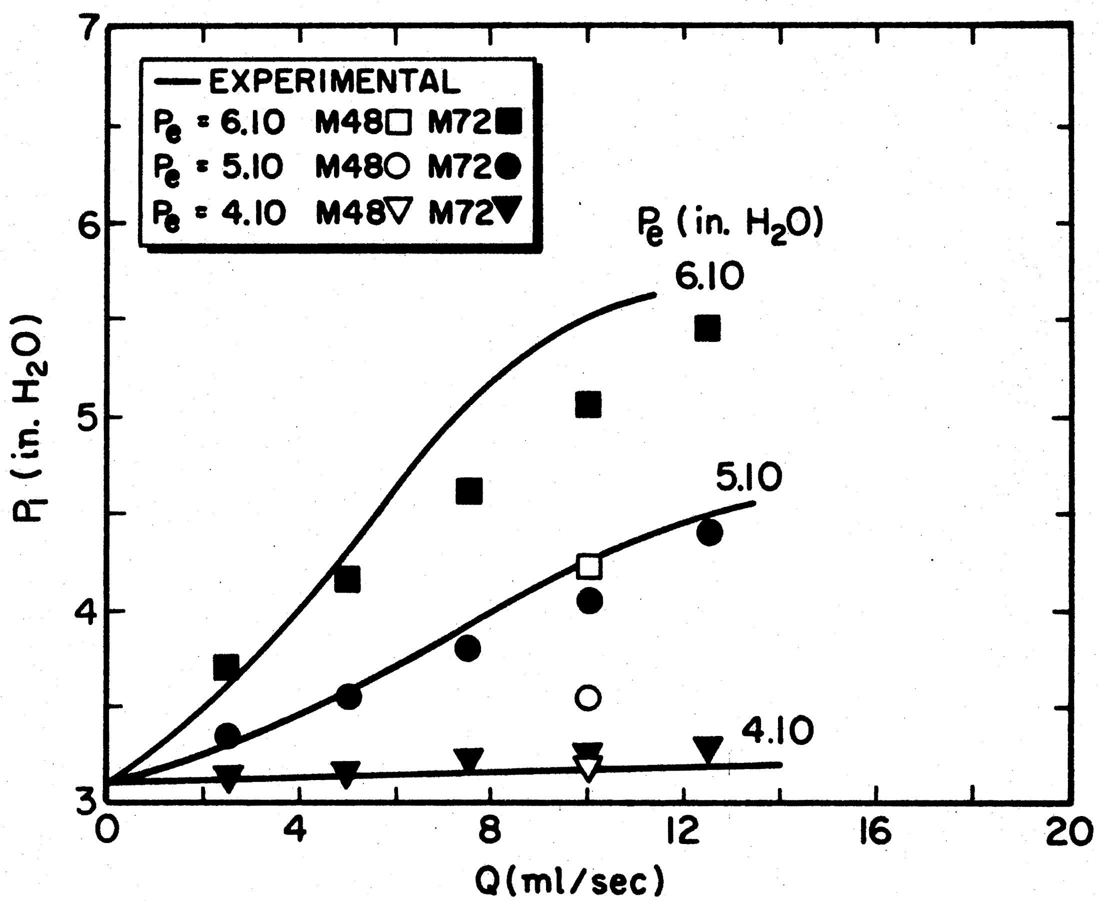

Figure 21. Prediction of the Characteristic at High Prestrain and Low Collapsing Pressure with P_2 = 3.10 in H_2O

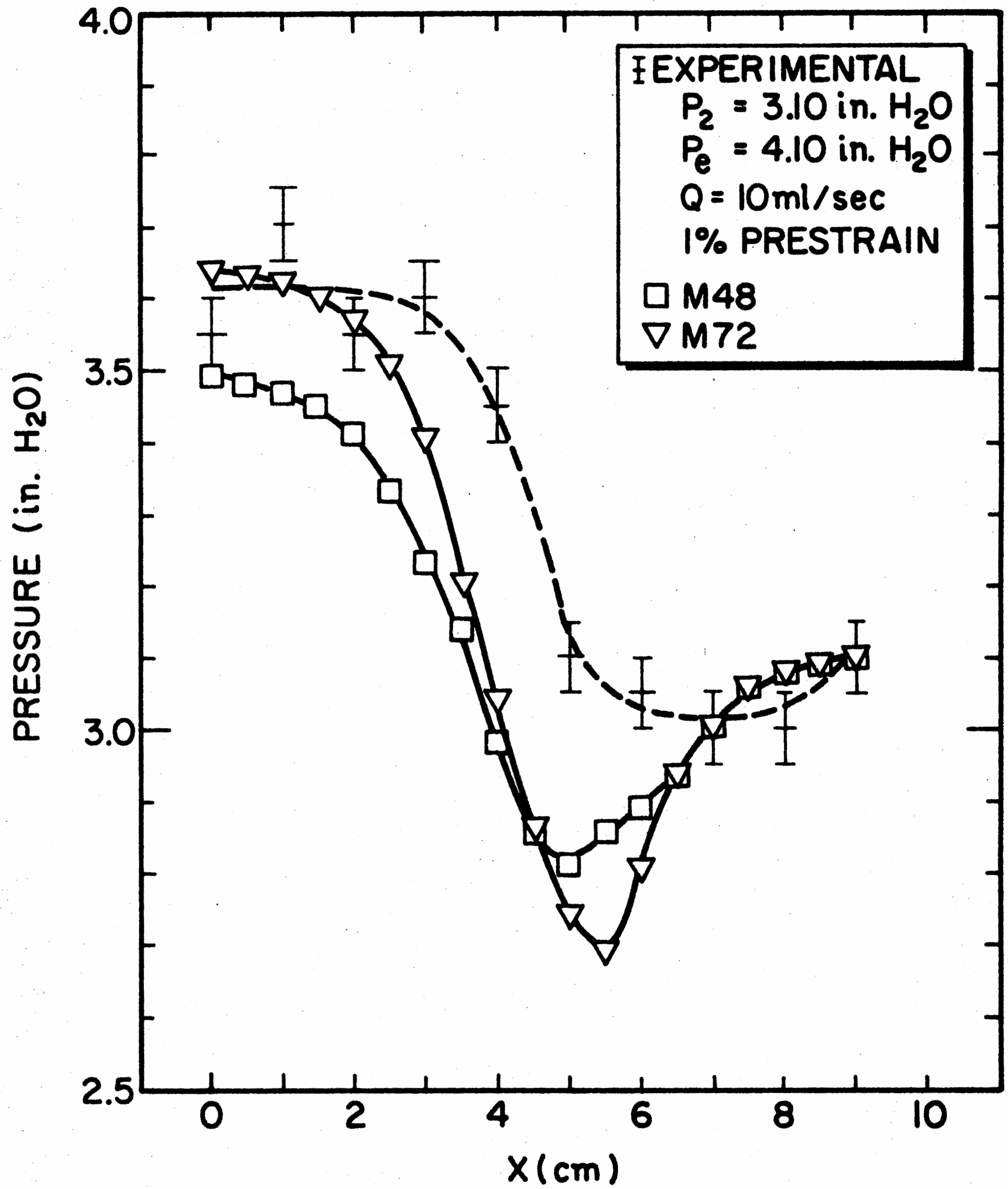

Figure 22. Measured and Predicted Axial Distribution of Fluid Pressure

CHAPTER V

SUMMARY AND RECOMMENDATIONS

The goal of this study was to measure and predict the steady-state pressure drop-flowrate characteristic of a collapsible tube. Previous investigators have emphasized the need for an analysis which is constructed solely upon basic physical principles. The present study was intended to fill this need.

Experimental data was presented in order to clarify and augment previously presented results. New pressure drop-flowrate data was presented which shows the importance of tube axial pretension, particularly in cases of low collapsing pressure. The data also shows that tube/fluid oscillation occurs at sufficiently high flowrates independently of interacting circuit elements. Another set of new data was presented which showed the fluid wall static pressure distribution as a function of flowrate. These measurements raise the question of the suitability of using fluid wall static pressure measurements to validate a one-dimensional fluid model in the present case. More sophisticated fluid experiments need to be conducted to answer this question.

A finite element structural model of the tube was presented which balanced axial membrane stresses plus hoopwise bending stresses against the applied fluid pressure loads. The finite element tube wall approximation was coupled to a one-dimensional fluid model in order to predict the tube inlet fluid pressure as a function of tube collapsing pressure and fluid flowrate.

Analytical results showed that the approach yielded considerable improvement in accuracy over that demonstrated by other methods. Previous investigators have complained of errors in predicted fluid pressure as large as 56% of measured values at the same flowrate. In the present study, at low pretension, the <u>maximum error</u> in predicted pressure was near 13% of measured values with a coarse finite element array, and near 9% with a fine element array. With a high pretension, the maximum error was 24% with the coarse array and 8% with the fine array. This improvement in accuracy can be attributed to an analytical foundation in first physical principles.

In general, the analytical predictions agree reasonably well with the experimental data, yet a consistent error pattern emerged. The predictions were too high at low flowrates and too low at high flowrates. A variation in finite element size did not alter this pattern. The error pattern was attributed to an incorrectly flexing model and possibly an underestimation of fluid viscous forces.

Consequently, the first priority for further work on these methods should be to include a more complete state of bending while retaining the one-dimensional fluid mechanics. A review of the results of such a study should indicate the necessity for attempting a more detailed two- or three-dimensional fluid mechanical analysis.

As Brower and Noordergraaf (11) have demonstrated, the predicted fluid flow characteristic can be used to evaluate circuit performance where a section of collapsible tubing is present. The characteristic in the present study had fluid flowrate forcing, but an important companion case has pressure forcing of the fluid through the tube (Figure 2a). In order to predict general circuit performance it is required to be able to predict both the pressure and flowrate forced characteristics. Consequently, a worthwhile goal of subsequent research would be to extend the techniques presented here to include the case of pressure forcing of the fluid.

The analysis methods of this study are applicable to engineering design as well as physiologic analysis of collapsible tube flows. Engineering devices which function as resistors, oscillators, amplifiers, and switches have been discussed. In addition to these, a collapsible tube may provide a useful means of signal interfacing; for example, between hydraulic and pneumatic circuitry. This is, after all, the role that the veins in the thorax appear to play during positive pressure lung ventilation. The analytical difficulty associated with physiologic collapsed tube flows appears to be primarily due to complications in the tube mechanics. Thus, the power of the finite element method of analysis used in this study becomes important. In fact, the finite element method can model the complex tube materials and environments which are often encountered in the physiology.

BIBLIOGRAPHY

(1) Guyton, A. C., Abernathy, B., Langston, J. B., Kaufmann, B. K., and Fairchild, H. M. "Relative Importance of Venous and Arterial Resistances in Controlling Venous Return and Cardiac Output." American Journal of Physiology, 196 (1959), 1008-1014.

(2) Bayliss, W. M. and Hill, L. "On Intracranial Pressure and Cerebral Circulation." Journal of Physiology (London), 18 (1895), 334-362.

(3) Knowlton, F. P. and Starling, E. H. "The Influence of Variations in Temperature and Blood Pressure on the Performance of the Isolated Mammalian Heart." Journal of Physiology (New York), 44 (1912), 206-219.

(4) Shapiro, A. H. "Physiologic and Medical Aspects of Flow in Collapsible Tubes." Proceedings of Sixth Canadian Congress of Applied Mechanics, 1977.

(5) Cournand, A., Motley, H. L., Werko, L., and Richards, Jr. D. W. "Physiological Studies of the Effects of Intermittent Positive Pressure Breathing on Cardiac Output in Man." American Journal of Physiology, 152 (1948), 162-174.

(6) Morgan, B. C., Martin, W. E., Hornbein, T. F., Crawford, E. W., and Guntheroth, W. G. "Hemodynamic Effects of Intermittent Positive Pressure Respiration." Anesthesiology, 27 (1966), 584-590.

(7) Permutt, S., Bromberger-Barnea, B. and Bane, H. N. "Alveolar Pressure, Pulmonary Venous Pressure and the Vascular Waterfall." Med. Thoracalis, 19 (1962), 239-260.

(8) Permutt, S. and Riley, R. L. "Hemodynamics of Collapsible Vessels with Tone: The Vascular Waterfall." Journal of Applied Physiology, 18 (1963), 924-932.

(9) Smith, H. C. and Butler, J. "Pulmonary Venous Waterfall and Perivenous Pressure in the Living Dog." Journal of Applied Physiology, 38 (1975), 304-308.

(10) West, J. B., Dollery, C. T. and Naimark, A. "Distribution of Blood Flow in the Isolated Lung: Relation to Vascular and Alveolar Pressures." Journal of Applied Physiology, 19 (1964), 713-724.

(11) Brower, R. W. and Noordergraaf, A. "Pressure-Flow Characteristics of Collapsible Tubes: A Reconciliation of Seemingly Contradictory Results." Annals of Biomedical Engineering, 1 (1973), 333-355.

(12) Katz, A. I., Chen, Y., and Moreno, A. H. "Flow Through a Collapsible Tube. Experimental Analysis and Mathematical Model." Biophysical Journal, 9 (1968), 1261-1279.

(13) Shapiro, A. H. "Steady Flow in Collapsible Tubes." ASME Journal of Biomechanical Engineering, 99 (1977), 126-147.

(14) Griffiths, D. J. "Steady Fluid Flow Through Veins and Collapsible Tubes." Medical and Biological Engineering, 9 (1971), 597-602.

(15) Lambert, R. K. and Wilson, T. A. "Flow Limitation in a Collapsible Tube." Journal of Applied Physiology, 33 (1972), 150-153.

(16) Conrad, W. A. "Pressure-Flow Relationships in Collapsible Tubes." IEEE Trans. on Biomedical Engineering, BME-16 (October, 1969), 284-295.

(17) Brower, R. W. "Pressure-Flow Characteristics of Collapsible Tubes." Unpublished Ph.D. dissertation, University of Pennsylvania, 1970.

(18) Rodbard, S. "Flow Through Collapsible Tubes: Augmented Flow Produced by Resistance at Outlet." Circulation, 11 (1955), 280-287.

(19) Ganong, W. F. Review of Medical Physiology. Los Altos: Lange Medical Publications, 1971.

(20) Rodbard, S. and Saiki, H. "Flow Through Collapsible Tubes." American Heart Journal, 46 (1953), 715-725.

(21) Rodbard, S. "A Hydrodynamic Mechanism for Autoregulation of Flow." Cardiologia, 48 (1966), 532-535.

(22) Holt, J. P. "The Collapse Factor in the Measurement of Venous Pressure: The Flow of Fluid Through Collapsible Tubes." American Journal of Physiology, 134 (1944), 292-299.

(23) Holt, J. P. "Flow of Liquids Through Collapsible Tubes." Circulation Research, 7 (1959), 342-353.

(24) Wild, R., Pedley, T. J. and Riley, D. S. "Viscous Flow in Collapsible Tubes of Slowly Varying Elliptical Cross-section." Journal of Fluid Mechanics, 81 (1976), 273-294.

(25) Zienkiewicz, O. C. The Finite Element Method. New York: McGraw-Hill, 1977.

(26) Donnell, L. H. Beams, Plates, and Shells. New York: McGraw-Hill, 1976.

(27) White, F. M. Viscous Fluid FLow. New York: McGraw-Hill, 1974.

(28) Hildebrand, F. B. Methods of Applied Mathematics. New Jersey: Prentice-Hall, Inc., 1965.

(29) Bergan, P. G., and Clough, R. W. "Large Deflection Analysis of Plates and Shallow Shells Using the Finite Element Method." Int. Journal for Numerical Methods in Engineering, 5 (1973), 543-556.

(30) Gallagher, R. H. "Finite Element Analysis of Geometrically Nonlinear Problems." Proceedings of the 1973 Tokyo Seminar on Finite Element Analysis, (1973).

APPENDIX A

SUBROUTINE KMATRI

The task of this subroutine was to assemble the overall structural stiffness matrix referred to a global axes coordinate system.

Preliminary Considerations

The analysis requires two sets of displacements, as discussed in Chapter III; these are the global displacements, q_G, and the local displacements, q_L. The two displacement sets are related by a coordinate rotation:

$$\underset{\sim}{q}_L = [T]\, \underset{\sim}{q}_G \tag{24}$$

Once the initial configuration is established, this relationship remains constant. In the following derivations, the subscripts are omitted and local coordinates are understood unless otherwise stated.

Basic to the analysis is the formulation of element stiffnesses in local coordinates in order to take advantage of the simplifying shell assumptions. The transformation of the "local" stiffness into a "global" stiffness is accomplished via Equation 24. The structural global stiffness emerges once the elemental contributions are summed in the proper manner.

The analysis first requires a relationship between the displacements, dq, and the generalized coordinates, da; this relationship comes from the first variation of the polynomial expressions for the displacements (Equations 3-6). That is,

$$\underset{\sim}{dq} = [C]\, \underset{\sim}{da} \tag{25}$$

or, in expanded form:

$$\begin{Bmatrix} du_j \\ dv_j \\ dw_j \\ d\Delta\theta_{xj} \\ du_k \\ dv_k \\ dw_k \\ d\Delta\theta_{xk} \\ du_l \\ dv_l \\ dw_l \\ d\Delta\theta_{xl} \end{Bmatrix} = \begin{bmatrix} 1 & x_j & y_j & 0 & 0 & 0 & 0 & 0 & 0 & 0 & 0 & 0 \\ 0 & 0 & 0 & 1 & x_j & y_j & 0 & 0 & 0 & 0 & 0 & 0 \\ 0 & 0 & 0 & 0 & 0 & 0 & 1 & x_j & y_j & 0 & 0 & 0 \\ 0 & 0 & 0 & 0 & 0 & 0 & 0 & 0 & 0 & 1 & x_j & y_j \\ 1 & x_k & y_k & 0 & 0 & 0 & 0 & 0 & 0 & 0 & 0 & 0 \\ 0 & 0 & 0 & 1 & x_k & y_k & 0 & 0 & 0 & 0 & 0 & 0 \\ 0 & 0 & 0 & 0 & 0 & 0 & 1 & x_k & y_k & 0 & 0 & 0 \\ 0 & 0 & 0 & 0 & 0 & 0 & 0 & 0 & 0 & 1 & x_k & y_k \\ 1 & x_l & y_l & 0 & 0 & 0 & 0 & 0 & 0 & 0 & 0 & 0 \\ 0 & 0 & 0 & 1 & x_l & y_l & 0 & 0 & 0 & 0 & 0 & 0 \\ 0 & 0 & 0 & 0 & 0 & 0 & 1 & x_l & y_l & 0 & 0 & 0 \\ 0 & 0 & 0 & 0 & 0 & 0 & 0 & 0 & 0 & 1 & x_l & y_l \end{bmatrix} \begin{Bmatrix} da_1 \\ da_2 \\ da_3 \\ da_4 \\ da_5 \\ da_6 \\ da_7 \\ da_8 \\ da_9 \\ da_{10} \\ da_{11} \\ da_{12} \end{Bmatrix}$$

Notice that the [C] matrix is a constant matrix regardless of the polynomials chosen for the deflections. Moreover, in general, the deflections are known while the corresponding generalized coordinates need to be found. Hence, the inverse relationship is needed:

$$d\underset{\sim}{a} = [C]^{-1}\, d\underset{\sim}{q} \tag{26}$$

The analysis also requires a relationship between strains and displacements:

$$d\underset{\sim}{\varepsilon} = [B]\, d\underset{\sim}{q} \tag{27}$$

To find the [B] matrix, the displacement polynomials are substituted into Equations 9-11, 13:

$$\varepsilon_x = a_2 + \frac{1}{2}(a_2^2 + a_5^2 + a_8^2) \tag{28}$$

$$\varepsilon_y = a_6 + \frac{1}{2}(a_3^2 + a_6^2 + a_9^2) \tag{29}$$

$$\gamma_{xy} = a_3 + a_5 + a_2 a_3 + a_5 a_6 + a_8 a_9 \tag{30}$$

$$\kappa = a_{12} \tag{31}$$

Taking the first variation of these equations yields:

$$d\,\varepsilon_x = (1 + a_2)\, da_2 + a_5 da_5 + a_8 da_8 \tag{32}$$

$$d\,\varepsilon_y = a_3 da_3 + (1 + a_6)\, da_6 + a_9 da_9 \tag{33}$$

$$d\gamma_{xy} = a_3 da_2 + (1 + a_2)\, da_3 + (1 + a_6)\, da_5 + a_9 da_8 + a_8 da_9 \tag{34}$$

$$d\kappa = da_{12} \tag{35}$$

which is, in matrix notation,

$$d\underset{\sim}{\varepsilon} = [B^*]\, d\underset{\sim}{a} \tag{36}$$

with [B*] equal to

$$\begin{bmatrix} 0 & (1+a_2) & 0 & 0 & 1 & 0 & 0 & a_8 & 0 & 0 & 0 & 0 \\ 0 & 0 & a_3 & 0 & 0 & (1+a_6) & 0 & 0 & a_9 & 0 & 0 & 0 \\ 0 & a_3 & (1+a_2) & 0 & (1+a_6) & a_5 & 0 & a_9 & a_8 & 0 & 0 & 0 \\ 0 & 0 & 0 & 0 & 0 & 0 & 0 & 0 & 0 & 0 & 0 & 1 \end{bmatrix}$$

This means that

$$d\underset{\sim}{\varepsilon} = [B^*][C]^{-1}\, d\underset{\sim}{q} \qquad (37)$$

and

$$[B] = [B^*][C]^{-1} \qquad (38)$$

Since [B*] depends on the values of $\underset{\sim}{a}$, it is thus position dependent. In fact, the position dependency of [B*] leads to the position dependency of the stiffness matrix, soon to be developed.

The strains can also be related to the stresses through an Hookean elasticity matrix:

$$d\underset{\sim}{\sigma} = [D]\, d\underset{\sim}{\varepsilon} \qquad (39)$$

In this scheme,

$$\begin{Bmatrix} d\sigma_x \\ d\sigma_y \\ d\tau_{xy} \\ dM_y \end{Bmatrix} = \frac{E}{(1-r^2)} \begin{bmatrix} 1 & r & 0 & 0 \\ r & 1 & 0 & 0 \\ 0 & 0 & \frac{(1+r)}{2} & 0 \\ 0 & 0 & 0 & \frac{h^2}{12} \end{bmatrix} \begin{Bmatrix} d\varepsilon_x \\ d\varepsilon_y \\ d\gamma_{xy} \\ d\kappa \end{Bmatrix} \qquad (40)$$

The Principle of Virtual Work

The stresses and strains produced by the external loading are represented by a set of equivalent external forces, F_e, which act at the finite element nodes. The virtual work done by the external nodal forces is:

$$dW = d\underset{\sim}{q}^T \underset{\sim}{F}_e \tag{41}$$

This work done must equal the structural internal work (e.g., the principle of virtual work). The internal work is calculated by integration of the stress-strain product over the volume of the element:

$$dU^i = \int d\underset{\sim}{\varepsilon}^T \underset{\sim}{\sigma}\, d\tau \tag{42}$$

Or, using Equation 27:

$$dU^i = d\underset{\sim}{q}^T \int [B]^T \underset{\sim}{\sigma}\, d\tau \tag{43}$$

and, equating the external and internal work:

$$d\underset{\sim}{q}^T \underset{\sim}{F}_e = d\underset{\sim}{q}^T \int [B]^T \underset{\sim}{\sigma}\, d\tau \tag{44}$$

Finally, given an arbitrary value of dq, the multipliers must be equal. Or,

$$\underset{\sim}{F}_e = \int [B]^T \underset{\sim}{\sigma}\, d\tau \tag{45}$$

Solution Method

If the right-hand side of Equation 45 is thought of as a vector of the internal nodal forces, F_i, then Equation 45 can be rewritten in terms of an equilibrium index, Ψ,

$$\underset{\sim}{\Psi} = \underset{\sim}{F}_i - \underset{\sim}{F}_e \tag{46}$$

Taking the first variation of this equation, holding the external forces constant, gives:

$$d\underset{\sim}{\Psi} = \int [dB]^T \underset{\sim}{\sigma}\, d\tau + \int [B]^T\, d\underset{\sim}{\sigma}\, d\tau \tag{47}$$

Using Equations 27 and 39,

$$d\underset{\sim}{\Psi} = \int [dB]^T \underset{\sim}{\sigma} d\tau + \left[\int [B]^T[D][B]\, d\tau\right] d\underset{\sim}{q} \tag{48}$$

so that

$$d\underset{\sim}{\Psi} = [K_T]\, d\underset{\sim}{q} \tag{49}$$

where

$$[K_T] = [K_\sigma] + [K_N] \tag{50}$$

$$[K_\sigma]\, d\underset{\sim}{q} = \int [dB]^T \underset{\sim}{\sigma} d\tau \tag{51}$$

$$[K_N] = \int [B]^T[D][B]\, d\tau \tag{52}$$

Here, $[K_\sigma]$ is known as the <u>initial stress</u> matrix, or the <u>geometric</u> matrix, while $[K_T]$ is known as the <u>tangential stiffness</u> matrix.

Calculation of the Stiffness Matrix Entries

The Zienkiewicz (25) procedure was used to find $[K_\sigma]$. This method begins with a definition:

$$\begin{Bmatrix} \partial u/\partial x \\ \partial v/\partial x \\ \partial w/\partial x \\ \partial u/\partial y \\ \partial v/\partial y \\ \partial w/\partial y \end{Bmatrix} \triangleq [G]\,\underset{\sim}{q} \tag{53}$$

substituting Equations 3 to 6:

$$\begin{Bmatrix} \partial u/\partial x \\ \partial v/\partial x \\ \partial w/\partial x \\ \partial u/\partial y \\ \partial v/\partial y \\ \partial w/\partial y \end{Bmatrix} = \begin{bmatrix} 0 & 1 & 0 & 0 & 0 & 0 & 0 & 0 & 0 & 0 & 0 & 0 \\ 0 & 0 & 0 & 0 & 1 & 0 & 0 & 0 & 0 & 0 & 0 & 0 \\ 0 & 0 & 0 & 0 & 0 & 0 & 0 & 1 & 0 & 0 & 0 & 0 \\ 0 & 0 & 1 & 0 & 0 & 0 & 0 & 0 & 0 & 0 & 0 & 0 \\ 0 & 0 & 0 & 0 & 0 & 1 & 0 & 0 & 0 & 0 & 0 & 0 \\ 0 & 0 & 0 & 0 & 0 & 0 & 0 & 0 & 1 & 0 & 0 & 0 \end{bmatrix} \underset{\sim}{a} \tag{54}$$

$$= [H]\,\underset{\sim}{a}$$

and, using Equation 26:

$$[H]\,\underset{\sim}{a} = [H][C]^{-1}\,\underset{\sim}{q} \tag{55}$$

so that

$$[G] = [H][C]^{-1} \tag{56}$$

and the well-known form of the geometric matrix can be used (25)

$$[K_\sigma] = \int [G]^T[M][G]\, d\tau \qquad (57)$$

where [M] is a matrix of the stress values:

$$[M] = \begin{bmatrix} \sigma_x & 0 & 0 & \tau_{xy} & 0 & 0 \\ 0 & \sigma_x & 0 & 0 & \tau_{xy} & 0 \\ 0 & 0 & \sigma_x & 0 & 0 & \tau_{xy} \\ \tau_{xy} & 0 & 0 & \sigma_y & 0 & 0 \\ 0 & \tau_{xy} & 0 & 0 & \sigma_y & 0 \\ 0 & 0 & \tau_{xy} & 0 & 0 & \sigma_y \end{bmatrix} \qquad (58)$$

In addition to the formulation of the tangential stiffness matrix, this subroutine computes the Lagrangian constraint equations. From Chapter III, the two constraint equations are:

$$\mathrm{Sin}\,\bar{\theta} = (Z_{L_o} + W_L) - (Z_{J_o} + W_J)\,/\ell_Y \qquad (8)$$

$$\varepsilon_y = 0 \qquad (12)$$

To apply the Lagrangian constraint method, the first variation of these equations must be computed (28):

$$(da_{10} + l_y da_{12}/2)\,\mathrm{Cos}\,\bar{\theta}_x = da_9 \qquad (59)$$

$$a_3 da_3 + (1 + a_6)\, da_6 + a_9 da_9 = 0 \qquad (60)$$

Equations 59 and 60 can be written in matrix form and appended to $[K_T]$ with Lagrange multipliers, so that

$$\begin{bmatrix} [K_T] & [CC]^T \\ [CC] & [0] \end{bmatrix} \begin{Bmatrix} d\underset{\sim}{q} \\ \underset{\sim}{\lambda} \end{Bmatrix} = \begin{Bmatrix} d\underset{\sim}{\Psi} \\ \underset{\sim}{0} \end{Bmatrix} \tag{61}$$

Equation 61 is the fundamental equation in the solution. In the following deck listing, the step-by-step procedure in the formulation is given.

A more compact formulation for the stiffness matrix could have been obtained if the internal energy were expressed directly in terms of the averaged rotational coordinates. A subsequent energy minimization would then yield a stiffness matrix which does not require the computation of the additional Lagrange multipliers.

```
      SUBROUTINE KMATRI
C
C  THIS SUBROUTINE CALCULATES THE STIFFNESS MATRIX IN GLOBAL COORDINATES
C
C
      COMMON D(4,4),PSI(450),STRAIN(300,4),CI(12,12),H(6,12),VOL
      COMMON STIFF(32215)
      COMMON VU(23),P(23),NY(23),PXB(23)
      COMMON XNODE(200),YNODE(200),ZNODE(200),IELEM(300,3)
      COMMON F(405),YMAX(23),IMAX(23,16)
      COMMON XO(135),YO(135),ZO(135),TR(300,10),SIGMA(300,4),NDOF(200)
      COMMON TX(200),TXO(200)
      COMMON DXIN,DXOUT,THK,RLS,FMU,E,P1,P2,PE,IIN,IOUT
      COMMON R,RHO,RL,DIA,Q,DPDX,REY,RMU,RNU,DRO
      COMMON UTEST,PTEST,DMAX,DP,DU,DPSI,SCALE
      COMMON LASTEL,LASTND,NELEM,NNODES,NIN,NTUBE,LASTJ,INFLAG
      COMMON NX,NNY,NTUBEX,NTUBEY,HX,HY,NUMBC
      COMMON IFORCE,TWX,TWY,TWZ,SIGXO,XC,YC
      DOUBLE PRECISION D,PSI,STRAIN,CI,H,VOL,STIFF
C
      DIMENSION DUM1(12,12),DUM2(12,12),DUM3(12),DUM4(12)
      DIMENSION DPT(12,12),A(12),RM(6,6),CC(2,12),CON(2,12)
      DIMENSION BSTAR(4,12),B(4,12),HMH(12,12),SIGMAL(4),RK(12,12)
      DOUBLE PRECISION DUM1,DUM2,DUM3,DUM4,DPT,A
      DOUBLE PRECISION BSTAR,B,SIGMAL,HMH,RK,RM,CC,CON
C
      YPRIME = Y3/2.0
C  INITIALIZE THE PSI VECTOR, -PSI IS ACTUALLY COMPUTED HERE.
      LAST = 4*NNODES + (NTUBEX-1)*NTUBEY*2
      DO 1502 J = 1,LAST
 1502 PSI(J) =    F(J)
C
C
C  INITIALIZE THE STIFFNESS MATRIX
C   THE STIFFNESS MATRIX IS STORED COLUMN-WISE
C
      KCOL = 4*NNODES
      ISTOP = LAST*(LAST+1)/2
      DO 1510 J = 1,ISTOP
 1510 STIFF(J) = 0.0
C
C  THE NEXT LOOP CONSIDERS THE MATRICIES ELEMENT-BY-ELEMENT.
      DO 1500 M = 1,NELEM
C
C  BUILD THE ROTATION MATRIX.
      DO 1505 J = 1,12
      DO 1505 K = 1,12
 1505 DPT(J,K) = 0.0
C
      L=0
      DO 1506 J = 1,3
      DO 1506 K = 1,3
      L = L+1
      DPT(J,K) = TR(M,L)
      DPT(J+4,K+4) = DPT(J,K)
      DPT(J+8,K+8) = DPT(J,K)
 1506 CONTINUE
      DPT(4,4) = TR(M,10)
      DPT(8,8) = TR(M,10)
      DPT(12,12) = TR(M,10)
C
C
C  COMPUTE THE NODE DEFLECTIONS IN GLOBAL COORDINATES.
      I = IELEM(M,1)
      J = IELEM(M,2)
      K = IELEM(M,3)
      DUM3(1) = XNODE(I) - XO(I)
      DUM3(2) = YNODE(I) - YO(I)
      DUM3(3) = ZNODE(I) - ZO(I)
      DUM3(4) = TX(I) - TXO(I)
      DUM3(5) = XNODE(J) - XO(J)
      DUM3(6) = YNODE(J) - YO(J)
      DUM3(7) = ZNODE(J) - ZO(J)
      DUM3(8) = TX(J) - TXO(J)
      DUM3(9) = XNODE(K) - XO(K)
      DUM3(10)= YNODE(K) - YO(K)
      DUM3(11)= ZNODE(K) - ZO(K)
      DUM3(12)= TX(K) - TXO(K)
C
C  ROTATE THE DEFLECTIONS TO LOCAL COORDINATES.
      DO 1582 J = 1,12
      DUM4(J) = 0.0
      DO 1582 K = 1,12
 1582 DUM4(J) = DUM4(J) + DPT(J,K)*DUM3(K)
C
C  COMPUTE THE GENERALIZED COORDINATES FOR THE LOCAL SYSTEM
      DO 1750 J = 1,12
      A(J) = 0.0
      DO 1750 K = 1,12
      A(J) = A(J) + CI(J,K)*DUM4(K)
 1750 CONTINUE
C
C**************COMPUTE BSTAR*************************************
C  FILL BSTAR
      DO 1530 J = 1,4
      DO 1530 K = 1,12
      BSTAR(J,K) = 0.0
 1530  CONTINUE
C
C CALCULATE THE DERIVATIVE TERMS.
      DWDX  = A(8)
      DWDX2 = DWDX*DWDX/2.0
      DWDY  = A(9)
      DWDY2 = DWDY*DWDY/2.0
      DWDXY = DWDX*DWDY
      THETAX = (DUM4(4) + DUM4(12))/2.0
C
      BSTAR(1,2) = 1.0 + A(2)
      BSTAR(1,5) = A(5)
      BSTAR(1,8) = A(8)
      BSTAR(2,3) = A(3)
      BSTAR(2,6) = 1.0 + A(6)
      BSTAR(2,9)  = A(9)
      BSTAR(3,2) = A(3)
      BSTAR(3,3) = 1.0 + A(2)
      BSTAR(3,5) = 1.0 + A(6)
      BSTAR(3,6) = A(5)
      BSTAR(3,8) = A(9)
      BSTAR(3,9) = A(8)
```

```
      BSTAR(4,12) = 1.0
C
C  FORM B = BSTAR*CI
      DO 1550 I = 1,4
      DO 1550 J = 1,12
      B(I,J) = 0.0
      DO 1550 K = 1,12
      B(I,J) = B(I,J) + BSTAR(I,K)*CI(K,J)
 1550 CONTINUE
C
C
C***********************CALCULATE STRESSES AND STRAINS****************
C
C  CALCULATE THE INCREMENTAL STRAIN FROM THE INITIAL POSITION.
C  IN LOCAL COORDINATES.
 1560 STRAIN(M,1) = A(2) + A(2)*A(2)/2.0 + A(5)*A(5)/2.0 + DWDX2
      STRAIN(M,2) = A(6) + A(3)*A(3)/2.0 + A(6)*A(6)/2.0 + DWDY2
      STRAIN(M,3) = A(3) + A(5) + A(2)*A(3) + A(5)*A(6) + DWDXY
      STRAIN(M,4) = A(12)
C
C  CALCULATE THE LOCAL STRESSES
      DO 1531 J = 1,4
      SIGMAL(J) = SIGMA(M,J)
      DO 1531 K = 1,4
         SIGMAL(J) = SIGMAL(J) + D(J,K)*STRAIN(M,K)
 1531 CONTINUE
C
C  CALCULATE THE INTERNAL FORCES, BT*SIGMAL, IN LOCAL COORDINATES.
 1715 DO 1630 J = 1,12
      DUM3(J) = 0.0
      DO 1630 K = 1,4
      DUM3(J) = DUM3(J) + B(K,J)*SIGMAL(K)
 1630 CONTINUE
C
C  ROTATE THE FORCES INTO THE GLOBAL SYSTEM
      DO 1735 J = 1,12
      DUM4(J) = 0.0
      DO 1735 K = 1,12
      DUM4(J) = DUM4(J) + DPT(K,J)*DUM3(K)
 1735 CONTINUE
C
C
C  BUILD THE PSI VECTOR
      DO 1650 L = 1,3
      N = IELEM(M,L)
      J = 4*N
      K = 4*L
      PSI(J-3) = PSI(J-3) - DUM4(K-3)*VOL
      PSI(J-2) = PSI(J-2) - DUM4(K-2)*VOL
      PSI(J-1) = PSI(J-1) - DUM4(K-1)*VOL
      PSI(J) = PSI(J) - DUM4(K)*VOL
 1650 CONTINUE
C
C
C
C
C*******************SET AND STORE THE HOOP CONSTRAINTS*************
      IF(M.GT.(NELEM-NTUBEY))  GO TO 1651
      NROW = (M-1)/NTUBEY
      IALT = (-1)**NROW
      IF(IALT.GT.0) GO TO 1651
C
C  SET THE HOOP STRAIN CONSTRAINT ENTRIES IN TERMS OF THE
C  GENERALIZED COORDINATES.
      DO 3000 K=1,12
      CC(1,K) = 0.0
 3000 CC(2,K) = BSTAR(2,K)
C
C SET THE THETA-SHAPE CONSTRAINT IN TERMS OF THE
C GENERALIZED COORDINATES.
      CC(1,9) = -1.0
      CC(1,10)= COS(THETAX)
      CC(1,12)= YPRIME*COS(THETAX)
C
C  COMPUTE THE CONSTRAINT ENTRIES IN TERMS OF DISPLACEMENTS
      DO 3010 L=1,2
      DO 3010 K = 1,12
      DUM1(L,K) = 0.0
      DO 3010 J = 1,12
 3010 DUM1(L,K) = DUM1(L,K) + CC(L,J)*CI(J,K)
C
C
C  ROTATE THE CONSTRAINT ENTRIES INTO THE GLOBAL REFERENCE SYSTEM.
      DO 3020 L=1,2
      DO 3020 K = 1,12
      CON(L,K) = 0.0
      DO 3020 J=1,12
      CON(L,K) = CON(L,K) + DUM1(L,J)*DPT(J,K)
 3020 CONTINUE
C
C
C  NUMERICAL CONDITIONING OF THE CONSTRAINTS.
      DO 1790 L=1,2
      BIG = 0.0
      DO 3030 J=1,12
      ACON = DABS(CON(L,J))
      IF(ACON.GT.BIG) BIG = ACON
 3030 CONTINUE
C
C  SCALE THE LARGEST ENTRY TO 10**6
      SCALEK = 1.0E06/BIG
      DO 3040 J=1,12
      CON(L,J) = SCALEK*CON(L,J)
 3040 CONTINUE
C
C  STORE THE ROW INTO THE GLOBAL STIFFNESS MATRIX.
      KCON = 0
      KCOL = KCOL+1
      DO 1790 I = 1,3
      KROW = 4*(IELEM(M,I) - 1)
      DO 1790 K = 1,4
      KROW = KROW + 1
      KCON = KCON + 1
      N = KROW + KCOL*(KCOL-1)/2
      STIFF(N) = STIFF(N) + CON(L,KCON)
 1790 CONTINUE
C
C
C*********************CALCULATE AND ASSEMBLE THE SIFFNESS********
C
```

```
C  SET THE RM MATRIX
 1651 DO 1532 J = 1,6
      DO 1532 K = 1,6
 1532 RM(J,K) = 0.0
C
      RM(1,1) = SIGMAL(1)
      RM(2,2) = SIGMAL(1)
      RM(3,3) = SIGMAL(1)
      RM(4,4) = SIGMAL(2)
      RM(5,5) = SIGMAL(2)
      RM(6,6) = SIGMAL(2)
      RM(1,4) = SIGMAL(3)
      RM(2,5) = SIGMAL(3)
      RM(3,6) = SIGMAL(3)
      RM(4,1) = SIGMAL(3)
      RM(5,2) = SIGMAL(3)
      RM(6,3) = SIGMAL(3)
C
C  MULTIPLY M*H
      DO 1770 J=1,6
      DO 1770 K=1,12
      DUM1(J,K) = 0.0
      DO 1770 L=1,6
      DUM1(J,K) = DUM1(J,K) + RM(J,L)*H(L,K)
 1770 CONTINUE
C
C  CALCULATE HMH = HT*DUM1
      DO 1780 J=1,12
      DO 1780 K=1,12
      HMH(J,K) = 0.0
      DO 1780 L=1,6
      HMH(J,K) = HMH(J,K) + H(L,J)*DUM1(L,K)
 1780 CONTINUE
C
C
C  THE FOLLOWING TWO LOOPS DEFINE THE GMG MATRIX
C  MULTIPLY HMH*CI
      DO 1540 I = 1,12
      DO 1540 J = 1,12
      DUM2(I,J) = 0.0
      DO 1540 K = 1,12
      DUM2(I,J) = DUM2(I,J) + HMH(I,K)*CI(K,J)
 1540 CONTINUE
C
C  SET GMG = DUM1 = CIT*DUM2
      DO 1541 I = 1,12
      DO 1541 J = 1,12
      DUM1(I,J) = 0.0
      DO 1541 K = 1,12
      DUM1(I,J) = DUM1(I,J) + CI(K,I)*DUM2(K,J)
 1541 CONTINUE
C
C  THE FOLLOWING TWO LOOPS DEFINE RK, THE ELEMENT STIFFNESS MATRIX.
C  MULTIPLY BT*D
 1542 DO 1535 I = 1,12
      DO 1535 J = 1,4
      DUM2(I,J) = 0.0
      DO 1535 K = 1,4
      DUM2(I,J) = DUM2(I,J) + B(K,I)*D(K,J)
 1535 CONTINUE
C
C  MULTIPLY DUM2*B AND ADD TO GMG(DUM1)
      DO 1545 I = 1,12
      DO 1545 J = 1,12
      RK(I,J) = DUM1(I,J)
      DO 1545 K = 1,4
      RK(I,J) = RK(I,J) + DUM2(I,K)*B(K,J)
 1545 CONTINUE
C
C  APPLY THE CONGRUENT AXIS TRANSFORMATION.
      DO 1551 J = 1,12
      DO 1551 K = 1,12
         DUM2(J,K) = 0.0
      DO 1551 L = 1,12
         DUM2(J,K) = DUM2(J,K) + RK(J,L)*DPT(L,K)
 1551 CONTINUE
C
      DO 1552 J = 1,12
      DO 1552 K = 1,12
         RK(J,K) = 0.0
      DO 1552 L = 1,12
         RK(J,K) = RK(J,K) + DPT(L,J)*DUM2(L,K)
 1552 CONTINUE
C
      DO 1562 J = 1,12
      DO 1562 K = 1,12
      RK(J,K) = RK(J,K)*VOL
 1562 CONTINUE
C
C  STORE THE STIFFNESS TERMS
      DO 1563 J = 1,3
      DO 1563 K = J,3
      JK = (IELEM(M,J)-1)*4
      KK = (IELEM(M,K)-1)*4
      KSAVE = KK
      KSYM = 0
      IF(JK.EQ.KK) KSYM = 1
      JR = (J-1)*4
      KR = (K-1)*4
      IF(JK.GT.KSAVE) GO TO 1555
      GO TO 1557
 1555 KK = JK
      JK = KSAVE
      JR = (K-1)*4
      KR = (J-1)*4
 1557 DO 1563 L1 = 1,4
      JK = JK+1
      JR = JR+1
      KS = KR
      KB = KK
      DO 1564 L2 = 1,4
      KS = KS+1
      KB = KB+1
      IF(JR.GT.KS .AND. KSYM.EQ.1) GO TO 1564
      N = JK + KB*(KB-1)/2
      STIFF(N) = RK(JR,KS) + STIFF(N)
 1564 CONTINUE
 1563 CONTINUE
C
 1500 CONTINUE
```

```
C
C
C CONDITION THE STIFFNESS MATRIX
      DO 4000 J = 1,LAST
      DO 4000 K = J,LAST
         N = J + (K-1)*K/2
         IF(DABS(STIFF(N)).LT.0.1) STIFF(N) = 0.0
 4000 CONTINUE
C
      RETURN
      END
```

APPENDIX B

SUBROUTINE FLOW1D

The object of this subroutine was to calculate the fluid variables of pressure and velocity on the interior of the tube. In order to accomplish this, the fluid region was subdivided into a connected set of finite fluid regions divided by a successive constant X planes and enclosed by the tube wall (Figure 10 and Figure 23).

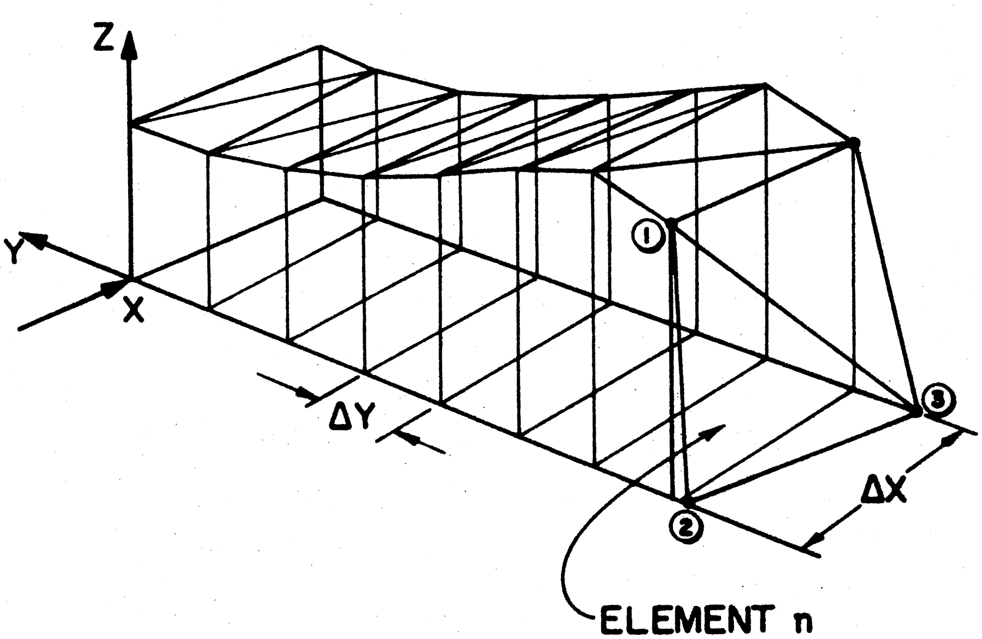

Figure 23. Wall Surface Approximation in a Fluid Integral Region

Given the tube shape, it is a straightforward task to apply continuity and determine the average velocity, $\overline{V}$, everywhere within the tube. The equation used is

$$\overline{V} = Q/A \tag{62}$$

Here, A is the cross-sectional area and Q is the flowrate through the tube. The trapezoidal method of integration is used to find the cross-sectional areas based upon the cartesian mesh values as determined by subroutine MESH.

As discussed in Chapter III, the term of interest in the momentum equation is

$$\int_{w} P dA_X = \overline{P}_w A_{wX} \tag{63}$$

Here, $\overline{P}_w$ is the average wall pressure and A_{wX} is the x-component of wall surface area of the tube in the region of interest. To obtain these values, the surface is approximated by a set of flat triangles. The surface approximation is shown in Figure 23. Notice that the surface triangles must be defined so that they enclose the volume between the X-plane boundaries. This means that the finite elements cannot be directly used since they are not, in general, related to the underlying cartesian grid. The computation is done by assuming a linear variation of pressure in the region.

$$P_d = mX + P_u \tag{64}$$

For this assumed linear variation in P and a planar triangle for a wall approximation, the average becomes:

$$\bar{P}_w = (P_1 + P_2 + P_3)/3 \tag{65}$$

where P_1, P_2, P_3 are pressures at the corners of the triangle, which are either P_u or P_d in magnitude. The x-component of the wall area, A_{wx}, is found by computing the area vector for each surface triangle. For element n in Figure 23:

$$\underset{\sim}{A}_{wn} = \begin{Bmatrix} A_{wX} \\ A_{wY} \\ A_{wZ} \end{Bmatrix}_n^T \hat{n} \tag{66}$$

Summation of all the surface element area contributions produces the value of A_{wx} for the region.

```
      SUBROUTINE FLOW1D
C
C THIS SUBROUTINE CALCULATES THE FLUID VARIABLES OF PRESSURE AND
C AVERAGE VELOCITY.
C
      COMMON D(4,4),PSI(450),STRAIN(300,4),CI(12,12),H(6,12),VOL
      COMMON STIFF(82215)
      COMMON VU(23),P(23),NY(23),PXB(23)
      COMMON XNODE(200),YNODE(200),ZNODE(200),IELEM(300,3)
      COMMON F(405),YMAX(23),ZMAX(23,15)
      COMMON XO(135),YO(135),ZO(135),TR(300,10),SIGMA(300,4),NDOF(200)
      COMMON TX(200),TXO(200)
      COMMON DXIN,DXOUT,THK,RLS,FMU,E,P1,P2,PE,IIN,IOUT
      COMMON R,RHO,RL,DIA,Q,DPDX,REY,RMU,RNU,DRO
      COMMON UTEST,PTEST,DMAX,DP,DU,DPSI,SCALE
      COMMON LASTEL,LASTND,NELEM,NNODES,NIN,NTUBE,LASTJ,INFLAG
      COMMON NX,NNY,NTUBEX,NTUBEY,HX,HY,NUMBC
      COMMON IFORCE,TWX,TWY,TWZ,SIGXO,XC,YC
      DOUBLE PRECISION D,PSI,STRAIN,CI,H,VOL,STIFF
C
C  THE FOLLOWING ARE PROGRAM SPECIFIC VARIABLES.
      DIMENSION YZAREA(23),XGC(40,3),YGC(40,3),ZGC(40,3),SEC(23)
      DIMENSION SMOOTH(23),SMAX(23),SMSUM(23),AXBAR(23),SUMBAR(23)
      DOUBLE PRECISION X21,Y21,Z21,X31,Y31,Z31,AX,AY,AZ,SAREA
      DOUBLE PRECISION XGC,YGC,ZGC
C
C  FIRST, CALCULATE THE CROSSECTIONAL AREAS AND AVERAGE VELOCITIES.
C  TRAPEZOIDAL INTEGRATION IS USED.
      JSTART = 1
      JSTOP = LASTJ+1
      UTEST = 0.0
      DO 1000 J=JSTART,JSTOP
      SUM = 0.0
      LASTK = NY(J)-1
      DO 1010 K=2,LASTK
      ZBAR = (ZMAX(J,K)+ZMAX(J,K+1))/2.0
      SUM = SUM+ZBAR*HY
 1010 CONTINUE
C
      RNY = NY(J)
      LAST = NY(J)
      Y = RNY*HY
      AINC = (YMAX(J)-Y)*ZMAX(J,LASTK)/2.0
      YZAREA(J) = 4.0*(SUM+AINC)
 1000 CONTINUE
C
C  SMOOTH THE CROSSECTIONAL AREA'S IN THE X DIRECTION.
C  THIS IS NECESSARY DUE TO THE COARSENESS OF THE WALL MODEL.
      NDIM = NTUBE - NIN
      JSTART = NIN+1
      JSTOP = NTUBE
      DO 1020 J=JSTART,JSTOP
      L=J-NIN
      SEC(L) = YZAREA(J)
 1020 CONTINUE
C
      CALL SE13(SEC,SMOOTH,NDIM,IER)
C  SUBROUTINE SE13 IS AN SSP SUBROUTINE WHICH SMOOTHS BY INTERPOLATING
C  A SECOND ORDER FUNCTION WHICH IS A LEAST-SQUARE-ERROR FIT TO THE
C  NEIGHBORING DATA POINTS.
C
      DO 1030 J=JSTART,JSTOP
      L = J-NIN
      YZAREA(J) = SMOOTH(L)
 1030 CONTINUE
C
C  CALCULATE THE AVERAGE VELOCITIES.
      JSTOP  = LASTJ+1
      DO 1040 J=1,JSTOP
      VBAR = Q/YZAREA(J)
      UDELT = VU(J)-VBAR
      VU(J) = VBAR
      IF(UDELT.LT.0.0) UDELT = -UDELT
      IF(UDELT.GT.UTEST) UTEST=UDELT
C  UTEST IS USED FOR CONVERGENCE TESTING BY SUBROUTINE STEP.
 1040 CONTINUE
C
C
C  THE ANALYSIS NEXT REQUIRES THAT THE FLEXIBLE SURFACE BE
C  APPROXIMATED WITH A SET OF TRIANGLES RELATED TO THE
C  GLOBAL COORDINATE SYSTEM.
C
      NSTART = NIN+1
      NSTOP = NTUBE+1
      DO 1100 N = NSTART,NSTOP
      MEL = 0
      J = NSTART+NSTOP-N
      JM1 = J-1
      LASTK = NY(J)
      IF(NY(JM1).LT.NY(J)) LASTK=NY(JM1)
      RJ=J-1
      X = RJ*HX
      XJM1 = X-HX
C
C  DEFINE THE ELEMENT CORNERS IN GLOBAL COORDINATES,
C  IN A COUNTER-CLOCKWISE FASHION.
      DO 1200 K =3,LASTK
      RK = K-2
      Y = RK*HY
      KM1 = K-1
      YKM1 = Y-HY
C
      MEL = MEL+1
      XGC(MEL,1) = XJM1
      YGC(MEL,1) = YKM1
      ZGC(MEL,1) = ZMAX(JM1,KM1)
      XGC(MEL,2) = X
      YGC(MEL,2) = YKM1
      ZGC(MEL,2) = ZMAX(J,KM1)
      XGC(MEL,3) = XJM1
      YGC(MEL,3) = Y
      ZGC(MEL,3) = ZMAX(JM1,K)
C
      MEL = MEL+1
      XGC(MEL,1) = XJM1
      YGC(MEL,1) = Y
      ZGC(MEL,1) = ZMAX(JM1,K)
      XGC(MEL,2) = X
      YGC(MEL,2) = YKM1
```

```
      ZGC(MEL,2) = ZMAX(J,KM1)
      XGC(MEL,3) = X
      YGC(MEL,3) = Y
      ZGC(MEL,3) = ZMAX(J,K)
C
 1200 CONTINUE
C
C  AN EXTRA ELEMENT MAY BE NECESSARY IF THE TUBE WALL IS ANGLED.
C  THE FOLLOWING LOGIC DEFINES IT.
      RK = LASTK-2
      Y = RK*HY
      YU = Y
      YD = Y
      ZU = ZMAX(JM1,LASTK)
      ZD = ZMAX(J,LASTK)
      IF(NY(J).EQ.NY(JM1)) GO TO 1300
      MEL = MEL+1
      IF(NY(J).GT.NY(JM1)) GO TO 1250
C  THE FOLOWING SECTION IS FOR NY(J).LT.NY(JM1)
      XGC(MEL,1) = XJM1
      YGC(MEL,1) = Y
      ZGC(MEL,1) = ZMAX(JM1,LASTK)
      XGC(MEL,2) = X
      YGC(MEL,2) = Y
      ZGC(MEL,2) = ZMAX(J,LASTK)
      XGC(MEL,3) = XJM1
      YGC(MEL,3) = Y+HY
      ZGC(MEL,3) = ZMAX(JM1,LASTK+1)
      YU = Y + HY
      YD = Y
      ZU = ZMAX(JM1,LASTK+1)
      ZD = ZMAX(J,LASTK)
      GO TO 1300
C
C  THIS LOGIC IS FOR NY(J).GT.NY(JM1)
 1250 XGC(MEL,1) = XJM1
      YGC(MEL,1) = Y
      ZGC(MEL,1) = ZMAX(JM1,LASTK)
      XGC(MEL,2) = X
      YGC(MEL,2) = Y
      ZGC(MEL,2) = ZMAX(J,LASTK)
      XGC(MEL,3) = X
      YGC(MEL,3) = Y+HY
      ZGC(MEL,3) = ZMAX(J,LASTK+1)
      YU = Y
      YD = Y+HY
      ZU = ZMAX(JM1,LASTK)
      ZD = ZMAX(J,LASTK+1)
C
C  THE FOLLOWING LOGIC DEFINES THE LAST TWO ELEMENTS.
 1300 MEL = MEL+1
      XGC(MEL,1) = XJM1
      YGC(MEL,1) = YU
      ZGC(MEL,1) = ZU
      XGC(MEL,2) = X
      YGC(MEL,2) = YD
      ZGC(MEL,2) = ZD
      XGC(MEL,3) = XJM1
      YGC(MEL,3) = YMAX(JM1)
      ZGC(MEL,3) = 0.0
C
      MEL = MEL+1
      XGC(MEL,1) = XJM1
      YGC(MEL,1) = YMAX(JM1)
      ZGC(MEL,1) = 0.0
      XGC(MEL,2) = X
      YGC(MEL,2) = YD
      ZGC(MEL,2) = ZD
      XGC(MEL,3) = X
      YGC(MEL,3) = YMAX(J)
      ZGC(MEL,3) = 0.0
C
C
C  NEXT, COMPUTE THE ELEMENT AREAS AND CORNER LOCATIONS IN LOCAL COORDS.
      SMAX(J-NIN) = 0.0
      SMSUM(J-NIN) = 0.0
      DO 1400 L = 1,MEL
      X31 = XGC(L,3)-XGC(L,1)
      Y31 = YGC(L,3)-YGC(L,1)
      Z31 = ZGC(L,3)-ZGC(L,1)
      X21 = XGC(L,2)-XGC(L,1)
      Y21 = YGC(L,2)-YGC(L,1)
      Z21 = ZGC(L,2)-ZGC(L,1)
C  AREA IS 1/2 R21 CROSS R31
      AX = (Y21*Z31-Z21*Y31)/2.0
      AY = (Z21*X31 - X21*Z31)/2.0
      AZ = (X21*Y31 - Y21*X31)/2.0
      SAREA = DSQRT(AX*AX + AY*AY + AZ*AZ)
C
      DXBAR = (X21 + X31)/3.0 - HX
      SMSUM(J-NIN) = SMSUM(J-NIN) + AX*DXBAR/HX
C SMSUM IS A TERM IN THE MOMENTUM BALANCE EQUATION.
      SMAX(J-NIN) = SMAX(J-NIN) + SAREA
C SMAX STORES THE INCREMENTAL WALL AREA BETWEEN SUCCESSIVE X=C PLANES.
C
 1400 CONTINUE
C
       SMSUM(J-NIN) = 4.0*SMSUM(J-NIN)
       SMAX(J-NIN) = 4.0*SMAX(J-NIN)
C
 1100 CONTINUE
C
C  SMOOTH THE INTEGRAL VALUES
C  THE TERMS ARE TREATED AS FUNCTIONS OF X AND MUST BE SMOOTHED IN
C  ORDER TO REDUCE COMPUTATIONAL IRREGULARITIES.
      NDIM = NTUBE-NIN+1
      CALL SE13(SMAX,AXBAR,NDIM,IER)
      CALL SE13(SMSUM,SUMBAR,NDIM,IER)
C
C******************COMPUTE THE FLUID VARIABLES************************
      PTEST=0.0
      DO 1600 N=NSTART,NSTOP
      J=NSTART+NSTOP-N
      JM1=J-1
C  SET THE DOWNSTREAM PRESSURE.
      PD = P(J)
C
C  SET THE VISCOUS FORCES
      ABAR = YZAREA(J)
      VBAR = VU(J)
```

```
      HD = 4.0*ABAR/RLS
      TAU = 8.0*RMU*VBAR/HD
C
C  CALCULATE THE UPSTREAM PRESSURE FROM THE MOMENTUM BALANCE EQN.
      PU = PD + (RHO*Q*(VU(J)-VU(JM1)) + TAU*AXBAR(J-NIN))
     $           /(YZAREA(JM1)+SUMBAR(J-NIN))
C
C  CALCULATE THE SLOPE OF THE PRESSURE DISTRIBUTION.
      A = (PD-PU)/HX
C  CALCULATE THE PRESSURE CHANGE FOR THE CONVERGENCE TESTING.
      PDELT = PU - P(JM1)
C
C  STORE THE PRESSURE VALUES
      P(JM1) = PU
      PXB(JM1) = A
C
C  SET THE CONVERGENCE TEST VALUE
      IF(PDELT.LT.0.0) PDELT=-PDELT
      IF(PDELT.GT.PTEST) PTEST=PDELT
C
 1600 CONTINUE
C
      RETURN
      END
```

APPENDIX C

SUBROUTINE FORCES

The purpose of this subroutine was to calculate the equivalent nodal forces exerted on the structure by the loads. Inputs were the hydrostatic collapsing pressure, P_e, and the internal fluid pressure, P. It was assumed that the fluid viscous forces on the wall are negligible. The effects of curvature were not included in the external loading calculations. The surface average internal pressure, $\overline{P}_i$, is used in the analysis. For arbitrary element n this is

$$\overline{P}_{in} = \frac{1}{A_n} \int_n P dA \tag{67}$$

$$\overline{P}_{in} = (P_1 + P_2 + P_3)_n/3 \tag{68}$$

Thus, the magnitude of the outward directed net force acting on the element is

$$F_e = (\overline{P}_{in} - P_e) A_n \tag{69}$$

This force is distributed uniformly at the nodes. To compute the total force vector, the forces are vectorily added at the three nodes, in turn. When contributions from all of the elements are summed, the total external force vector, $\underset{\sim}{F}_e$, is obtained.

```
      SUBROUTINE FORCES
C
C THE PURPOSE OF THIS ROUTINE IS TO COMPUTE THE EQUIVALENT SET
C OF NODAL FORCES.
C
C
      COMMON D(4,4),PSI(450),STRAIN(300,4),CI(12,12),H(6,12),VOL
      COMMON STIFF(82215)
      COMMON VU(23),P(23),NY(23),PXB(23)
      COMMON XNODE(200),YNODE(200),ZNODE(200),IELEM(300,3)
      COMMON F(405),YMAX(23),ZMAX(23,18)
      COMMON XO(135),YO(135),ZO(135),TR(300,10),SIGMA(300,4),NDOF(200)
      COMMON TX(200),TXO(200)
      COMMON DXIN,DXOUT,THK,RLS,FMU,E,P1,P2,PE,IIN,IOUT
      COMMON R,RHO,RL,DIA,Q,DPDX,REY,RMU,RNU,DRO
      COMMON UTEST,PTEST,DMAX,DP,DU,DPSI,SCALE
      COMMON LASTEL,LASTND,NELEM,NNODES,NIN,NTUBE,LASTJ,INFLAG
      COMMON NX,NNY,NTUBEX,NTUBEY,HX,HY,NUMBC
      COMMON IFORCE,TWX,TWY,TWZ,SIGXO,XC,YC
      DOUBLE PRECISION D,PSI,STRAIN,CI,H,VOL,STIFF
C
C THE FOLLOWING ARE PROGRAM SPECIFIC VARIABLES.
      DIMENSION XB(300,3),YB(300,3),ZB(300,3)
      DOUBLE PRECISION X21,Y21,Z21,X31,Y31,Z31
      DOUBLE PRECISION AX,AY,AZ,AREA
C
C INITIALIZE THE FORCES
      LAST = 4*NNODES + (NTUBEX-1)*NTUBEY*2
 1201 DO 1200 MM = 1,LAST
      F(MM) = 0.0
 1200 CONTINUE
C
C
C THE FOLLOWING LOOP IS THE CONTROLLING LOOP, EACH ELEMENT MUST BE
C LOOKED AT IN TURN.
      DO 1210  M = 1,NELEM
C
C
C RECOVER THE ELEMENT NODES IN THE CORRECT ORDER.
C IT IS IMPORTANT TO OBTAIN THE OUTWARD POINTED DIRECTION, HENCE
C THE NODES WERE STORED IN A COUNTER-CLOCKWISE FASHION.
 1310 NODE1 = IELEM(M,1)
      NODE2 = IELEM(M,3)
      NODE3 = IELEM(M,2)
 1311 XB(M,1) = XNODE(NODE1)
      YB(M,1) = YNODE(NODE1)
      ZB(M,1) = ZNODE(NODE1)
      XB(M,2) = XNODE(NODE2)
      YB(M,2) = YNODE(NODE2)
      ZB(M,2) = ZNODE(NODE2)
      XB(M,3) = XNODE(NODE3)
      YB(M,3) = YNODE(NODE3)
      ZB(M,3) = ZNODE(NODE3)
C
      X21 = XB(M,2) - XB(M,1)
      Y21 = YB(M,2) - YB(M,1)
      Z21 = ZB(M,2) - ZB(M,1)
      X31 = XB(M,3) - XB(M,1)
      Y31 = YB(M,3) - YB(M,1)
      Z31 = ZB(M,3) - ZB(M,1)
C CALCULATE THE AREA AND OUTWARD POINTED NORMAL.
C  AREA = 1/2(R21 CROSS R31)
      AX = (Y21*Z31 - Z21*Y31)/2.0
      AY = (Z21*X31 - X21*Z31)/2.0
      AZ = (X21*Y31 - Y21*X31)/2.0
      AREA     = DSQRT(AX*AX+AY*AY+AZ*AZ)
C
C
C TEST FOR THE SPECIFIED FORCE CONDITION.
      IF(IFORCE.EQ.0) GO TO 1215
      GO TO 3010
 1215 XGC = (XB(M,1) + XB(M,2) + XB(M,3))/3.0
      RX = RL+DXIN+DXOUT-XGC
      PW = P2 - RX*DPDX
      GO TO 1250
C
 3010 SUM = 0.0
      DO 3020 I=1,3
      J = XB(M,I)/HX
      J = J+1
      RJ = J-1
      PX = PXB(J)
      SUM = SUM + P(J) + PX*(XB(M,I)-RJ*HX)
 3020 CONTINUE
      PW = SUM/3.0
C
C THE FORCES ARE  AREA*STRESSES, DISTRIBUTED EQUALLY.
 1250 AREAX = AX
      AREAY = AY
      AREAZ = AZ
      FX = (PW-PE)*AREAX/3.0 + TWX*AREA/3.0
      FY = (PW-PE)*AREAY/3.0+ TWY*AREA/3.0
      FZ = (PW-PE)*AREAZ/3.0 + TWZ*AREA/3.0
C CONSTRUCT THE FORCE VECTOR
      N = 4*NODE1 - 3
      F(N) = F(N) + FX
      F(N+1) = F(N+1) + FY
      F(N+2) = F(N+2) + FZ
      N = 4*NODE2 - 3
      F(N) = F(N) + FX
      F(N+1) = F(N+1) + FY
      F(N+2) = F(N+2) + FZ
      N = 4*NODE3 - 3
      F(N) = F(N) + FX
      F(N+1) = F(N+1) + FY
      F(N+2) = F(N+2) + FZ
C
 1210 CONTINUE
C
      RETURN
      END
```

APPENDIX D

SUBROUTINE STEP

The goal of this subroutine was to compute the vector of incremental displacements. This included application of the boundary conditions, inversion of the stiffness matrix, and comparison of variables to the convergence criteria.

Two planes of symmetry were assumed in order to reduce computations, these being the x-z and x-y planes as shown in Figure 24. Here, the y = 0 edge must be restrained from y motion and rotation ($v, \Delta\theta_x = 0$), while the z = 0 edge must be restrained from z motion and rotation ($w, \Delta\theta_x = 0$). In addition, the ends of the flexible tube were fastened to rigid supports; consequently, the ends are assumed to be simply supported ($u, v, w = 0$) and held in the hoop direction, $\Delta\theta_x = 0$.

Given the formulation of the augmented stiffness matrix discussed in Chapter III, the problem was to evaluate:

$$\begin{Bmatrix} d\underset{\sim}{q}^n \\ \underset{\sim}{\lambda}^n \end{Bmatrix} = - \begin{bmatrix} [K_T]^n & [CC]^{T\ n} \\ [CC]^n & [0] \end{bmatrix}^{-1} \begin{Bmatrix} \underset{\sim}{\psi}^n \\ \underset{\sim}{0} \end{Bmatrix} \qquad (23)$$

at computation step n.

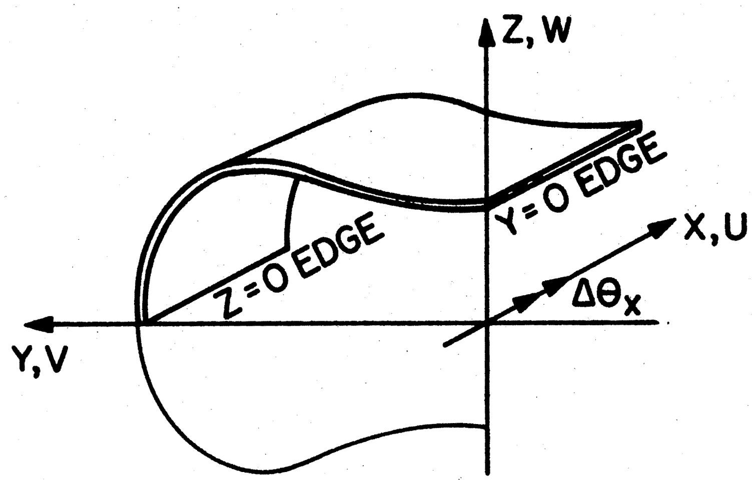

Figure 24. Cutaway View of the Tube Showing Nomenclature of the Boundary Conditions

The boundary conditions are enforced by zeroing out the appropriate row and column of the stiffness matrix, excluding the diagonal. The appropriate row of the Ψ vector is also zeroed. Thus, an incremental step, dq = 0, is computed for all constrained degrees of freedom.

In order to ensure convergence to an accurate prediction, the step size, dq, must be kept "small." If dq is allowed to become excessive, then the approximation of constant external forces during the step becomes a poor one. Furthermore, the nonlinearities may lead to convergence at a non-physical prediction. One way to ensure the smallness of dq is to test the maximum in the vector against some smallness criteria, eps. If the criteria is exceeded, then the entire vector is scaled so that the maximum is acceptable. That is, if

$$\max \left| \underset{\sim}{dq} \right| > eps \qquad (70)$$

then,

$$\max S \left| \underset{\sim}{dq} \right| \leq eps \qquad (71)$$

The net effect of this process is the same as if a smaller force were originally applied to produce the smaller displacement associated with eps.

A mini-maximum in the global Z position of the nodes is used to determine the smallness criteria. The structure is separated into a set of hoopwise rings. For each ring, the maximum Z coordinate of all nodes on the ring is calculated. The maximum allowable step is then determined to be a preset fraction of the <u>smallest</u> Z-maximum. Thus, the maximum step adjusts to the changing shape of the tube: it shrinks as the tube collapses.

Contact of opposite walls occurs when $z = 0$ occurs at an unconstrained node. In this scheme, $z < 0$ is tested for on each step. When this condition is detected, the dq vector is scaled so that $z = 0$ is established. The appropriate degrees of freedom (dW and $\Delta\theta_x$) are then constrained from further motion in the same manner as the boundary conditions are enforced.

Numerical convergence is assessed in three ways simultaneously based on changes in pressure, velocity, and wall position. The problem of numerical convergence becomes acute when very small cross-sectional areas are encountered at extreme collapse conditions. At this point, very small changes in wall position will produce large changes in the fluid pressure gradient through fluid viscous forces. Hence, at this time a pressure criteria is suitable for convergence testing. Conversely, at only slightly collapsed shapes, viscous effects are minimal and a wall position criterion may be best. At intermediate times, a combination of these or a velocity criteria may be best. To simply enforce a very small wall position criteria at all times would be computationally wasteful; hence, a multiple criteria is advantageously used.

```
      SUBROUTINE STEP(LOUT)
C
C  THIS SUBROUTINE APPLIES THE BOUNDARY CONDITIONS, COMPUTES THE
C  INVERSION OF THE AUGMENTED STIFFNESS MATRIX, AND TESTS FOR
C  CONVERGENCE.  THE PARAMETER LOUT INDICATES CONVERGENCE TO THE
C  CALLING PROGRAM,
C                     LOUT = 1 IS A CONVERGED SOLUTION
C                     LOUT = 0 IS AN UNCONVERGED SOLUTION
C
      COMMON D(4,4),PSI(450),STRAIN(300,4),CI(12,12),H(6,12),VOL
      COMMON STIFF(82215)
      COMMON VU(23),P(23),NY(23),PXB(23)
      COMMON XNODE(200),YNODE(200),ZNODE(200),IELEM(300,3)
      COMMON F(405),YMAX(23),ZMAX(23.18)
      COMMON XO(135),YO(135),ZO(135),TR(300,10),SIGMA(300,4),NDOF(200)
      COMMON TX(200),TXO(200)
      COMMON DXIN,DXOUT,THK,RLS,FMU,E,P1,P2,PE,IIN,IOUT
      COMMON R,RHO,RL,DIA,Q,DPDX,REY,RMU,RNU,DRO
      COMMON UTEST,PTEST,DMAX,DP,DU,DPSI,SCALE
      COMMON LASTEL,LASTND,NELEM,NNODES,NIN,NTUBE,LASTJ,INFLAG
      COMMON NX,NNY,NTUBEX,NTUBEY,HX,HY,NUMBC
      COMMON IFORCE,TWX,TWY,TWZ,SIGXO,XC,YC
      DOUBLE PRECISION D,PSI,STRAIN,CI,H,VOL,STIFF
C
C  THE FOLLOWING ARE PROGRAM SPECIFIC VARIABLES.
      DIMENSION AUX(404),RO(450)
      DOUBLE PRECISION AUX,SCALEF
C
      LAST = 4*NNODES + (NTUBEX-1)*NTUBEY*2
      LASTP = 4*NNODES
C
C  APPLY THE CONSTRAINED DEGREES OF FREEDOM TO PSI.
      DO 1890 M = 1,NUMBC
      J = NDOF(M)
      PSI(J) = 0.0
 1890 CONTINUE
C
C
C
C  APPLY THE  CONSTRAINTS TO STIFF
 1680 DO 1590 M = 1,NUMBC
      J = NDOF(M)
      K = J
      ISTART = K+1
      IF(ISTART.GT.LAST) GO TO 1576
      DO 1575 KL = ISTART,LAST
      N = J + KL*(KL-1)/2
      STIFF(N) = 0.0
 1575 CONTINUE
 1576 ISTOP = J-1
      IF(ISTOP.LT.1) GO TO 1590
      DO 1585 JL = 1,ISTOP
      N = JL + K*(K-1)/2
      STIFF(N) = 0.0
 1585 CONTINUE
C
 1590 CONTINUE
C
C
C ***********INVERSION OF THE AUGMENTED GLOBAL STIFFNESS MATRIX.*******
C  SSP ROUTINE TO FIND DEFLECTIONS, PSI STORES THE DEFECTIONS ON RETURN
 1695 CALL DGELS(PSI,STIFF,LAST,1,1.0E-13,IER,AUX)
      IF(IER) 1513,1512,1513
 1513 WRITE(IOUT,1511) IER
 1511 FORMAT(1H ,5X,6HIER = ,I3,26H,-1 IS A SINGULAR K MATRIX  )
      STOP
C
C FIND THE MINI-MAX
 1512 N=0
      SMALL = R-DRO
      NTX = NTUBEX+1
      NTY = NTUBEY+1
      DO 100 L = 1,NTX
      ZBIG = 0.0
        DO 200 K = 1,NTY
        N = N+1
        IF(ZNODE(N).GT.ZBIG) ZBIG=ZNODE(N)
  200 CONTINUE
      IF(ZBIG.LT.SMALL) SMALL = ZBIG
  100 CONTINUE
C
C  CALCULATE THE MAXIMUM ALLOWABLE STEP.
      ALLOW = SMALL*SCALE
C
C
C COMPUTE THE SCALE FACTOR FOR THE DISPLACEMENT INCREMENTS.
      BIG = 0.0
      DO 1800 J=1,LASTP
      IF(PSI(J).GT.BIG) BIG = PSI(J)
      IF(PSI(J).LT.-BIG) BIG = -PSI(J)
 1800 CONTINUE
      IF(BIG.GT.ALLOW) SCALEF = ALLOW/BIG
      IF(BIG.LE.ALLOW) SCALEF = 1.0
C
C  TEST FOR THE CONTACT OF OPPOSITE WALLS.
      JFLAG = 0
      .. 1571 J=1,NNODES
      IF((PSI(4*J-1)*SCALEF+ZNODE(J)) .LT. 0.0) GO TO 1577
      GO TO 1571
 1577 SCALEF = -ZNODE(J)/PSI(4*J-1)
      JFLAG = J
 1571 CONTINUE
C UPON EXIT FROM THIS LOOP, SCALEF IS THE SMALLEST SCALE FACTOR,
C  THE ONE WHICH PERMITS ONLY ONE NODE AT MOST TO CONTACT.
C
C  SCALE THE DISPLACEMENT INCREMENTS.
      DO 1760 J = 1,LASTP
      RO(J) = SCALEF*PSI(J)
 1760 CONTINUE
C
C  COMPUTE THE NEW NODE POSITIONS
 1597 DO 1570 J = 1,NNODES
          XNODE(J) = XNODE(J) + RO(4*J-3)
          YNODE(J) = YNODE(J) + RO(4*J-2)
          ZNODE(J) = ZNODE(J) + RO(4*J-1)
          TX(J)  = TX(J) + RO(4*J)
        IF(J.NE.JFLAG) GO TO 1570
          ZNODE(J) = 0.0
          NUMBC = NUMBC + 1
```

```
         NDOF(NUMBC) = 4*J-1
C  CONTACT OF OPPOSITE WALLS MEANS THAT THE SLOPE IS ZERO TOO.
         TX(J) = 0.0
         NUMBC = NUMBC + 1
         NDOF(NUMBC) = 4*J
 1570 CONTINUE
C***********************CONVERGENCE TESTING****************************
 1910 ICONV = 0
      IF(UTEST.GT.DU) GO TO 1655
      IF(PTEST.GT.DP) GO TO 1655
      ICONV = 1
C
C  FIND THE MAXIMUM RO VALUE
 1655 DMAX = 0.0
      DO 1660 L = 1,LASTP
      TESTP = ABS(RO(L))
      IF(TESTP.LE.DMAX) GO TO 1660
      DMAX = TESTP
      ROOUT = RO(L)
 1660 CONTINUE
      WRITE(IOUT,1656) UTEST,PTEST,ROOUT
 1656 FORMAT(1H ,2X,8HDUMAX = ,E12.5,9H DPMAX = ,E12.5,10H  ROMAX = ,
     $E12.5)
      IF(DMAX.GT.DPSI .OR. JFLAG.GT.0) GO TO 1598
      IF(ICONV) 1598,1598,1665
C
C  THE ONLY WAY TO ACHIEVE LOUT=1 IS FOR ALL PARTS TO CONVERGE.
C  SET CONVERGENCE FLAG FOR THE SOLUTION.
 1665 LOUT = 1
C
C
 1598 RETURN
      END
```

APPENDIX E

SUBROUTINE INIT

The purpose of this subroutine was to establish the initial database prior to the iterative solution process. This goal is accomplished via the following tasks:

1. Establish the initial node locations.
2. Set the initial constrained degrees of freedom according to the boundary conditions.
3. Make the nodal connections which define the finite elements. This also sets the direction of the local axes.
4. Build the constant matrices:

    [C]

    [CI]

    [H]

    [TR]
5. Define other necessary constants.

```
      SUBROUTINE INIT
C
C  THIS SUBROUTINE INITIALIZES THE SHAPE OF THE TUBE AND FLUID
C  MECHANICAL PARAMETERS PRIOR TO THE ACTUAL SOLUTION ITERATION.
C
      COMMON D(4,4),PSI(450),STRAIN(300,4),CI(12,12),H(6,12),VOL
      COMMON STIFF(82215)
      COMMON VU(23),P(23),WY(23),PXB(23)
      COMMON XNODE(200),YNODE(200),ZNODE(200),IELEM(300,3)
      COMMON F(405),YMAX(23),ZMAX(23,18)
      COMMON XO(135),YO(135),ZO(135),TR(300,10),SIGMA(300,4),NDOF(200)
      COMMON TX(200),TXO(200)
      COMMON DXIN,DXOUT,THK,RLS,FMU,E,P1,P2,PE,IIN,IOUT
      COMMON R,RHO,RL,DIA,Q,DPDX,REY,RMU,RNU,DRO
      COMMON UTEST,PTEST,DMAX,DP,DU,DPSI,SCALE
      COMMON LASTEL,LASTND,NELEM,NNODES,NIN,NTUBE,LASTJ,INFLAG
      COMMON NX,NNY,NTUBEX,NTUBEY,HX,HY,NUMBC
      COMMON IFORCE,TWX,TWY,TWZ,SIGXO,XC,YC
      DOUBLE PRECISION D,PSI,STRAIN,CI,H,VOL,STIFF
C
C THE FOLLOWING VARIABLES ARE USED INTERNAL TO THIS ROUTINE ONLY.
C
      DIMENSION XB(300,3),YB(300,3),ZB(300,3)
      DIMENSION MIN(8),MOUT(8),C(144),DUM3(12),DUM4(12)
      DIMENSION MOL(12),MOM(12),YEDGE(12)
      DIMENSION SIGMAG(3),DUM1(3,3),DUM2(3,3),STRESS(3,3)
      DIMENSION DPT(12,12)
      DOUBLE PRECISION X21,Y21,Z21,X31,Y31,Z31,AX,AY,AZ,AREA,DTHK,DIST21
      DOUBLE PRECISION SIGMAG,DUM1,DUM2,STRESS
      DOUBLE PRECISION DUM3,C,DPT,DET,DUM4
C
C THE FOLLOWING CALCULATIONS ARE FOR THE INITIAL, ELLIPTIC SHAPE.
      A = R+DRO
      B = R-DRO
      ASQ = A*A
      BSQ = B*B
      YEDGE(1) = 0.0
      YEDGE(2) = 0.1651
      YEDGE(3) = 0.3302
      YEDGE(4) = 0.4890
      YEDGE(5) = 0.6312
      YEDGE(6) = 0.7430
      YEDGE(7) = 0.7938
      DIA = SQRT(4*A*B)
C
C CALCULATE THE FLUID MECHANICAL PARAMETERS.
      RMU = RNU*RHO
      REY = 4.0*Q/RMU/DIA/3.1416
      IF(IFORCE) 145,150,145
  145 DPDX = -4.0*(ASQ + BSQ)*RMU*Q/(A*ASQ*B*BSQ*3.1416)
  150 P1 = P2 - DPDX*(DXIN+RL+DXOUT)
C
      WRITE(IOUT,152) DIA
  152 FORMAT(1H1,5X,31HTHE INLET HYDRAULIC DIAMETER IS ,F7.2,4H CM.)
      WRITE(IOUT,151) RL
  151 FORMAT(1H ,5X,15HTHE LENGTH IS   , F7.2,4H CM.)
      WRITE(IOUT,153) P2
  153 FORMAT(1H ,5X,28HTHE DOWNSTREAM PRESSURE IS  ,F9.2,12H DYNES/SQCM.
     $)
      WRITE(IOUT,156) Q
  156 FORMAT(1H ,5X,15HTHE FLOWRATE IS, F7.2,10H CUCM/SEC.)
      WRITE(IOUT,154) REY
  154 FORMAT(1H ,5X,29HTHE INLET REYNOLDS NUMBER IS ,F7.1)
      WRITE(IOUT,155) P1
  155 FORMAT(1H ,5X,43HTHE INITIAL ESTIMATE OF THE INLET PRESSURE ,F9.1,
     $12H DYNES/SQCM.)
C
C  FILL D, THE MATERIAL STRESS-STRAIN RELATIONSHIP MATRIX
      DO 1100 J = 1,4
      DO 1100 K = 1,4
 1100 D(J,K) = 0.0
      RD = E/(1.0-FMU*FMU)
      D(1,1) = RD
      D(1,2) = RD*FMU
      D(2,1) = RD*FMU
      D(2,2) = RD
      D(3,3) = RD/2.0*(1.0-FMU)
      D(4,4) = RD*THK*THK/12.0
C
C*****************BOUNDARY DEFINITION AND TUBE INITIALIZATION***********
C SET THE PARAMETERS FOR THE AUTOMATIC TUBE DEFINITION.
      NTX = NTUBEX + 1
      NTY = NTUBEY + 1
      RNTX = NTUBEX
      RNTY = NTUBEY
      DX = RL/RNTX
      DTHETA = 3.14159265/2.0/RNTY
      NNODES = 0
      NELEM = 0
      NUMBC = 0
      JSTOP = NTX
      KSTOP = NTY
C   INITIALIZE TUBE SHAPE
C   THIS SECTION DEFINES THE TUBE ITSELF WITH PROPER CONSTRAINTS.
      DO 1110 J = 1,JSTOP
      RJ = J -1
      X = DXIN + RJ*DX
      NELEM = (J-2)*2*NTUBEY
      DO 1110 K = 1,KSTOP
      RK = K-1
C ************DEFINE THE INITIAL POSITIONS OF THE NODES**********
      THETA = RK*DTHETA
      Y = YEDGE(K)
      Z = B*SQRT(1.0-Y*Y/ASQ)
      NNODES = NNODES + 1
      IF(J.EQ.1) MIN(K) = NNODES
      IF(J.EQ.JSTOP) MOUT(K) = NNODES
 1118 XNODE(NNODES) = X
      YNODE(NNODES) = Y
      ZNODE(NNODES) = Z
      DENOM = SQRT(ASQ-Y*Y)
      IF(DENOM.GT.0.00001) GO TO 2000
      THETAX = -THETA
      GO TO 2100
 2000 THETAX = ATAN(-B*Y/A/DENOM)
 2100 XO(NNODES) = X
      YO(NNODES) = Y
      ZO(NNODES) = Z
      TXO(NNODES) = THETAX
```

```
      TX(NNODES) = TXO(NNODES)
      IF(K.LT.KSTOP) GO TO 1104
         ZNODE(NNODES) = 0.0
         ZO(NNODES) = 0.0
C ***************IDENTIFY THE CONSTRAINED DEGREES OF FREEDOM*********
 1104 IF(J.EQ.1.OR.J.EQ.JSTOP) GO TO 1106
      GO TO 1107
 1106 NUMBC = NUMBC + 1
      N = 4*NNODES-3
      NDOF(NUMBC) = N
      NUMBC = NUMBC+1
      N = 4*NNODES - 2
      NDOF(NUMBC) = N
      NUMBC = NUMBC + 1
      N = 4*NNODES - 1
      NDOF(NUMBC) = N
      NUMBC = NUMBC + 1
      N = 4*NNODES
      NDOF(NUMBC) = N
      GO TO 1115
 1107 IF(K.EQ.1) GO TO 1108
      GO TO 1109
 1108 NUMBC = NUMBC + 1
      N = 4*NNODES - 2
      NDOF(NUMBC) = N
      NUMBC = NUMBC+1
      N = 4*NNODES
      NDOF(NUMBC) = N
      GO TO 1115
 1109 IF(K.EQ.KSTOP) GO TO 1111
      GO TO 1115
 1111 NUMBC = NUMBC + 1
      N = 4*NNODES-1
      NDOF(NUMBC) = N
      NUMBC = NUMBC+1
      N = 4*NNODES
      NDOF(NUMBC) = N
C ***************CONNECT THE NODES TO MAKE THE ELEMENTS*************
 1115 IF(J.EQ.1 .OR. K.EQ.1) GO TO 1110
      NELEM = NELEM + 1
      M = NELEM
      IELEM(M,1) = NNODES-NTY
      IELEM(M,2) = NNODES
      IELEM(M,3) = NNODES-NTY-1
C
      M = NELEM + NTUBEY
      IELEM(M,1) = NNODES-1
      IELEM(M,2) = NNODES-NTY-1
      IELEM(M,3) = NNODES
 1110 CONTINUE
      NELEM = 2*NTUBEX*NTUBEY
C
C A SET OF CONTROLLING PARAMETERS MUST BE DEFINED FOR THE INLET
C AND OUTLET MOUNTING TUBES IN ORDER TO DISTINGUISH THEM FROM THE
C FLEXIBLE TUBE.
      LASTEL = NELEM
      LASTND = NNODES
      NTX = 2
      RNTX = NTX
C
      DX = DXOUT/RNTX
C
C ***************DEFINE THE RIGID OUTLET MOUNTING FIXTURE.**************
      DO 1120 J = 1,NTX
      RJ = J
      X = RJ*DX + RL + DXIN
      DO 1120 K = 1,NTY
      RK = K-1
      THETA = RK*DTHETA
      DR = DRO*COS(2.0*THETA)
      Y = (R-DR)*SIN(THETA)
      Z = (R-DR)*COS(THETA)
      LASTND = LASTND + 1
      XNODE(LASTND) = X
      YNODE(LASTND) = Y
      ZNODE(LASTND) = Z
      IF(K.LT.NTY) GO TO 1125
         YNODE(LASTND) = R+DRO
         ZNODE(LASTND) = 0.0
 1125 IF(K.EQ.1) GO TO 1120
      N = LASTND-NTY
      NM1 = N-1
      IF(J.EQ.1) N = MOUT(K)
      IF(J.EQ.1) NM1 = MOUT(K-1)
 1130 LASTEL = LASTEL + 1
      IELEM(LASTEL,1) = NM1
      IELEM(LASTEL,2) = LASTND - 1
      IELEM(LASTEL,3) = LASTND
      LASTEL = LASTEL + 1
      IELEM(LASTEL,1) = NM1
      IELEM(LASTEL,2) = LASTND
      IELEM(LASTEL,3) = N
 1120 CONTINUE
C
C ***************DEFINE THE RIGID INLET MOUNTING FIXTURE.*************
      DX = DXIN/RNTX
      DO 1150 J = 1,NTX
      RJ = J
      X = DXIN - DX*RJ
      DO 1150 K = 1,NTY
      RK = K-1
      THETA = RK*DTHETA
      DR = DRO*COS(2.0*THETA)
      Y = (R-DR)*SIN(THETA)
      Z = (R-DR)*COS(THETA)
      LASTND = LASTND + 1
      XNODE(LASTND) = X
      YNODE(LASTND) = Y
      ZNODE(LASTND) = Z
      IF(K.LT.NTY) GO TO 1155
         YNODE(LASTND) = R+DRO
         ZNODE(LASTND) = 0.0
 1155 IF(K.EQ.1) GO TO 1150
C  PATCH INLET TO THE FLEXIBLE TUBE
      N = LASTND - NTY
      NM1 = N-1
      IF(J.EQ.1) N = MIN(K)
      IF(J.EQ.1) NM1 = MIN(K-1)
 1160 LASTEL = LASTEL + 1
      IELEM(LASTEL,1) = LASTND - 1
```

```
      IELEM(LASTEL,2) = NM1
      IELEM(LASTEL,3) = LASTND
      LASTEL = LASTEL + 1
      IELEM(LASTEL,1) = LASTND
      IELEM(LASTEL,2) = NM1
      IELEM(LASTEL,3) = N
 1150 CONTINUE
C
C  SET FLAG TO SIGNAL SUBROUTINE MESH THAT INITIALIZATION WAS RUN.
      INFLAG = 1
C
C
C  CALCULATE  ROTATIONS  TO  GLOBAL  COORDINATES FOR ALL ELEMENTS
C THAT ARE PART OF THE FLEXIBLE TUBE.
      DO 1140 M = 1,NELEM
      NODE1 = IELEM(M,1)
      XB(M,1) = XO(NODE1)
      YB(M,1) = YO(NODE1)
      ZB(M,1) = ZO(NODE1)
      NODE2 = IELEM(M,2)
      XB(M,2) = XO(NODE2)
      YB(M,2) = YO(NODE2)
      ZB(M,2) = ZO(NODE2)
      NODE3 = IELEM(M,3)
      YB(M,3) = YO(NODE3)
      ZB(M,3) = ZO(NODE3)
      XB(M,3) = XO(NODE3)
C
      X21 = XB(M,2) - XB(M,1)
      Y21 = YB(M,2) - YB(M,1)
      Z21 = ZB(M,2) - ZB(M,1)
      X31 = XB(M,3) - XB(M,1)
      Y31 = YB(M,3) - YB(M,1)
      Z31 = ZB(M,3) - ZB(M,1)
C  CALCULATE THE NORMAL FROM THE AREA VECTOR
C   AREA = 1/2(R21 CROSS R31)
      AX = (Y21*Z31 - Z21*Y31)/2.0
      AY = (Z21*X31 - X21*Z31)/2.0
      AZ = (X21*Y31 - Y21*X31)/2.0
      AREA     = DSQRT(AX*AX+AY*AY+AZ*AZ)
      XN = AX/AREA
      YN = AY/AREA
      ZN = AZ/AREA
C
C
C  THE LOCAL X-AXIS IS R21
      DIST21 = DSQRT(X21*X21+Y21*Y21+Z21*Z21)
      XX = X21/DIST21
      XY = Y21/DIST21
      XZ = Z21/DIST21
      TR(M,1) = XX
      TR(M,2) = XY
      TR(M,3) = XZ
C  THE LOCAL Y-AXIS IS Z CROSS X
      TR(M,4) = YN*XZ - ZN*XY
      TR(M,5) = ZN*XX - XN*XZ
      TR(M,6) = XN*XY - YN*XX
C  THE NORMAL IS THE LOCAL Z-AXIS
      TR(M,7) = XN
      TR(M,8) = YN
      TR(M,9) = ZN
C  THE TRANSFORMATION FOR THE ANGLULAR DEFLECTION.
      TR(M,10) = XX
C
C  BUILD THE ROTATION MATRIX.
      DO 1505 J = 1,12
      DO 1505 K = 1,12
 1505 DPT(J,K) = 0.0
      L=0
      DO 1506 J = 1,3
      DO 1506 K = 1,3
      L = L+1
      DPT(J,K) = TR(M,L)
      DPT(J+4,K+4) = DPT(J,K)
      DPT(J+8,K+8) = DPT(J,K)
 1506 CONTINUE
      DPT(4,4) = XX
      DPT(8,8) = XX
      DPT(12,12) = XX
C
C
C
C  SET THE INITIAL STRESS VECTOR
      SIGMA(M,1) = SIGXO
      SIGMA(M,2) = 0.0
      SIGMA(M,3) = 0.0
      SIGMA(M,4) = 0.0
C
 1140 CONTINUE
C
C  EXTRACT THE LOCATIONS OF THE ELEMENT CORNERS IN GLOBAL COORDINATES.
C  THE ORIGIN IS ALWAYS AT NODE 1.
      I = IELEM(NELEM,1)
      J = IELEM(NELEM,2)
      K = IELEM(NELEM,3)
      DUM3(1) = 0.0
      DUM3(2) = 0.0
      DUM3(3) = 0.0
      DUM3(4) = 0.0
      DUM3(5) = XO(J) - XO(I)
      DUM3(6) = YO(J) - YO(I)
      DUM3(7) = ZO(J) - ZO(I)
      DUM3(8) = 0.0
      DUM3(9) = XO(K) - XO(I)
      DUM3(10)= YO(K) - YO(I)
      DUM3(11)= ZO(K) - ZO(I)
      DUM3(12)= 0.0
C
C
C  ROTATE THE LOCATIONS TO LOCAL COORDINATES.
      DO 1507 J = 1,12
      DUM4(J) = 0.0
      DO 1507 K = 1,12
 1507 DUM4(J) = DUM4(J) + DPT(J,K)*DUM3(K)
C
C  COMPUTE THE ELEMENT CENTROID. NOTICE THAT THE ELEMENTS ARE ALL
C  THE SAME SIZE, THUS THE CENTROID IS AT THE SAME LOCATION FOR ALL.
      XC = (DUM4(1)+DUM4(5)+DUM4(9))/3.0
      YC = (DUM4(2)+DUM4(6)+DUM4(10))/3.0
C
```

```
C ***********************INTIIALIZE C.*****************************
      DO 1515 J = 1,144
 1515 C(J) = 0.0
C  FILL THE C MATRIX
      C(1) = 1.0
      C(5) = 1.0
      C(9) = 1.0
      C(13) = DUM4(1)
      C(17) = DUM4(5)
      C(21) = DUM4(9)
      C(25) = DUM4(2)
      C(29) = DUM4(6)
      C(33) = DUM4(10)
      C(38) = 1.0
      C(42) = 1.0
      C(46) = 1.0
      C(50) = DUM4(1)
      C(54) = DUM4(5)
      C(58) = DUM4(9)
      C(62) = DUM4(2)
      C(66) = DUM4(6)
      C(70) = DUM4(10)
      C(75) = 1.0
      C(79) = 1.0
      C(83) = 1.0
      C(87) = DUM4(1)
      C(91) = DUM4(5)
      C(95) = DUM4(9)
      C(99) = DUM4(2)
      C(103)= DUM4(6)
      C(107)= DUM4(10)
      C(112)= 1.0
      C(116)= 1.0
      C(120)= 1.0
      C(124)= DUM4(1)
      C(128)= DUM4(5)
      C(132)= DUM4(9)
      C(136)= DUM4(2)
      C(140)= DUM4(6)
      C(144)= DUM4(10)
C
C  COMPUTE THE INVERSE OF C. SUBROUTINE DINV IS AN SSP SUBROUTINE
C  WHICH COMPUTES THE INVERSE IN DOUBLE PRECISION.
      CALL DINV(C,12,DET,MOL,MOM)
      IF(DET) 1517,1516,1517
 1516 WRITE(IOUT,1581)
 1581 FORMAT(1H1,5X,25HTHE C MATRIX IS SINGULAR. )
      STOP
 1517 DO 1580 K = 1,12
      DO 1580 J = 1,12
      N = (K-1)*12 + J
      CI(J,K) = C(N)
 1580 CONTINUE
C
C ***************SET THE H MATRIX.*******************************
      DO 1600 J=1,6
      DO 1600 K=1,12
 1600 H(J,K) = 0.0
C
      H(1,2)  = 1.0
      H(2,5)  = 1.0
      H(3,8)  = 1.0
      H(4,3)  = 1.0
      H(5,6)  = 1.0
      H(6,9)  = 1.0
C
C
C   COMPUTE THE VOLUME OF THE ELEMENTS.
      DTHK = THK
      VOL = AREA*DTHK
C
C
C   CALCULATE THE CARTESIAN MESH SPACING.
      LASTJ = NX
      RNX = NX
      RNY =NNY
      HX = (RL + DXIN + DXOUT)/RNX
      HY = R/RNY
      NIN = DXIN/HX + 1.0
      IF(NIN.LT.2) NIN = 2
      NTUBE = (DXIN + RL)/HX + 1.0
C
C   INITIALIZE THE FLUID PRESSURE
      LAST = LASTJ+1
      P(LAST) = P2
      DO 2150 J=1,LASTJ
      M = LAST-J
      P(M) = P(M+1) - DPDX*HX
 2150 CONTINUE
C
 2200 RETURN
      END
```

APPENDIX F

SUBROUTINE MESH

The goal of this routine was to define the variables necessary to describe the cartesian mesh which is enclosed by the tube and its rigid end mountings. This procedure was greatly simplified by the planar nature of the finite elements since it means that linear interpolation can be used when needed to locate the tube wall. Conceptually, the approach is to establish an x-y grid under the finite element wall approximation. The algorithm then moves through this grid and calculates the z distance to the finite element surface.

```
      SUBROUTINE MESH
C
C  THIS SUBROUTINE COMPUTES THE PARAMETERS NECESSARY TO SPECIFY THE
C  CARTESIAN MESH WHICH IS ENCLOSED BY THE TUBE AND MOUNTING FIXTURES.
C
      COMMON D(4,4),PSI(450),STRAIN(300,4),CI(12,12),H(5,12),VOL
      COMMON STIFF(82215)
      COMMON VU(23),P(23),NY(23),PXB(23)
      COMMON XNODE(200),YNODE(200),ZNODE(200),IELEM(300,3)
      COMMON F(405),YMAX(23),ZMAX(23,18)
      COMMON XO(135),YO(135),ZO(135),TR(300,10),SIGMA(300,4),NDOF(200)
      COMMON TX(200),TXO(200)
      COMMON DXIN,DXOUT,THK,RLS,FMU,E,P1,P2,PE,IIN,IOUT
      COMMON R,RHO,RL,DIA,Q,DPDX,REY,RMU,RNU,DRO
      COMMON UTEST,PTEST,DMAX,DP,DU,DPSI,SCALE
      COMMON LASTEL,LASTND,NELEM,NNODES,NIN,NTUBE,LASTJ,INFLAG
      COMMON NX,NNY,NTUBEX,NTUBEY,HX,HY,NUMBC
      COMMON IFORCE,TWX,TWY,TWZ,SIGXO,XC,YC
      DOUBLE PRECISION D,PSI,STRAIN,CI,H,VOL,STIFF
C
C  THE FOLLOWING ARE ROUTINE SPECIFIC VARIABLES.
      DIMENSION YEDGE(60),ZEDGE(60)
      DIMENSION XB(300,3),YB(300,3),ZB(300,3)
C
C  INITIALIZE THE LOOP PARAMETERS
      JSTART = 2
      JSTOP = LASTJ
      MSTOP = LASTEL
C  IF THE INITIALIZATION HAS JUST BEEN RUN, THE ENTIRE INTERIOR MUST
C  BE ANALYZED, OTHERWISE ONLY THE VOLUME UNDER THE FLEXIBLE TUBE
C  NEED BE ANALYZED.
      IF(INFLAG.EQ.1) GO TO 240
         JSTART = NIN
         JSTOP = NTUBE + 1
C
C
C  REFORMAT THE NODE DEFINITIONS.
  240 DO 330 M = 1,MSTOP
      ID = IELEM(M,1)
      XB(M,1) = XNODE(ID)
      YB(M,1) = YNODE(ID)
      ZB(M,1) = ZNODE(ID)
      ID = IELEM(M,2)
      XB(M,2) = XNODE(ID)
      YB(M,2) = YNODE(ID)
      ZB(M,2) = ZNODE(ID)
      ID = IELEM(M,3)
      XB(M,3) = XNODE(ID)
      YB(M,3) = YNODE(ID)
      ZB(M,3) = ZNODE(ID)
  330 CONTINUE
C
C
C  ARRANGE THE X,Y,Z VALUES OF THE NODES BY X ORDER IN EACH ELEMENT.
C
      DO 230 M =1,MSTOP
      IBIG = 0
      IF(XB(M,2).GE.XB(M,1) .AND. XB(M,2).GE.XB(M,3)) IBIG = 2
      IF(XB(M,3).GE.XB(M,1) .AND. XB(M,3).GE.XB(M,2)) IBIG = 3
      IF(XB(M,1).GE.XB(M,2) .AND. XB(M,1).GE.XB(M,3)) IBIG = 1
      IF(IBIG.EQ.1) GO TO 220
      XSAVE = XB(M,1)
      YSAVE = YB(M,1)
      ZSAVE = ZB(M,1)
      XB(M,1) = XB(M,IBIG)
      YB(M,1) = YB(M,IBIG)
      ZB(M,1) = ZB(M,IBIG)
      XB(M,IBIG) = XSAVE
      YB(M,IBIG) = YSAVE
      ZB(M,IBIG) = ZSAVE
  220 IF(XB(M,2).GE.XB(M,3)) GO TO 230
      XSAVE = XB(M,2)
      YSAVE = YB(M,2)
      ZSAVE = ZB(M,2)
      XB(M,2) = XB(M,3)
      YB(M,2) = YB(M,3)
      ZB(M,2) = ZB(M,3)
      XB(M,3) = XSAVE
      YB(M,3) = YSAVE
      ZB(M,3) = ZSAVE
  230 CONTINUE
C
C
C  THE FOLLOWING LOOP CALCULATES THE Y,Z COORDINATES FOR EACH
C  INTERSECTION OF AN X=C LINE WITH AN ELEMENT EDGE.
C
      DO 410 J = JSTART,JSTOP
      RJ = J - 1
      X = RJ*HX
C  THE NEXT LOOP CALCULATES THE ELIGIBLE ELEMENTS AND THE Y,Z PAIRS.
C  LINEAR INTERPOLATION IS USED.
      ICOUNT = 0
      DO 520 M = 1,MSTOP
      IF(XB(M,1).LT.X .OR. XB(M,3).GE.X) GO TO 520
      ICOUNT = ICOUNT + 1
      YEDGE(ICOUNT) = YB(M,3) + (X-XB(M,3))*(YB(M,1)-YB(M,3))
     $/(XB(M,1)-XB(M,3))
      ZEDGE(ICOUNT) = ZB(M,3) + (X-XB(M,3))*(ZB(M,1)-ZB(M,3))
     $/(XB(M,1)-XB(M,3))
      ICOUNT = ICOUNT + 1
      IF(X.NE.XB(M,2)) GO TO 540
      YEDGE(ICOUNT) = YB(M,2)
      ZEDGE(ICOUNT) = ZB(M,2)
      GO TO 520
  540 IF(X.LT.XB(M,2)) GO TO 530
      YEDGE(ICOUNT) = YB(M,2) + (X-XB(M,2))*(YB(M,1)-YB(M,2))
     $/(XB(M,1)-XB(M,2))
      ZEDGE(ICOUNT) = ZB(M,2) + (X-XB(M,2))*(ZB(M,1)-ZB(M,2))
     $/(XB(M,1)-XB(M,2))
      GO TO 520
  530 YEDGE(ICOUNT) = YB(M,3) + (X-XB(M,3))*(YB(M,2)-YB(M,3))
     $/(XB(M,2)-XB(M,3))
      ZEDGE(ICOUNT) = ZB(M,3) + (X-XB(M,3))*(ZB(M,2)-ZB(M,3))
     $/(XB(M,2)-XB(M,3))
  520 CONTINUE
C
C  SORT THE PAIRS INTO ASCENDING Y ORDER.
      LAST = ICOUNT - 1
      DO 610 M = 1,LAST
```

```
      SMALL = YEDGE(M)
      YSAVE = YEDGE(M)
      ZSAVE = ZEDGE(M)
      MP1 = M + 1
      MSAVE = M
         DO 620 N = MP1,ICOUNT
         IF(YEDGE(N).GE.SMALL) GO TO 620
         MSAVE = N
         SMALL = YEDGE(N)
  620 CONTINUE
      IF(MSAVE.EQ.M) GO TO 610
      ZEDGE(M) = ZEDGE(MSAVE)
      YEDGE(M) = YEDGE(MSAVE)
      YEDGE(MSAVE) = YSAVE
      ZEDGE(MSAVE) = ZSAVE
  610 CONTINUE
      ITOTAL = ICOUNT
C
C ********************SET THE MESH PARAMETERS.****************
C
C
C  CALCULATE THE MAXIMUM Y COORDINATE (YMAX) AND THE NUMBER OF Y
C  INCREMENTS (NY).
      NY(J) = YEDGE(ITOTAL)/HY + 2.0
      YMAX(J) = YEDGE(ITOTAL)
C
C  CALCULATE THE MAXIMUM Z COORDINATE (ZMAX)
      ZMAX(J,2) = ZEDGE(1)
      IF(ZMAX(J,2).LT.0.0) ZMAX(J,2) = 0.0
  705 LASTY = NY(J)
      DO 730 M = 3,LASTY
      RM = M-2
      TESTY = RM*HY
      NSAVE = 0
      DO 710 N = 2,ITOTAL
         IF(YEDGE(N).LE.TESTY) GO TO 710
         IF(YEDGE(N).EQ.YEDGE(N-1)) GO TO 706
         NSAVE = N
         GO TO 720
  706    ZMAX(J,M) = ZEDGE(N)
         GO TO 725
  710 CONTINUE
      ZMAX(J,M) = ZEDGE(ITOTAL)
      GO TO 725
  720 IK = NSAVE - 1
      ZMAX(J,M) = ZEDGE(IK) + (ZEDGE(NSAVE)-ZEDGE(IK))*(TESTY-YEDGE(IK))
     $/(YEDGE(NSAVE)-YEDGE(IK))
  725 IF(ZMAX(J,M).LT.0.0) ZMAX(J,M) = 0.0
  730 CONTINUE
      ZMAX(J,1) = ZMAX(J,3)
C
  410 CONTINUE
C
C
C  SET PARAMETERS FOR THE INLET PLANE.
      IF(INFLAG.EQ.0) GO TO 755
      YMAX(1) = YMAX(2)
      NY(1) = NY(2)
      LASTK = NY(2)
      DO 745 K = 2,LASTK
  745   ZMAX(1,K) = ZMAX(2,K)
C  SET OUTLET PARAMETERS.
      YMAX(LASTJ+1) = YMAX(LASTJ)
      NY(LASTJ+1) = NY(LASTJ)
      KEND = NY(LASTJ)
      DO 750 K = 2,KEND
  750 ZMAX(LASTJ+1,K) = ZMAX(LASTJ,K)
C
C
C  RESET THE INITIALIZATION FLAG
      INFLAG = 0
C
  755 RETURN
      END
```

VITA[2]

David Lee Smith

Candidate for the Degree of

Doctor of Philosophy

Thesis: INCOMPRESSIBLE FLUID FLOW IN COLLAPSIBLE TUBES

Major Field: Mechanical Engineering

Biographical:

Personal data: Born in Dayton, Ohio, November 27, 1945, to Mr. and Mrs. M. D. Smith.

Education: Attended University of Minnesota at Minneapolis, enrolled in Aeronautical Engineering 1963-1967; received Bachelor of Science degree in Mechanical Engineering with an Aerospace option from Oklahoma State University in 1971; received Master of Science degree in Mechanical Engineering from Oklahoma State University in 1972; completed requirements for the Doctor of Philosophy degree at Oklahoma State University in December, 1979.

Professional Experience: Data Processor, Twin Cities Milk Producers Association 1965-67; enlisted service, Air Weather Observer, United States Air Force, 1967-71; commissioned service, Satellite Command Engineer, United States Air Force, 1972-76; graduate teaching and research associate, Oklahoma State University, school of Mechanical and Aerospace Engineering, 1976-79; Senior Aerodynamics Engineer, General Dynamics, 1979.